

2017

Rapid, label-free disease diagnostics by surface enhanced Raman spectroscopy

<https://hdl.handle.net/2144/28986>

Boston University

2017

Rapid, Label-Free Disease Diagnostics by Surface Enhanced Raman Spectroscopy

Chen, Ying

Boston University

BOSTON UNIVERSITY
GRADUATE SCHOOL OF ARTS AND SCIENCES

Dissertation

**RAPID, LABEL-FREE DISEASE DIAGNOSTICS BY
SURFACE ENHANCED RAMAN SPECTROSCOPY**

by

MELISSA (YING) CHEN

B.S., Polytechnic Institute of New York University, 2012
M.S., Polytechnic Institute of New York University, 2012

Submitted in partial fulfillment of the
requirements for the degree of
Doctor of Philosophy

2017

© 2017 by
Melissa (Ying) Chen
All rights reserved

Approved by

First Reader

Lawrence D. Ziegler, Ph.D.
Professor and Chair of Chemistry

Second Reader

Björn Reinhard, Ph.D.
Professor of Chemistry

DEDICATION

To my family, my friends and my colleagues

ACKNOWLEDGMENTS

I want to thank my dissertation advisor Professor Lawrence Ziegler for giving me the opportunity to join the Bio-Raman Lab. What I learned from this remarkable place shall be a lifetime benefit. With the increasing emergence of drug-resistant bacteria strains worldwide, the ability for rapid, easy-to-use, sensitive and specific diagnostic of the causative agent is paramount. In this laboratory I learned about, and honor to be part of, how SERS can be a valuable tool for not only diagnostic purpose but also for studying the underlying molecular mechanism of the disease. I am also equally thankful to the Research Scientist in our lab Dr. Ranjith Premasiri, whose experience and invention of the SERS substrate laid the foundation of all the work I described here.

I also want to thank all my colleagues in the lab, both present and graduated, for their supports in my dissertation works and co-authoring the manuscripts. I want to thank our collaborators for their generous support and providing the bacterial strains and cancer cell lines for my SERS work. I want to thank my dissertation committee members for their effort and guidance to my work.

Additionally, I am also grateful to my parents for their sacrifices and support throughout my education. Without them I would not be able to accomplish what I got today. At last, I am indebted to my husband who have been always by my side.

**RAPID, LABEL-FREE DISEASE DIAGNOSTICS BY
SURFACE ENHANCED RAMAN SPECTROSCOPY**

MELISSA (YING) CHEN

Boston University Graduate School of Arts and Sciences, 2017

Major Professor: Lawrence D. Ziegler, Professor and Chair of Chemistry

ABSTRACT

Surface-Enhanced Raman Scattering (SERS) has the potential to be a rapid disease diagnostic platform. SERS is a well-known ultrasensitive, label-free method for the detection and identification of molecules at low concentrations. The Raman cross-sections are primarily enhanced by plasmonic effects for molecules close to (< 5 nm) the surface of nanostructured metal substrates. Due to the unique Raman vibration features that provide molecular signatures, we have shown that SERS can provide a rapid (< one hour), label-free, sensitive and specific diagnosis for a number of diseases. This work demonstrates the capability of SERS to be an effective optical diagnostic approach, in particular, for bacterial infectious diseases such as urinary tract infections (UTI) and sexually transmitted diseases (STD), and cancer cell identification. More specifically, this work demonstrates the ability of SERS to distinguish different vegetative bacterial cells with species and strain specificity based on their intrinsic SERS molecular signatures. With the exception of *C. trachomatis* - the causative agent of chlamydia - whose SERS molecular signatures are found to be aggregated proteins on the cell membrane, all bacterial SERS molecular signatures are due to purine molecules resulting from nucleic acid metabolism as part of the rapid onset of the starvation response of these pathogens.

The differences in relative contribution of different purine metabolites for each bacterium gives rise to the SERS strain and species specificity. The ability of SERS to distinguish cancer and normal cells grown *in vitro* based on changes of SERS spectral feature as a function of time after sample processing is also demonstrated. Furthermore, the difference of spectral features on the gold and silver SERS substrate of the same bacteria can be used as additional attribute for identification. This work demonstrate the potential of SERS platform to provide antibiotic-specific diagnostics in clinical settings within one hour when combined with a portable Raman microscopy instrument, an effective enrichment procedure, multivariate data analysis and an expendable SERS reference library with drug-susceptibility profile for each bacterial strain determined *a priori*, as well as the ability of SERS platform as a powerful bioanalytical probe for learning about near cell membrane biochemical processes.

TABLE OF CONTENTS

DEDICATION	iv
ACKNOWLEDGMENTS	v
ABSTRACT	vi
TABLE OF CONTENTS	viii
LIST OF TABLES	xi
LIST OF FIGURES	xii
LIST OF ABBREVIATED KEYWORDS	xvi
1. Introduction.....	1
1.1 – Theory of Surface Enhanced Raman Scattering (SERS).....	1
1.1.1 - The Electromagnetic Enhancement Mechanism of SERS.....	3
1.1.2 - The chemical enhancement mechanism of SERS.....	6
1.2 – The Advantages of SERS.....	7
2. SERS Diagnostic Platform: Urinary Tract Infections.....	9
2.1 - Prevalence and Significance of Urinary Tract Infections.....	9
2.2 - Overview of Current UTI Diagnostic Methods.....	10
2.3 - Introduction of SERS-based UTI Diagnostic Platform.....	12
2.4 - Methods and Materials.....	15
2.5 - Results and Discussion.....	20
2.6 – Introduction to linear regression machine-learning methods for strain identification from SERS spectra of an unknown sample.....	27
2.7 - Conclusion.....	34
2.8 - Extended study: Time evolution of UTI bacteria SERS signature.....	36
3. SERS Diagnostic Platform: Sexually Transmitted Disease.....	38

3.1	- Chlamydia and Gonorrhea – the Silent Killer	38
3.2	- Current Chlamydia and Gonorrhea Diagnostic Methods	40
3.3	- Materials and Methods	42
3.4	- Results and Discussion	45
3.5	- Conclusion and Future work	61
4.	The SERS Vibrational Signature of Proteins	62
4.1	- Introduction to SERS study of proteins	62
4.2	- Materials and Methods	65
4.3	- Results and Discussion	68
4.3.1	- SERS spectra of proteins on gold and silver substrates	68
4.3.2	- Perturbing the SERS Protein Spectra	72
4.3.3	- Origin of the Protein SERS Signature	79
4.4	- Conclusion	82
5.	SERS Diagnostic Platform: Cancer Cell Detection	83
5.1	- Basis of Metabolomic-based Cancer Identification	83
5.2	- Current Analytical Techniques for Cancer Metabolomic Study and Introduction of SERS-based Cancer Identification	85
5.3	- Materials and Methods	87
5.4	- Results and Discussions	91
5.5	- Conclusion and Future work	97
6.	Conclusion	99
7.	Supplementary Figures and Information	101
7.1	- SERS Diagnostic Platform: Urinary Tract Infection	101

7.2	- SERS Diagnostic Platform: Sexually Transmitted Disease	105
7.3	- SERS Diagnostic Platform: Cancer Cell Detection.....	106
7.4	- Modeling compound SERS spectra.....	107
8.	Appendix.....	109
8.1	- General laboratory cultivation guideline for vegetative bacteria	109
8.2	- Quantitation of Bacterial Cells by Serial Dilution.....	110
8.3	- Special Laboratory Cultivation Guideline for <i>Neisseria gonorrhoeae</i>	111
8.4	- <i>In vitro</i> cultivation for non- LGV serovar <i>Chlamydia trachomatis</i>	114
8.5	- Common tissue culture protocols	121
8.6	- Receipt for Common Buffer System	130
	BIBLIOGRAPHY	133
	CURRICULUM VITAE	147

LIST OF TABLES

Table 3-1 Contribution of purine metabolite to gold and silver <i>N. gonorrhoeae</i> spectra at each time point determined by linear combination of the normalized component spectra.....	52
Table 3-2 Band Assignment for Silver <i>C. trachomatis</i> SERS spectrum.	59
Table 4-1 The frequency and vibrational assignment of Amide A, B and I-III relevant to the protein structural analysis by IR and Raman spectroscopy.....	63
Table 4-2 Frequencies of Amide I, II and III bands for different secondary structures. .	64
Table S-7-1 Gram-negative UTI Clinical Isolates	101
Table S-7-2 Gram-positive Clinical Isolates	102
Table S-7-3 PLS-DA classification confusion table results for the cross validation model treatment of the SERS spectra of 12 UTI causative clinical isolates.	103
Table S-7-4 PLS-DA classification sensitivity and specificity for twelve UTI bacteria SERS spectra.....	103
Table S-7-5 Relative contribution of purine components to UTI bacteria SERS spectra.....	104
Table S-7-6 Relative contribution of molecular components to M1 and M3 SERS spectra at each time point.....	107

LIST OF FIGURES

Figure 1-1	Schematic representation of plasmonic oscillation (re-created based on)	3
Figure 1-2	The energy level diagram for a model adsorbed on a metal surface.....	6
Figure 2-1	The overall workflow of the SERS UTI diagnostic platform for recovering <i>E.coli</i> BD6594 cells grown in spiked, unprocessed urine from anonymous healthy donor.....	16
Figure 2-2	Scanning electron microscopy (SEM) image of the gold SERS active substrate showing the gold nanoparticle aggregate covering the surface of the substrate.	19
Figure 2-3	SERS spectra of twelve UTI clinical isolate grown in processed urine. The shaded area indicates the standard deviation for each spectrum.....	22
Figure 2-4	Best fits (red) resulting from a linear combination of various amounts of the seven purine molecule SERS spectra to the observed (blue) SERS spectra of the six <i>E.coli</i> bacterial strains.....	25
Figure 2-5	Best fits (red) resulting from a linear combination of various amounts of the seven purine molecule SERS spectra to the observed (blue) SERS spectra of each of <i>S. saprophyticus</i> , <i>E. faecalis</i> and <i>K. pneumoniae</i> strains.....	26
Figure 2-6	The relative contribution of each of the seven purine molecules to each bacterial spectrum is summarized in this bar graph	27
Figure 2-7	Schematic Outline of PLS method.....	29
Figure 2-8	Result of a cross-validated PLS-DA classification of the SERS spectra of the twelve bacterial strains grown in and enriched from processed urine.....	32
Figure 2-9	SERS spectra of different growths of <i>E. coli</i> BD6594 grown and enriched from unprocessed and processed urine.	33
Figure 2-10	Using the PLS-DA model constructed with SERS spectra of twelve UTI bacterial strain grown in processed urine, a set of twenty spectra of an unknown bacterial strain grown in unprocessed urine is correctly identified as <i>E. coli</i> BD6594	34
Figure 2-11	SERS spectra of <i>E.coli</i> BD6880 as a function of time post washing. The increasing contribution of guanine evident from the increasing intensity of the ~ 665 cm^{-1} band is indicated by the vertical dash line.	37

Figure 2-12 SERS spectra of <i>E.coli</i> BD67023 as a function of time post washing. The increasing contribution of guanine evident from the increasing intensity of the ~ 665 cm^{-1} band is indicated by the vertical dash line.	37
Figure 3-1 SEM image of the aggregated Ag nanoparticles-covered SiO_2 substrate. ...	42
Figure 3-2 Compare <i>C. trachomatis</i> (top) and <i>N. gonorrhoeae</i> (bottom) SERS spectra on the gold and the silver substrate.	45
Figure 3-3 Gold and silver SERS spectra comparing the signal from <i>N. gonorrhoeae</i> cell and from the unfiltered supernatant fluid around the cell as a function of time post sample processing.	49
Figure 3-4 The gold and silver SERS spectra of <i>N. gonorrhoeae</i> as a function of time post washing are shown with their best-fit calculated by a linear combination of three purine components: adenine, nicotinamide adenine dinucleotide (NAD/NADH) and guanine	51
Figure 3-5 (Left) Comparing the gold SERS spectra from <i>N. gonorrhoeae</i> from the cell and from the supernatant at $t = 0$ min (initial wash) and after re-washing at $t = 60$ min further show that the NAD/NADH molecules are bound to the bacteria cell membrane.....	55
Figure 3-6 Comparing the SERS gold and silver spectra from <i>C. trachomatis</i> cell with the spectra from the supernatant reveal that the molecule contributing the spectra locates only on the cells. Compare with spectra from HSA and avidin show that protein molecules on the cell membrane are the major contributor to the SERS spectra of <i>C. trachomatis</i>	56
Figure 3-7 Comparing the KEGG purine degradation pathway for <i>C. trachomatis</i> and <i>N. gonorrhoeae</i>	60
Figure 4-1 Ribbon diagram representing the tertiary structures of five protein molecules studied by SERS.	68
Figure 4-2 SERS spectra of various protein molecule solutions in water on the gold substrate (left) and the silver substrate (right).....	71
Figure 4-3 After removing the three broad spectral features by MATLAB function <i>msbackadj</i> distinct, narrower spectral features can be seen for each of the four protein molecules on the gold substrate.....	71
Figure 4-4 The optimized baseline determined by MATLAB function <i>msbackadj</i> is shown with the original spectrum.....	72
Figure 4-5 SERS gold spectra of HSA in 100 μM salt solutions: silver nitrate (AgNO_3), sodium chloride (NaCl), potassium chloride (KCl) and in water as reference	75

Figure 4-6	SERS gold spectra of HSA in NaCl of different concentration to study the effect of ion strength to the three spectral features.....	75
Figure 4-7	Dilution of HSA and avidin, two protein molecules of similar size but having alpha-helix and beta-sheet respectively, as main secondary structure on the gold SERS substrate	76
Figure 4-8	Dilution of HSA and avidin in water on the silver SERS substrate. The intensity and the S/N ratio of the SERS spectral features of both protein molecules on the silver substrate increase with dilution.....	76
Figure 4-9	Simultaneous comparisons between SERS (bottom) and DLS (top) measurements of HSA solution in three solvent systems before and after agitation confirm the molecular origin of the three broad spectral features on the gold SERS spectrum of HSA as protein aggregation in the solutions.....	82
Figure 5-1	Side-by-side comparison of the SERS spectra of non-tumorigenic M1 cells (red) and invasive breast cancer cell M3 (blue) as function of time post-washing. The time-dependent red-shift of the 733 cm^{-1} band on M1 cells is contrasted with the M3 cells which show no red-shift in the zoom-in view on the right.	93
Figure 5-2	Best fits (black) resulting from linear combination of SERS spectra of four purines, NAD/NADH and protein for M1 and M3 cells at each time point are shown. The relative contributions of each molecular components are shown as bar graph on the top.	93
Figure 5-3	Summary of the non-lytic mechanism for release of ATP to extracellular region.....	96
Figure 5-4	The inactivation mechanism of ATP purinergic signaling cascade by membrane-bound nucleotide converting-ectoenzymes.	97
Figure S-7-1	Plot of the PLS-DA classification cross validation root mean square error (RMSECV) as a function of the number of latent variables (LV) selected	104
Figure S-7-2	Sensitivity of <i>C. trachomatis</i> (<i>Ct</i>) on gold and silver SERS substrate at t = 0 min (right after sample processing)..	105
Figure S-7-3	Sensitivity of <i>N. gonorrhoeae</i> (<i>Ng</i>) on gold and silver SERS substrate at t = 60 minutes post sample processing.	105
Figure S-7-4	Gold and silver SERS spectra comparing the signal from <i>C. trachomatis</i> cell and from the unfiltered supernatant fluid around the cell as a function of time post sample processing.	106
Figure S-7-5	SERS spectral features are strongly affected by the local pH environment on the M3 cells.	106

Figure S-7-6	Normalized SERS spectra on gold substrate for seven purine compounds found contributing to the twelve UTI bacterial spectra.....	107
Figure S-7-7	Normalized SERS gold (red) and silver (blue) spectra of the three purine molecules found to be the components of the SERS spectra of <i>N. gonorrhoeae</i>	108
Figure S-7-8	The absolute intensity of adenine, NAD/NADH and guanine found in <i>N. gonorrhoeae</i> spectra are shown here on the gold and the silver substrate.	108
Figure S-7-9	Normalized (left) and baselined (right) SERS spectra on gold substrate of molecular components (four purines, protein and NAD/NADH) found contributing to the SERS spectra of M1 and M3 cells.	109

LIST OF ABBREVIATED KEYWORDS

ATCC.....	American Type Culture Collection
BD	Becton Dickinson®, Inc.
DFA.....	direct fluorescent antibody stain
DLS.....	dynamic light scattering
EB.....	<i>C. trachomatis</i> elementary body
EIA	enzyme immunoassay
HIV	human immunodeficiency virus
HSA.....	human serum albumin
LV.....	latent variables
MOMP.....	<i>C. trachomatis</i> major outer membrane protein
MS	mass spectrometry
NAAT.....	nucleic acid amplification
NMR.....	nuclear magnetic resonance
OD	optical density
PCA.....	principle component analysis
PLS	partial least square
RB.....	<i>C. trachomatis</i> reticulated body
SERS.....	Surface Enhanced Raman Spectroscopy
STD.....	sexually transmitted disease
UTI	Urinary Tract Infection

1. Introduction

Surface Enhanced Raman Scattering (SERS) arises from the resonant excitation of localized surface plasmons which enhance the local fields close to (< 5 nm) the surface of nanostructured metal surfaces. Raman scattering enhancements, typically of the order¹ of $\sim 10^4 - 10^8$ provided by surface plasmon resonance effects allow SERS to be a sensitive molecular spectroscopy for detection and identification of molecules at low concentrations ($\sim \mu\text{M}$ range) without the need of fluorescent labeling at least for molecules that are very near the metal surface. The electromagnetic and the chemical mechanisms that account for the SERS enhancement, which lead to the advantages of SERS as label-free, easy-to-use, sensitive and specific optical biosensor for biomedical applications, are summarized in this introductory chapter.

1.1 – Theory of Surface Enhanced Raman Scattering (SERS)

SERS was discovered, though not recognized at that time, by Fleischmann *et al.*² in 1974 who observed intense Raman scattering from pyridine adsorbed onto a roughened silver electrode surface, which couldn't be explained simply by an increased molecular concentration on the roughened electrode. Since then SERS effect has been observed for many molecules adsorbed onto the surface of metals with a variety of morphologies and local chemical environments. Silver, gold and copper³ are the common choices of metal for SERS substrate. These metals contain lots of free electrons and we will see mathematically how this property lead to large enhancement of the Raman Scattering signal. The large electric field enhancement results from metal surfaces that are

roughened on the nanoscale, which could be single or aggregated colloidal metal particles, etched metal surface, metallic nanoparticles deposited onto glass surface by evaporation or sputtering and arrays of nanoparticles created by lithographic techniques as examples.³

SERS differs from normal Raman spectroscopy in several ways. For examples, there are no strong correlation between the Raman and the SERS spectrum of the same molecule as the Raman selection rule do not fully apply to SERS. It's not uncommon to observe forbidden Raman modes in the SERS spectrum. The intensity of bands observed falls off with increasing frequency, for example C-H stretches tend to be relatively weak in SERS.³ In addition, fluorescent background which is problematic especially in Raman spectrum of hydrocarbon molecules is effectively quenched by energy transfer to the metal surface.

The signal enhancement mechanism of SERS was proposed independently by two groups of researchers Van Duyne *et al.*⁴ and Creighton *et al.*⁵. Van Duyne *et al.* proposed an electric field enhancement of the Raman Scattering for molecules in close proximity to the metal surface due to the presence of localized surface plasmon resonances, while Creighton *et al.* believed the broadening of the electronic state of the molecule due to the interaction with the metal surface resulted in the large Raman scattering cross-sections. As will be shown, both theories are correct conceptually but not in detail.

1.1.1 - The Electromagnetic Enhancement Mechanism of SERS

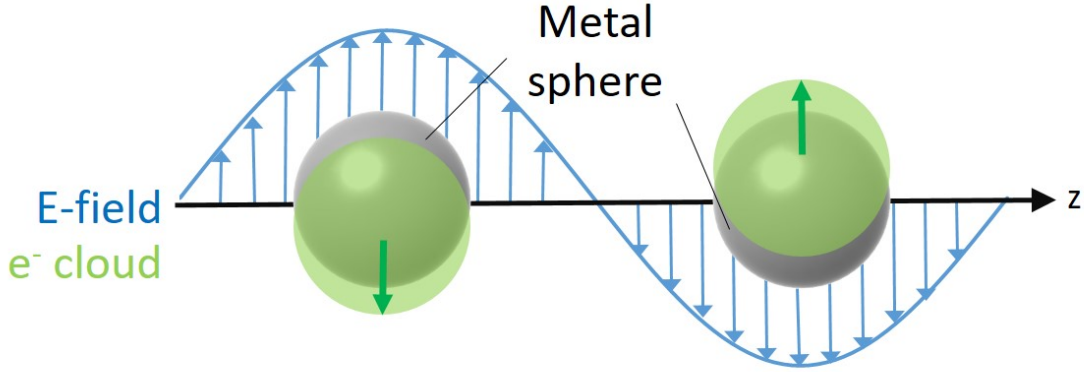


Figure 1-1 Schematic representation of plasmonic oscillation (re-created based on⁶)

In this theory the electric field of the incident and the scattered light are enhanced by the electromagnetic field from the plasmonic resonance.⁷ A plasmon is the collective oscillation of the electron cloud of a metal when excited by an incident electromagnetic wave. The excitation of the resonant oscillation of conduction electrons at the interface of the nanostructured metal surface is called a surface plasmon. This excitation can be propagating, such as on the surface of a grating, or can be localized, such as on the surface of a spherical metal nanoparticle. For a simple description of SERS, we will focus on the latter case. If the incident direction of propagation of the electromagnetic wave relative to the spherical nanoparticle is along the z-axis, as shown in Figure 1-1, then the electric field outside of the sphere E_{out} can be expressed as,

$$E_{out} = E_0 \vec{z} - \alpha E_0 \left[\frac{\vec{z}}{r^3} - \frac{3z}{r^5} (z\vec{z} + x\vec{x} + y\vec{y}) \right] \quad \text{Equation 1}$$

The first term is the electric field of the incident electromagnetic wave, and the second term is the dipole moment induced by the polarization of the electron cloud of the metal sphere. r is the radial distance and $z\vec{z}, x\vec{x}, y\vec{y}$ are the Cartesian coordinates of the induced

dipole which can be neglected at a distance very close to the surface of the sphere. The polarizability of the electron cloud of the metal α is described as,

$$\alpha = ga^3 \text{ and } g = \frac{\epsilon_i - \epsilon_0}{\epsilon_i + 2\epsilon_0} \quad \text{Equation 2}$$

where a is the radius of the metal sphere, ϵ_0 is the dielectric constant of the medium around the metal particle, and ϵ_i is the dielectric constant of the metal.

The displacement of the electron cloud from its equilibrium position is maximized when the frequency of the incident electromagnetic wave matches the intrinsic frequency of the collective plasmon oscillation, i.e. at the plasmonic resonant frequency. Excitation at near the plasmonic resonance wavelength greatly increases the local field experienced by a molecule adsorbed onto the metal surface. Mathematically, plasmonic resonance occurs when $Re(\epsilon_i) = -2\epsilon_0$, which means E_{out} will be very large if α is large. This is the reason metals such as gold and silver are able to provide good enhancement to Raman Scattering with visible/near-infrared excitation, because they have free electrons that make the real part of ϵ_i a large negative value and the imaginary part to be very small. The value of the real part of ϵ_i will dictate the resonance frequency, while the imaginary part will apply to the loss of the resonance. As shown in Equation 2, the plasmonic resonance condition depends on the dielectric constant of the surround medium ϵ_0 , therefore the plasmonic condition of a metal nanoparticle can be modified by changing the dielectric of the external environment, e.g. addition of salt.

It's clear from Equation 1 that the electric field strength falls off with radial distance r from the metal surface as $E_{out} \propto \frac{1}{r^3}$. The SERS intensity depends on the

absolute square of E_{out}^2 evaluated on the surface of the sphere ($r = a$). From Equation 1, this is given as,

$$E_{out}^2 = E_0^2 [1 - |g|^2 + 3 \cos^2 \theta (2\text{Re}(g) + |g|^2)] \quad \text{Equation 3}$$

θ is the angle between the incident field direction and the location r on the sphere surface.

At resonance when $|g|$ is large, Equation 3 can be simplified as $E_{out}^2 = E_0^2 |g|^2 (1 + 3 \cos^2 \theta)$. This means the field intensity is largest when the angle θ is either 0° or 180° , i.e. along the polarization direction. The ratio between the largest and smallest field enhancement as a function of θ is 4.

It's important to note that the surface plasmon will not only excite the incident but also the scattered field. A physical way to look at the field enhancement by plasmonic resonance is the metal particle acts as an antenna that amplifies both the incident and the scattered light. Therefore the overall electric field enhancement will need to consider both the incident and the scattered field enhancements,

$$G_R = \frac{E_{out}^2 E_{out}'^2}{E_0^4} = 16 |g|^2 |g'|^2 \quad \text{Equation 4}$$

where the primed symbols refer to fields for the scattered light. For Stokes shifts at lower frequency, $|g|^2$ and $|g'|^2$ is maximized at approximately the same wavelength, then the enhancement will be about g^4 .⁴ This may also help to explain why SERS intensity typically fall off for highest frequency modes. At higher frequency the plasmonic resonance can excite either the incident or the scattered field but not both, resulting at lower overall SERS enhancement.³

1.1.2 - The chemical enhancement mechanism of SERS

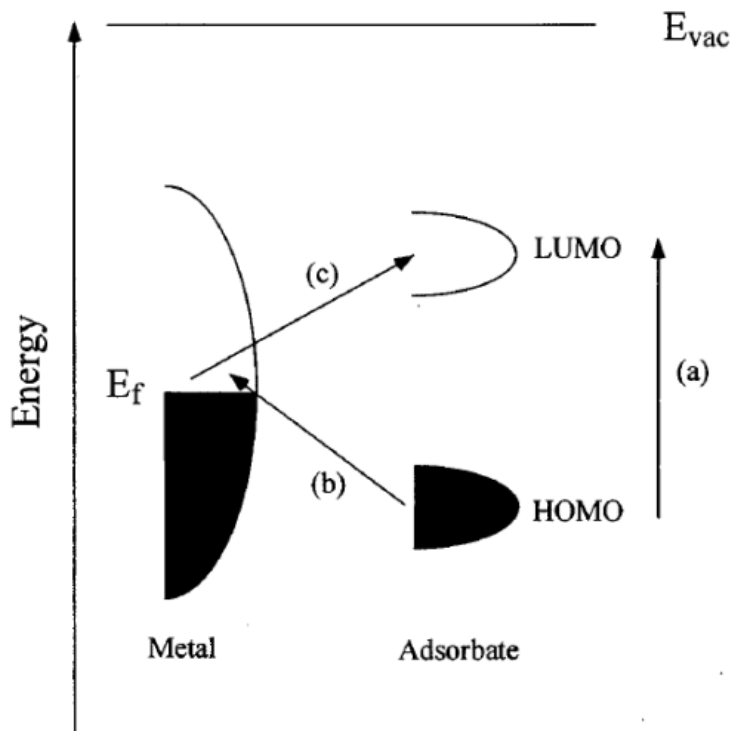


Figure 1-2 The energy level diagram for a model adsorbed on a metal surface. The HOMO and LUMO molecular orbitals of the molecule are broadened by their interaction with the metal states. The charge-transfer excitation is indicated by the arrow.³

The primary evidence suggesting the presence of a second SERS enhancement mechanism independent of the electromagnetic enhancement comes from the observation that nitrogen-containing molecules have stronger SERS intensities than other molecules under the same experimental condition. This observation is difficult to explain by the electromagnetic enhancement mechanism alone because this mechanism should be chemically nonselective. A second line of evidence supporting a second enhancement mechanism comes from the electric potential-dependence of Raman intensity as observed in Fleischmann's experiment.² The chemical enhancement mechanism suggested by Creighton *et al.*⁵ offers an explanation for this chemical selectivity of SERS. In this

mechanism, the electronic states of the adsorbed molecule are broadened due to interaction with the metal surface and new electronic states can also be created by combining with the metal states (“charge-transfer”), causing a shift of the electronic transitions of the molecule (usually from UV visible region). Both processes are illustrated in Figure 1-2. As discussed above, both the electromagnetic and chemical mechanism offer partial explanation but neither theory offers a complete picture of SERS.

1.2 – The Advantages of SERS

It’s easy to see from Equation 4 why SERS is a sensitive method: a modest increase in the local electric field of 10 – 100 produces an overall Raman enhancement that scales as E^4 or approximately a $10^4 – 10^8$ amplification at the surface plasmon frequency. When SERS is coupled with the electronic resonance effect the combined enhancement can allow detection of a single molecule.⁸ Additionally, the narrow Raman scattering spectral features make possible for precise determination of a molecular identity because vibrational motions are intrinsic markers of the molecule itself. Different molecules in a mixture can be simultaneously detected and identified because each molecule has unique narrow spectral signatures. As seen in later discussions, this multiplexing capability will allow us to accurately determine the composition and relative concentration of each component in complex biological samples to be determined. Since the localized plasmonic enhancement requires molecules to be at close proximity to the nanostructured metal surface, SERS is a useful tool for studying biochemical processes occurring at near-cell-membrane extracellular region as well as cell membrane

components when living cells are placed on a nanoparticle substrate. Potential interferences from water at near-infrared excitation frequencies have minimal impact on the SERS spectrum because water has a weak inherent Raman scattering cross-section. This is a particular beneficial property for studying biological systems especially relative to IR vibrational techniques. Since Raman depends on the inherent vibrational motions of samples for identifying characteristic signal, no extrinsic labeling as often employed in fluorescence studies of biological systems is required. Furthermore, the fluorescent background which can sometimes be problematic in Raman spectroscopy, particularly for biological systems, is minimized as mentioned above by energy transfer to the metal surface.

In the next few chapters, the advantages of SERS as label-free, easy-to-use, rapid, sensitive and specific disease diagnostic platform with multiplexing capability are demonstrated. Specifically, the potential of SERS platforms is demonstrated for urinary tract infection, sexually transmitted diseases and cancer diagnostic are discussed. These diseases are chosen for SERS study because they are some of the most common health concerns worldwide and result in billions of dollars in healthcare costs. It is shown that the SERS platform can find molecular biomarkers that identify the causative agents of bacterial infectious diseases and distinguish normal and tumorigenic cells which are grown in laboratory environment. At the same time we will also use SERS to study the biochemical process that lead to the observation of these biomarkers on the SERS spectrum. These proof-of-concept experiments show the ability of SERS as a novel

biosensor for these diseases as well as a powerful bioanalytical probe for studying extracellular metabolomics.

2. SERS Diagnostic Platform: Urinary Tract Infections

2.1 - Prevalence and Significance of Urinary Tract Infections

Urinary tract infection (UTI) is one of the most common types of bacterial infection in human evident by the appearance of large amounts ($\geq 10^5$ cfu/mL, colony forming unit) of bacteria in mid-stream urine.⁹ UTI is among the leading reasons for primary care medicine treatments.^{10, 11} Approximately 50% of all women will have UTI at least once in their lifetime, about 20% will have a recurrent UTI and large portion of this group will turn into chronic UTI.^{11,12} UTIs pose a heavy burden to the health care system. In the US alone, UTIs are responsible for more than 7 million doctor's office visits and over one million hospital admissions, at a cost of ~\$1 billion per year.^{13,14,15} UTI is also one of the most common hospital-acquired infections, responsible for up to 35% of nosocomial infections.¹⁶

Among the causative bacterial strains for UTI, *Escherichia. coli* is the predominant bacterial species accounting for up to 70% of UTI clinical presentations.¹⁰ Other common UTI pathogens include *Staphylococcus saprophyticus* (5-10%), *Klebsiella pneumoniae* (4-7%), *Proteus mirabilis* (4-5%), *Pseudomonas aeruginosa*, and *Enterococcus faecalis*.^{10,16,17} A mid-stream bacterial count of 10^5 cfu/mL (colonies forming unit/mL) in free collection urine is used as indication of UTI in symptomatic

patients and the recommended level for antibiotic treatment.⁹ Amid the growing concern of antimicrobial resistance, more drug-resistant bacterial strains are associated with UTI cases, such as the discovery of fluoroquinolone-resistant *E. coli* strains, extended spectrum beta lactamase (ESBL) *E.coli*, *K. pneumoniae*, and other Gram-negative strains as well as the increasing resistance to the combined trimethoprim/sulfamethoxazole antibiotic by many UTI strains.^{18,19,20} The number of antibiotics available for successful treatment has been significantly reduced due to these growing trends of drug-resistance.

2.2 - Overview of Current UTI Diagnostic Methods

The current UTI diagnostic method can be summarized into two categories: nonculture and culture methods. Examples of non-culture methods are urine microscopy, the nitrite test and the leukocyte esterase test.²¹ In the urine microscopy method bacteria cells are counted after being fixed with Gram stain in the patient's urine sample. The presence of bacteria in urine can also be detected indirectly by the amount of leukocyte cells in the urine sample which will increase dramatically in immune-response to an UTI episode.²² Both tests are simple and the cost per test is low. However both tests are insensitive to low bacteria concentration ($\leq 10^5$ cfu/mL), and a first-void urine sample with two hours incubation time in the lab is required for both tests to work properly.²³ Alternatively bacteriuria can be detected through a nitrite test that measures the chemical conversion of nitrite to nitrate by bacterial activity in the urine sample. The nitrite test is the basis for commercially available dip-strip test. The nitrite test is susceptible for members of the *Enterobacteriaceae* family,²² but its usefulness is limited because nitrite

production is not associated with other common UTI-causing pathogens such as the *S. saprophyticus* and the *Pseudomonas* species.²⁴ Moreover first-void urine and ~4 hours incubation time is necessary for bacterial conversion of nitrate to nitrite to reach sufficient level for detection.²² The leukocyte esterase test utilizes the hydrolysis of ester substrate by esterase released by neutrophils.²⁵ The esterase test detects esterase from both the intact and lysed leukocytes, but the test can yield false positive results when the urine is contaminated with bacteria from the vaginal fluid which naturally contain esterase or containing eosinophils or the *Trichomonas* species.²² These non-culture tests are simple, inexpensive and easy-to-use, but they detect the presence of bacteria through indirect measurement and thus provide no information about the species or strain identity, essential for establishing the antibiotic susceptibility profile required for drug prescription, or the quantity of the causative pathogen which can help monitor drug efficacy and disease progression.

The advances of genotyping-based techniques such as nucleic acid amplification tests (NAAT) allow more rapid molecular-based approaches and offer the advantage of high sensitivity and specificity compare to other non-culture detection methods. However, the high sensitivity and specificity of NAAT could mean false positive due contamination by exogenous sources of DNA.^{26,27} The need for matching genetic primers and the requirement of a laboratory setting can be problematic for NAAT as point-of-care diagnostic method.^{28,29}

Bacteria culturing, on the other hand, is the current gold standard method for UTI diagnosis. It remains the only method that provides information about bacterial strain

identity, quantity and antibiotic susceptibility simultaneously in patient urine sample.²² However this method typically required 24-48 hours incubation time for bacterial growth, and even longer incubation required for antibiotic susceptibility determination. The long incubation time is the major drawback especially when recurrent or chronic infections are suspected and multiple urine samples from the patient are needed for definitive diagnosis.³⁰ As a result of this long waiting period, physicians are often resort to prescribing broad spectrum antibiotics based on patient symptoms, which has significantly contributed to infective treatment, increased care cost and the rising occurrence of multi-drug resistant bacterial strains.¹⁸ Therefore, a rapid diagnostic method that provides microbial identification and drug susceptibility within the time frame of a patient presenting at a clinic (<1 hour) is urgently needed to allow appropriate use of narrow spectrum antibiotics. Rapid diagnostics is also cited as a critical need to aid the clinical development of new antibacterial drugs.³¹

2.3 - Introduction of SERS-based UTI Diagnostic Platform

SERS is an attractive candidate for bacterial diagnostics because it is a rapid, ease-to-use, information-rich method that does not require additional labeling procedures for identification purposes. SERS arises from the well-known Raman cross-section enhancement effect on molecules close to (< 5 nm) the surfaces of nanostructured metal substrates. Since Raman vibrational features are uniquely dependent on molecular structure, precise determination of the molecular identity from a SERS spectrum is possible. It's also possible to identify different molecular components in a mixture in a

single spectrum based on the unique narrow vibrational signatures of each component, which is essential for analyzing biological mixture.

SERS spectra of laboratory-cultured bacterial cells have been reported over the past fifteen years.^{32,33,34,35,36} The use of SERS as a novel approach to rapid, growth free UTI diagnostics has been proposed in several previous studies.^{37,38,39,40,41,42} In these studies clinical isolates or bacterial species known to cause UTI are cultured in standard growth media and SERS signatures are obtained. In a previous study it was shown that a group of six *E. coli* clinical isolates grown in bacterial growth media can be distinguished by their SERS spectra when combined with multivariate classification algorithm.³⁸ This study also demonstrated that the potential of SERS to provide strain specificity. In nearly all of these bacterial SERS studies, the major vibrational bands of the observed bacterial spectra are attributed to components of the outer bacterial cell wall structures, such as peptidoglycan, lipids, lipopolysaccharides or membrane proteins and nucleic acids.

Our efforts in the laboratory have been resulted in development of a SERS-based UTI diagnostic platform with the advantages of speed and ease-of-use with the potential to be a point-of-care diagnostic device. A crucial component of the SERS UTI diagnostic platform is a gold nanoparticle covered silica substrate which results from a metal ion doped sol-gel procedure which are used here for the acquisition of highly sensitive and robust SERS spectra of vegetative bacterial cells with 785 nm excitation.³⁴ After the acquisition of the bacteria SERS spectra a multivariate analysis “barcode” procedure based on the sign of the spectral second derivative as a function of the scattered wavelength are applied to allow rapid determination of the bacterial strain identity.⁴³

Furthermore, in contrast to the usually reported molecular origin of these SERS spectra being attributable to cell wall structures, we have shown that the dominant molecular species contributing to the 785 nm excited SERS spectra of bacteria are the metabolites of purine degradation: adenine, hypoxanthine, xanthine, guanine, uric acid and AMP⁴⁴. These molecules result from the starvation response of the bacterial cells in pure water washes following enrichment from nutrient rich environments.

In contrast to previous SERS UTI studies described above, our primary objective is to determine if high quality SERS spectra can be obtained from UTI causative bacteria grown in human urine and to demonstrate these obtained SERS spectra can provide growth-free species and strain specificity when combine with multivariate classification algorithms. We show that our SERS-based UTI diagnostic platform can identify the bacterial strain grown in the urine sample at clinically relevant concentration (10^5 cfu/mL) in less than a one hour time frame. Twelve UTI clinical isolates with previously determined antibiotic susceptibilities are used in this study, hence successful SERS-based classification will also provide growth-free determination of antibiotic susceptibility or resistance for this set of organisms. In addition, a prototype procedure for bacterial enrichment from urine is developed as part of the SERS UTI diagnostic platform. The molecular origins of the bacterial SERS signature will be discussed as well. The success of the rapid SERS UTI diagnostic platform will make possible the administration of appropriate narrow spectrum antibiotics, earlier initiation of appropriate therapy and better real time monitor of treatment efficacy for patients with UTIs.

2.4 - Methods and Materials

Bacterial samples and preparation. The twelve bacterial strains used in this study (see and Table S-7-2) were donated by BD® Life Sciences and were all isolated from clinical urine specimens. Their antimicrobial susceptibility profiles were determined by the BD Phoenix™ Automated Microbiology System⁴⁵ prior to these SERS investigations and are summarized for a range of antibiotics (See Table S-7-1 and Table S-7-2). These samples include strains of two Gram-negative bacteria, *Escherichia coli* (6 strains) and *Klebsiella pneumoniae* (2 strains), and two Gram-positive bacterial species, *Staphylococcus saprophyticus* (2 strains) and *Enterococcus faecalis* (2 strains).

All twelve bacterial strains were grown in freshly collected human urine that had been previously processed to remove solid materials. To prepare the processed urine, first or second urine of the day from anonymous healthy donor was collected (100 mL) into two 50-ml sterile centrifuge tubes and centrifuged at 10,000 rpm (Eppendorf® 5805) for 20 minutes at (18 °C). After centrifugation, the pellet at the bottom is discarded and the supernatant urine is transferred to sterile containers. The optical density (OD_{600nm}) of the supernatant urine is recorded and is used to compare with the OD after spiking with bacteria to verify the urine collected is initially free of bacterial cells. Then 10 mL of the supernatant urine are transferred from the container to a sterile test tube. Approximately three loops (~ 30 µL) of overnight bacterial culture grown in tryptic soy broth (BD®) are inoculated into this urine supernatant and allowed to grow to OD of 0.1. The bacterial concentration at this OD is determined by serial dilution to ~10⁷ cfu/mL (See Appendix 8.2). 0.5 mL of this ~10⁷ cfu/mL urine culture are spiked into about 50 mL of the

remaining urine supernatant and incubated for 30 minutes at room temperature.

To isolate the bacterial cells from the spiked urine sample, the urine sample is centrifuged at 10,000 rpm for 20 min and the resulting bacterial pellet is quantitatively transferred to a 2 mL micro-centrifuge tube. The bacterial pellet is then washed with 0.5 mL of ice-cold distilled water four times and centrifuged for 1 minute at 10,000 rpm between each washing cycle. Washing in ice-cold water will ensure consistent synchronization of bacterial stress response for each experiment. This centrifuging-washing procedure will result in a final enriched concentration of $\sim 10^8$ cfu/mL in a volume of ~ 50 μ L. For the subsequent SERS spectra acquisition, 1 μ L of the enriched sample is pipetted onto the SERS active substrate and allowed to air-dry for about 5 minutes. This procedure was repeated for all twelve bacterial strains. The total time for sample enrichment to placement on the SERS substrate for Raman acquisition was ~ 40 min.

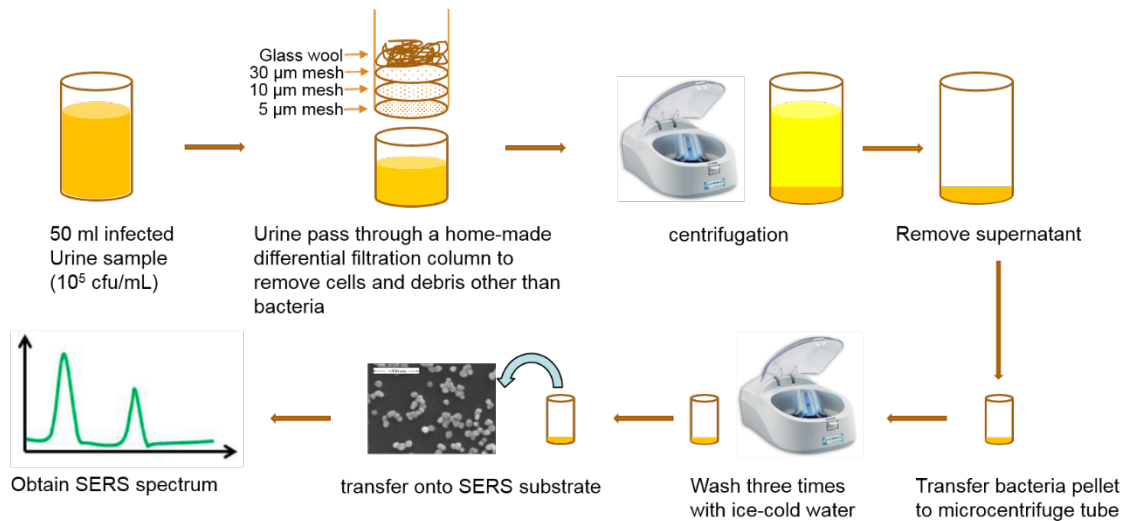


Figure 2-1 The overall workflow of the SERS UTI diagnostic platform for recovering *E. coli* BD6594 cells grown in spiked, unprocessed urine from anonymous healthy donor.

In another set of SERS measurements, bacterial cells from one of the twelve UTI bacterial strains, *E.coli* BD6594, were spiked into non-processed, i.e. non-centrifuged urine which thus contain natural sedimentary materials. The amount of the natural sedimentary material, which consists of whole cells and cell debris from the lining of the urinary tract and inorganic crystals,⁴⁶ is approximately 1-2 mL in 50 mL urine from anonymous healthy donor and may be more in real UTI patient samples due to presence of white blood cells.²² Therefore, the centrifugation method mentioned above alone will not be sufficient to consistently recover all bacterial cells from the urine sample. Hence for this proof-of-concept experiment a differential filtration scheme was developed to remove these sedimentary materials while retaining the bacterial cells, as shown in Figure 2-1. About 10 mL of the urine from anonymous healthy donor is inoculated using overnight *E.coli* BD6594 bacterial culture in tryptic soy broth and allow to grow to an OD of 0.1. Then 0.5 mL of the inoculated urine is spiked into 50 mL non-processed urine from the same donor to bring to concentration of bacterial to 10^5 cfu/ml. Meanwhile, a four-stage gravitational filtration system with decreasing pore size is assembled as shown in the figure. The filters used in the system are 30, 10 and 5 micron Nylon mesh filter (Cole-Palmer®). Three sterile 50 mL conical centrifuge tubes are obtained and their bottoms are cut off. The mesh filter are capped at the bottom of the conical centrifuge tube and secured by tape and parafilm to prevent leaking. Then the three centrifuged tubes are stacked on top of each other in the order of decreasing pore size. In addition, ~200 mg of glass wool is added to the bottom of the first tube to complete the four-stage filtration system. To use the four-stage filtration system to recover the bacterial cells, the

50 mL bacteria spiked urine sample is slowly pour into the system and the filtered urine is collected after the 5 micron mesh into a sterile 50 mL centrifuge tube. The subsequent steps of the bacterial enrichment procedure are identical to that for the processed urine samples described above. The total preparation time using this procedure is still around ~40 minutes since the filtration step takes ~1-2 minutes. This procedure was not carried out for all twelve bacterial strains because a new four-stage filtration system needs to be re-constructed for each new sample. However an analogous re-usable filtration/centrifugation scheme like this can be developed for a SERS UTI diagnostic system for real-world clinical samples. This prototype apparatus is intended to demonstrate how bacterial cells can be enriched and recovered from un-processed urine for successful acquisition of SERS spectra at clinically relevant concentrations as shown below.

SERS active substrate All SERS spectra are obtained using an *in-situ* grown, aggregated gold nanoparticle covered SiO₂ substrate developed in our laboratory.³⁴ Characterization and performance of these SERS active substrate have been previously described and characterized.^{34, 43, 44,47,48,49,50} These substrates are produced by a two-stage reduction by sodium borohydride of an Au³⁺ ion doped sol-gel that results in small (1-10 particles) aggregates of ~80 nm diameter gold nanoparticle covered SiO₂ substrate. Figure 2-2 shows the SEM image of the gold SERS active substrate. Ag⁺ doped sol-gels can also be prepared by this methodology.

SERS spectra acquisition Bacterial SERS spectra are acquired by an RM-2000 Renishaw® Raman microscope employing a 50x (infinity-corrected, 0.75 numerical

aperture) objective and 785 nm excitation. Incident laser powers of ~ 0.45 mw and ~ 10 seconds of illumination time are typically used to obtain the reported bacterial SERS spectra. The illuminated Raman excitation field of view is $\sim 30 \mu\text{m} \times 2.5 \mu\text{m}$. The 520 cm^{-1} band of a silicon wafer is used for frequency calibration. Typically ten spectra per sample range from $200\text{-}1800 \text{ cm}^{-1}$ were obtained for each experimentally reported bacterial spectrum. The peak frequency precision is $\pm 0.5 \text{ cm}^{-1}$. Spectral acquisition took less than 10 min. The acquired SERS spectra are averaged and baseline-corrected with GRAMS® (Thermo®). The SERS spectra are normalized and plotted by MATLAB® (r2013b) and the spectra are displayed vertically offset for clarity.

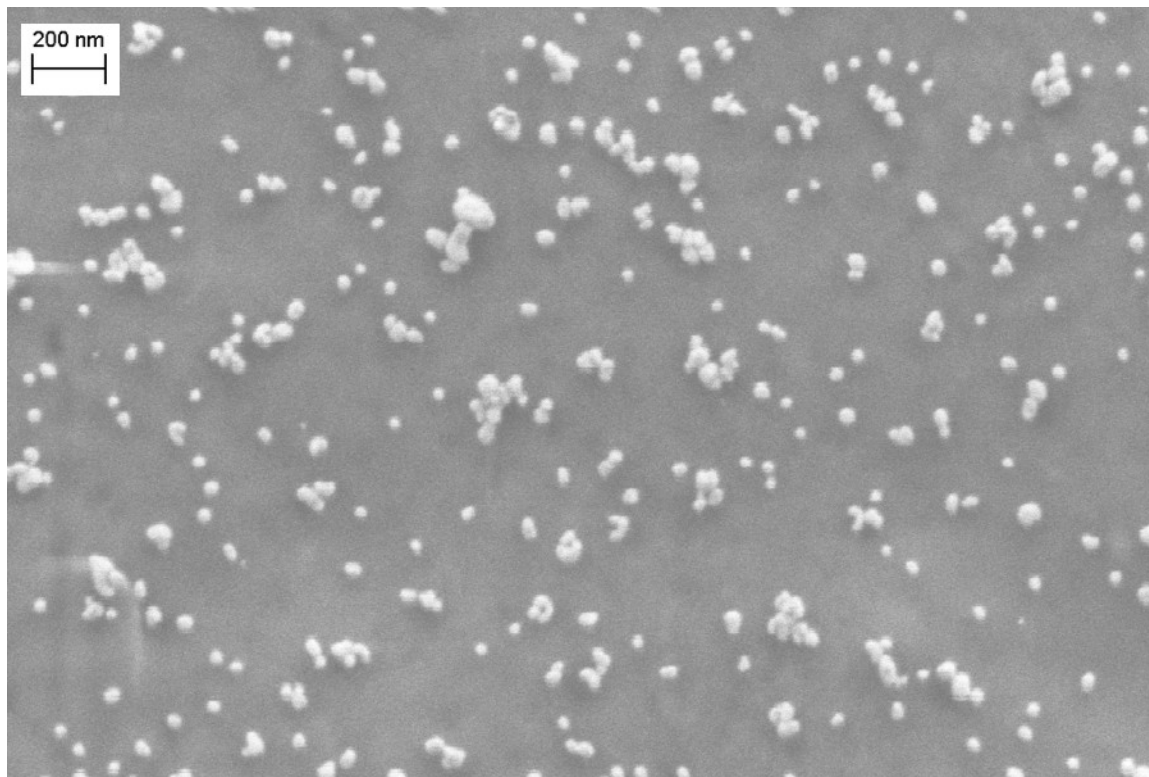


Figure 2-2 Scanning electron microscopy (SEM) image of the gold SERS active substrate showing the gold nanoparticle aggregate covering the surface of the substrate.

Data analysis Classification by multivariate machine-learning algorithm is an important component of our SERS UTI diagnostic platform. Machine-learning algorithm allow rapid processing and information gathering from large amount of spectral data and can be used to identify unknown spectra based libraries built from previously collected data. In this analysis, a partial least square – discriminant analysis (PLS-DA) algorithm was used to achieve bacterial strain identification based on SERS spectra. The PLS-DA algorithm is part of the PLS toolbox (v7.3.1) developed by Eigenvector Research, Inc. (Seattle, WA) based on MATLAB® (r2013b) platform. A polynomial fitting function in MATLAB® was employed to remove broad variable baseline features from individual SERS spectrum. A previously developed barcode methodology⁴³ based on the sign of the second derivative of the baselined SERS spectra as a function of scattered wavelength converts all baselined spectra into a barcode, a series of “1”’s or “0”’s, which are the input vectors to the PLS toolbox. This combination of barcode and multivariate classification algorithm results in greater sensitivity and specificity for this SERS-based spectral classification technique.

2.5 - Results and Discussion

SERS spectra of bacterial strains grown in filtered urine

SERS spectra of twelve bacterial clinical isolates grown in filtered urine and diluted with urine to 10^5 cfu/mL are shown in Figure 2-3. The shaded area indicates \pm one standard deviation of the averaged intensity of each spectrum. Six strains of *E.coli*, and two strains each of *S. saprophyticus*, *K. pneumoniae* and *E. faecalis* are shown in this

figure and color coded by species. Each spectrum is an average of ~10 individual SERS spectra acquired on our gold SERS active substrate. All spectra exhibit excellent S/N as seen on this figure. As already indicated, the total time for acquisition of the SERS spectra of bacteria from spiked processed urine sample is ~40 minutes, and the bulk of this time is spent on the sample enrichment and centrifugation steps in this bench-top prototype procedure. Figure 2-3 demonstrates the ability of our SERS UTI diagnostic platform to obtain high quality SERS spectra from enriched bacteria sample which are grown in spiked urine within one hour time-frame. Furthermore, this figure shows that our SERS platform has the ability to report UTI cases with bacterial concentration below 10^5 cfu/mL which is the current clinical definition.

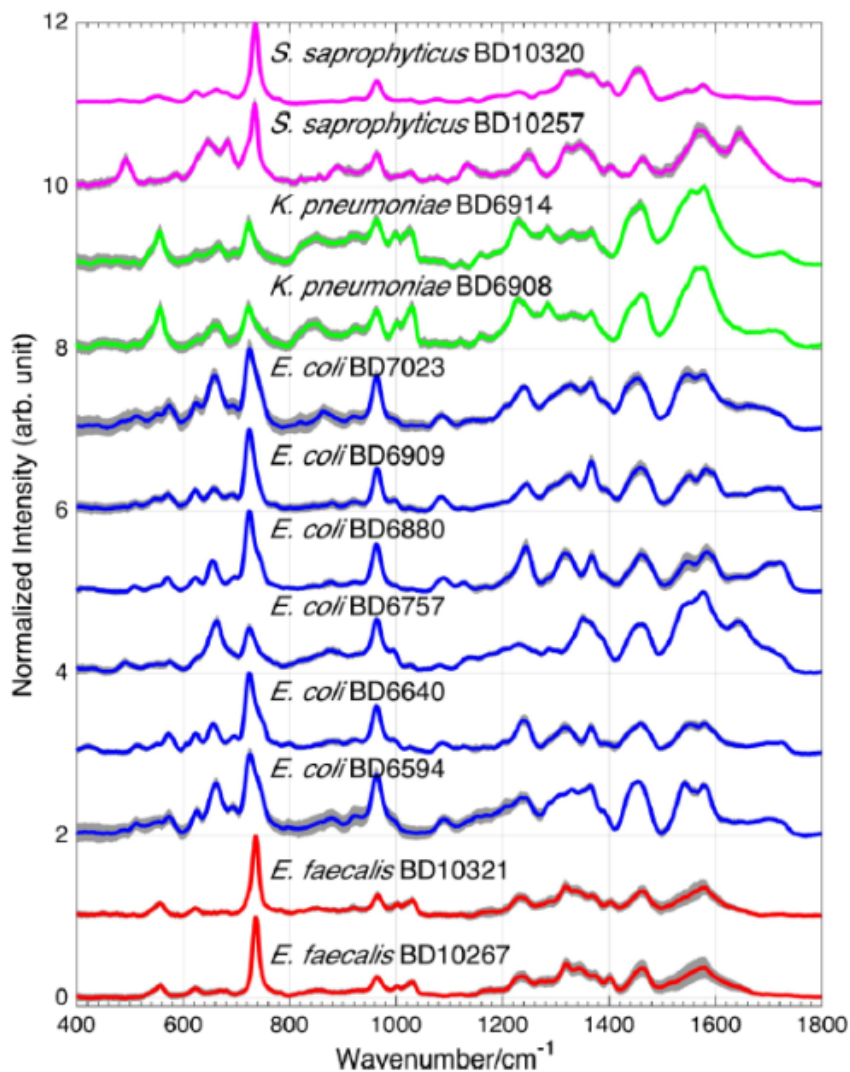


Figure 2-3 SERS spectra of twelve UTI clinical isolate grown in processed urine. The shaded area indicates the standard deviation for each spectrum.

As seen in Figure 2-3, with the exception of the two *S. saprophyticus* strains, the differences between the SERS spectra of the *E. coli*, *K. pneumoniae* and *E. faecalis* strains are greater than the difference between the strains of a given species. A number of vibrational bands are common among these bacterial spectra, such as the strong band in the 725-735 cm^{-1} region in all spectra as well as the 660 cm^{-1} , 960 cm^{-1} , 1240 cm^{-1} , 1315 cm^{-1} , and 1450 cm^{-1} bands. The molecules contributing to these vibrational bands

will be discussed shortly. Comparing Figure 2-3 with the drug susceptibility profile in Table 4-1 and in Table S-7-2 shows that there are no clear correlation between the SERS spectra similarity and the drug susceptibility profile. However, a larger dataset is needed to definitively determine the relationship between SERS spectral similarity and the drug susceptibility.

Molecular origin of SERS signal and species/strain specificity

In our previous reports of SERS spectra of vegetative bacterial cells^{44, 48, 49, 50} we found that virtually all observed vibrational features could be assigned to the spectral contributions of six purines molecules: adenine, hypoxanthine, xanthine, guanine, uric acid and AMP. The presences of these molecular species in our bacterial SERS spectra are attributed to the nucleotide metabolic degradation pathway due to the rapid onset of the bacterial starvation response. These molecules are secreted by the bacterial cells to the extracellular regions near the outer cell membrane in rapid response to being in a nutrient-depleted environment. The identity of these molecular components have been determined by isotopic labeling, model compound studies, bacterial supernatant studies, gene knockout studies, enzyme reactant effects and mass spectrometry.^{44,51} In the UTI bacterial SERS spectra we also found that nearly all the vibrational bands can be assigned to these six molecules with the addition of another purine molecular component, guanosine, identified here. Each of the bacterial strain spectra in Figure 2-3 is best-fit by a linear combination of these seven purine components and is shown in Figure 2-4 and Figure 2-5. The linear coefficient of the best-fit for each strain is given in Table S-7-5. The normalized SERS spectra of the seven purine compounds are shown in Figure S-7-6

and are used for this best-fitting procedure. Nearly all vibrational features in the bacteria spectra are captured in the calculated, best-fit spectra. Each bacterial spectrum has different amount of these purine components and the different relative contributions of each purine molecule is the intrinsic biomarker for the identification of the bacteria via this SERS diagnostic platform. To visualize the relative contributions of these seven purine molecular components to each bacterial spectrum, a bar graph showing these best-fit determined relative amounts (in Table S-7-5) is shown in Figure 2-6. This figure shows that each species has a different reproducible mixture of purine molecules contributing to its spectrum. For example, adenine and guanosine are the largest and second largest contributors respectively to the *E. faecalis* spectra, but for *E. coli* the two largest molecular components are hypoxanthine and xanthine. This difference in main purine contributors between these two species give rise to the species specificity observed with SERS. Furthermore, strains of a given species have similar composition of these seven purines, but the amount of each purine is not identical. For example, *E. coli* BD6594 spectrum has more hypoxanthine contribution than xanthine contribution, while for the *E. coli* BD6880 spectrum xanthine contributes more than hypoxanthine. The differing amount of these purine components within the same species give rise to the strain as well as species specificity of SERS, as well as a basis for the successful classification and diagnostic capability by multivariate analysis methods.

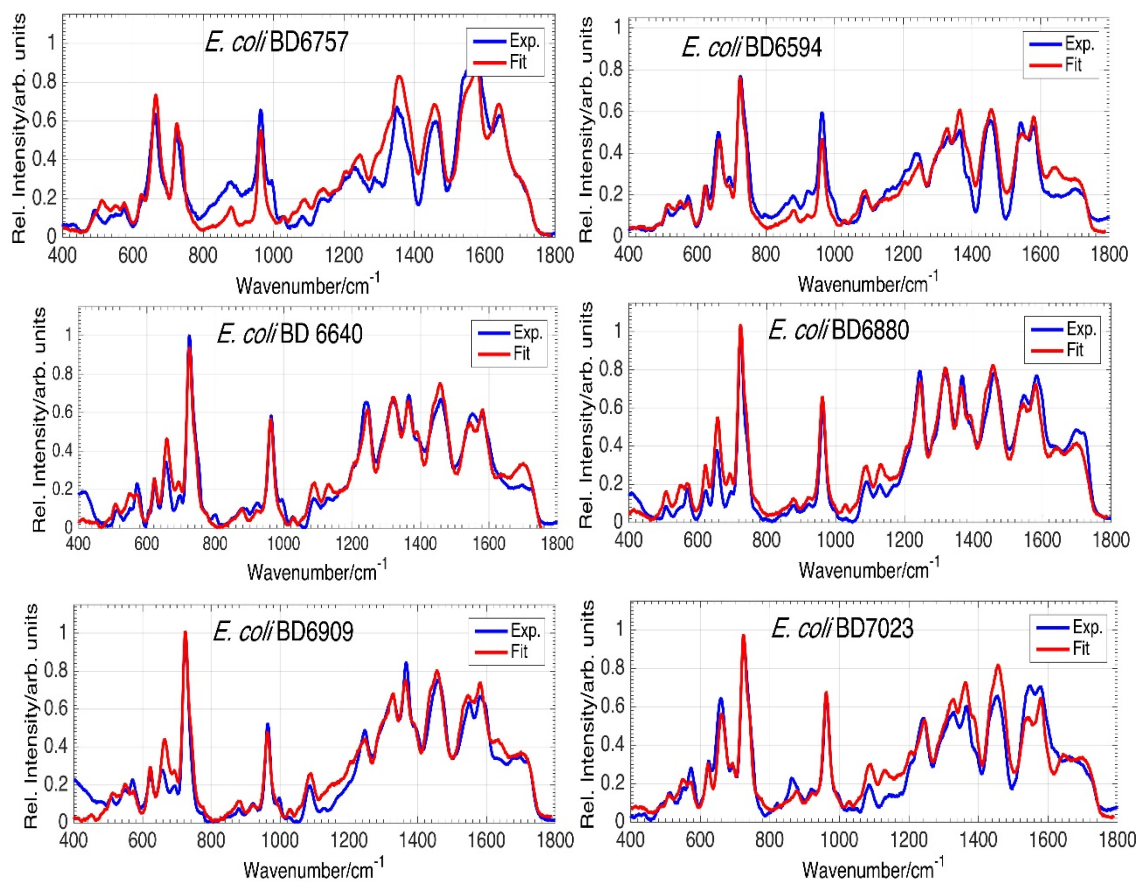


Figure 2-4 best fits (red) resulting from a linear combination of various amounts of the seven purine molecule SERS spectra to the observed (blue) SERS spectra of the six *E.coli* bacterial strains.

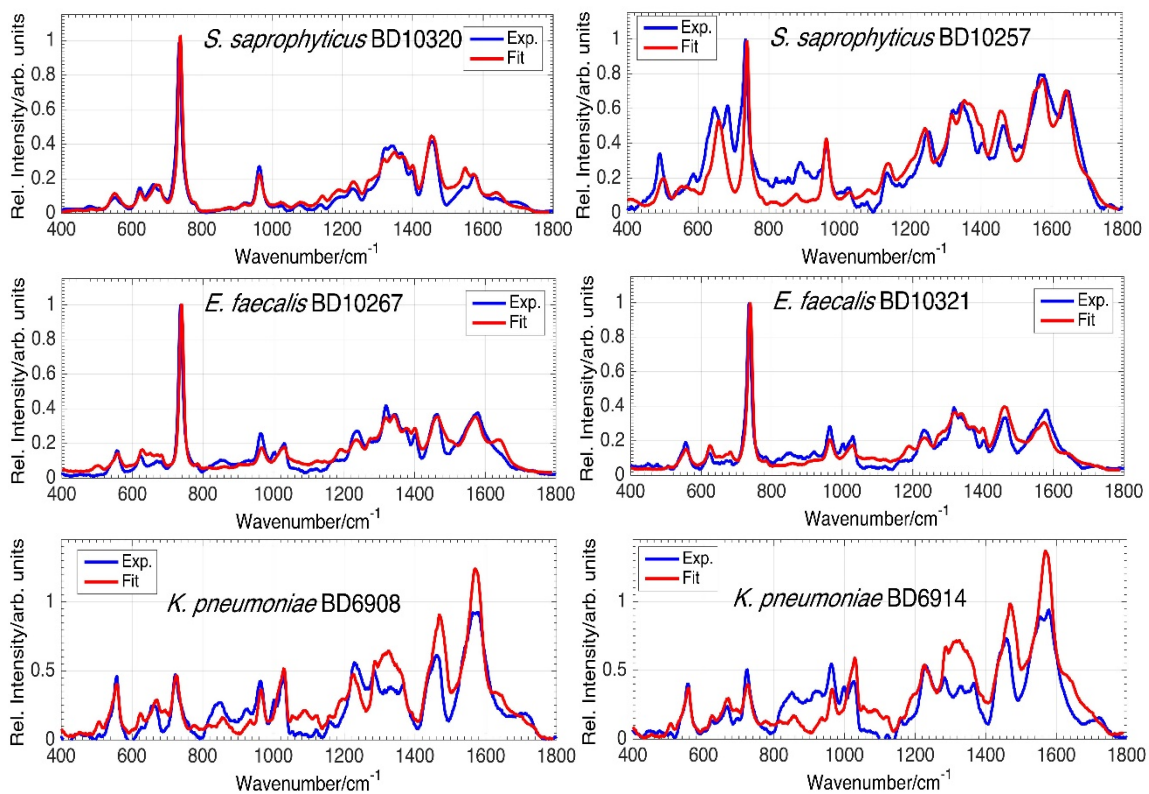


Figure 2-5 best fits (red) resulting from a linear combination of various amounts of the seven purine molecule SERS spectra to the observed (blue) SERS spectra of each of *S. saprophyticus*, *E. faecalis* and *K. pneumoniae* strains.

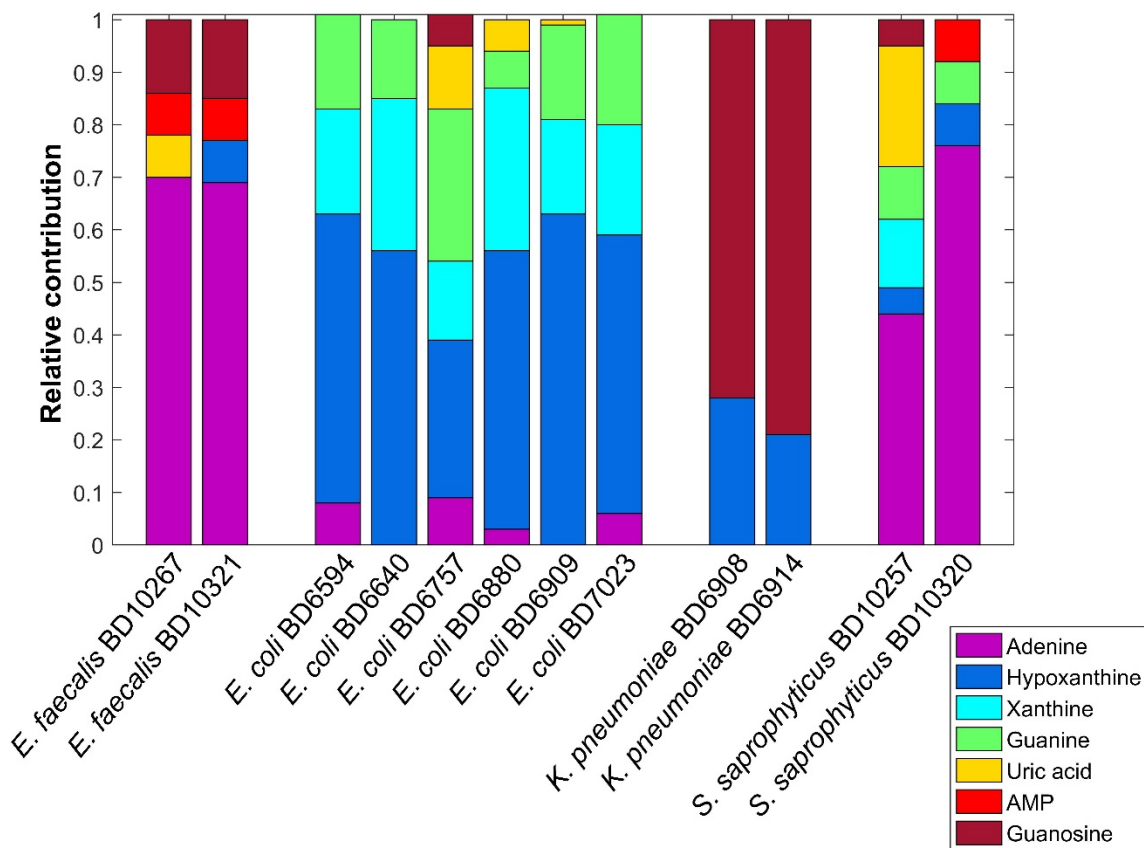


Figure 2-6 the relative contribution of each of the seven purine molecules to each bacterial spectrum is summarized in this bar graph. The numerical value is shown in Table S-7-4 PLS-DA classification sensitivity and specificity for twelve UTI bacteria SERS spectra.

2.6 – Introduction to linear regression machine-learning methods for strain identification from SERS spectra of an unknown sample

A partial least square (PLS) statistical method (Eigenvector Research Inc., Seattle, MA) was used to construct a predictive model based on the SERS spectra of the twelve UTI bacterial strains. A set of SERS spectra for a bacterial strain of an unknown identity grown in unprocessed urine (i.e. not centrifuged prior to spiking with bacterial cells) was

used to test the predictive model to see if the model can correctly identify the strain and hence offer antibiotic-specific diagnostic capability.

Introduction to Linear Regression

Scientific research often involves using controllable and/or easy-to-measure variables (*factors*) to explain or predict the behavior of other variables (*response*). If there are only few factors which are not significantly redundant (collinear) and a well-understood relationship exists between the factors and the response, a linear regression can be a good way to gather as much information from the dataset of interest as possible. Most of the time the primary objective for a researcher is merely identifying the most important factors and use them to construct a good predictive models. For example, the multiplexing capability of SERS allows the estimation of the amount of different chemical components in a UTI bacterial spectrum as shown in Figure 2-6. In this case the factors are the data-points that comprise the SERS spectrum; they are numbered in the thousands but are highly collinear. The response are the chemical components contributing to the SERS spectra of a particular UTI bacterial strain that we want to know and use as unique signature to indicate the presence of this strain in future samples.⁵²

Partial least squares (PLS) is a method for constructing predictive models when the factors are many but highly collinear. PLS was developed in the 1960's by Herman Wold as an econometric techniques, but quickly found use in chemical engineers and chemometricians. In principle, linear regression can be used when the number of factors is very large. However, not every one of these factors are needed to construct a good predictive model; there are only few important underlying factors that account for most

of the variation in a set of SERS spectra. The goal of PLS is to try to extract these few important underlying factors, or so-called latent variables (LV) that account for as much variation in the spectral dataset as possible. In this sense PLS bears some resemblance to principle component analysis (PCA) since both methods aim to find the important variables to describe the spectral dataset.

How does PLS works

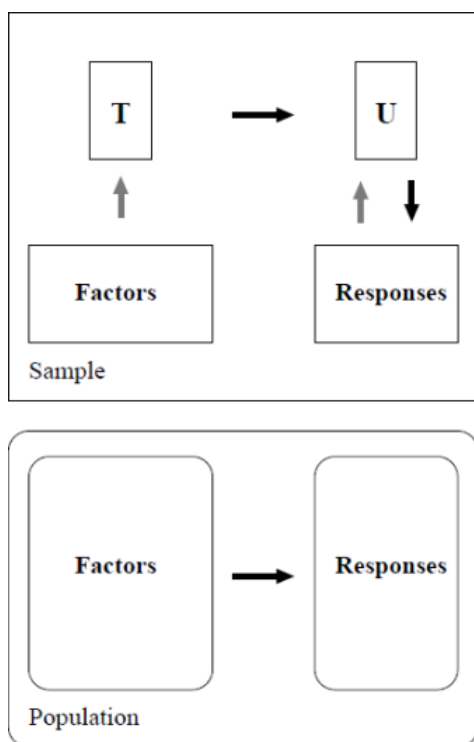


Figure 2-7 Schematic Outline of PLS method.⁵²

Figure 2-7 shows a schematic outline of the PLS method. In this application, the sample will be the SERS spectra of each of the twelve UTI bacterial strains and the population will be the SERS spectra acquired from an unknown urine sample. The overall goal (shown in the lower box) is to build a model that uses the most important factors (latent variables) gathered from the samples to predict the response when applying to the population. This goal is achieved indirectly by extracting latent variables T and U from the factors and response, respectively, in the sample. The extracted factors T (also known as X -scores) are used to predict the extracted factors U (also known as Y -scores) and the predicted Y -scores are used to construct prediction for the responses in the sample. After confirming the robustness of the constructed prediction through cross-validation, this prediction model can be used to predict the response from the population.⁵³

The importance of the cross-validation process

Cross-validation is a very important and useful tool in the classification process which serves two critical functions: (1) to assess the complexity of a model, i.e. is the number of latent variable being utilized to build the model large enough to capture sufficient variance from the dataset and (2) to provide an estimate of performance when the model is applied to unknown data. In other words, the cross-validation process is a “quality-control” step for the classification model. For any given dataset the cross validation process is a series of experiments (called sub-validation experiments) that starts with the removal of a subset of spectra from the dataset to form a test set, then construction of a model using the remaining objects in the dataset and application of resulting model to the objects in the test set. In this way each validation experiment involves testing the model with objects that are *not* used to build the model. Typically the cross-validation process involves more than one sub-validation experiments.

The success of any cross-validation process relies on unbiased selection of test sets objects. Therefore several different cross-validation methods are available depending on the size of the dataset, and these cross-validation methods differ in *how* the test set objects are selected. Each cross-validation method has two most important parameters, the splits and the iterations. The split is the total number of test sets that will be created and the iteration is how many times the sub-validation experiment is performed. The value of splits must be smaller than half of the total number of objects in the dataset, i.e. the number of test objects per sub-validation experiment = total number of object in data set/splits. For the UTI bacterial spectra dataset which consist of 150 spectra from the 12

strains, we employed random subsets with 27 splits and 21 iterations. These numbers are chosen such that there are at least 2 spectra from each of the twelve strains that participate in the cross-validation process.

Using barcoded spectra as input vectors improve sensitivity and specificity

Using the spectral second derivative-based barcodes (curvature up = 1; curvature down = 0) instead of the first or the raw spectra as input vectors for multivariate classification has been shown to result in improved sensitivity and specificity for bacterial strain identification.⁴³ In this study each individual UTI bacterial SERS spectra is converted into barcode, or an array of one and zero based on the sign of the second derivative at each wavenumber. The use of barcode effectively minimizes classification errors due to broad baseline contributions and intensity variability between individual spectra resulting from the SERS substrate and all sources of biological sample inhomogeneity.

Building PLS-DA predictive model with twelve UTI bacteria SERS spectra

The result of cross-validated PLS-DA classification is shown in Figure 2-8. The choice of 24 LV corresponds to a number after which additional LV *does not* improve classification quality, as evident from plotting the *cross-validated* root mean square error (RMSECV) against each LV as shown in Figure S-7-1. The corresponding confusion matrix is given in Table S-7-3 and the sensitivity and specificity for each bacterial strain is shown in Table S-7-4. The analytical sensitivity (true positive rate) and specificity (true negative rate), averaged over all 12 classes, is 95.8% and 99.3% respectively, for this classification model. The average classification error for the model is just 2.3%. This

result demonstrates the potential for SERS spectra bacterial strains grown in urine to serve as a rapid (less than one hour) diagnostic at clinical concentrations.

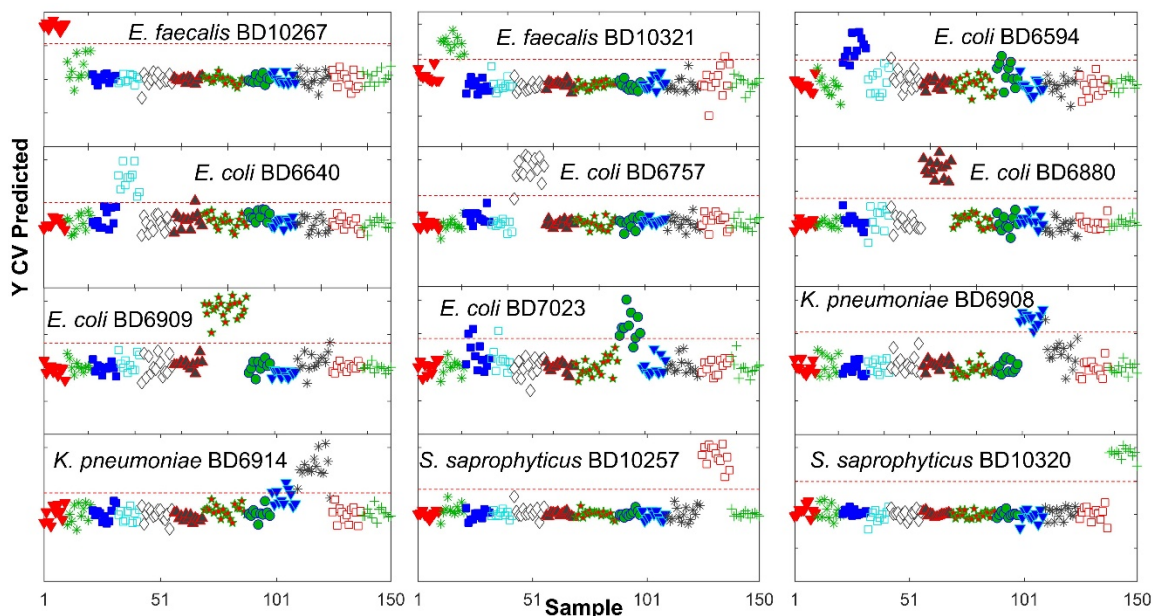


Figure 2-8 Result of a cross-validated PLS-DA classification of the SERS spectra of the twelve bacterial strains grown in and enriched from processed urine. The horizontal dashed line is the model threshold.

Application of constructed PLS-DA model for diagnostic test of unknown UTI strain in unprocessed urine

To test the robustness of the PLS-DA classification model using the SERS spectra of these twelve UTI bacteria strain grown in processed urine, a set of SERS bacteria spectra for one of the UTI clinical isolate, *E.coli* BD6594 grown and enriched in non-processed urine is supplied to the classification as unknown. As described previously the urine sample used for growing this bacteria strain was not subject to prior solid material removal via centrifugation. The bacteria grown in this urine is enriched with the four-

stage filtration/centrifugation system described in Figure 2-1. The resulting SERS spectrum is shown in Figure 2-9 and is compared to the SERS spectrum that result from spiking this strain into processed urine which had solid material removed by centrifugation prior to inoculation. Two spectrum are nearly identical.

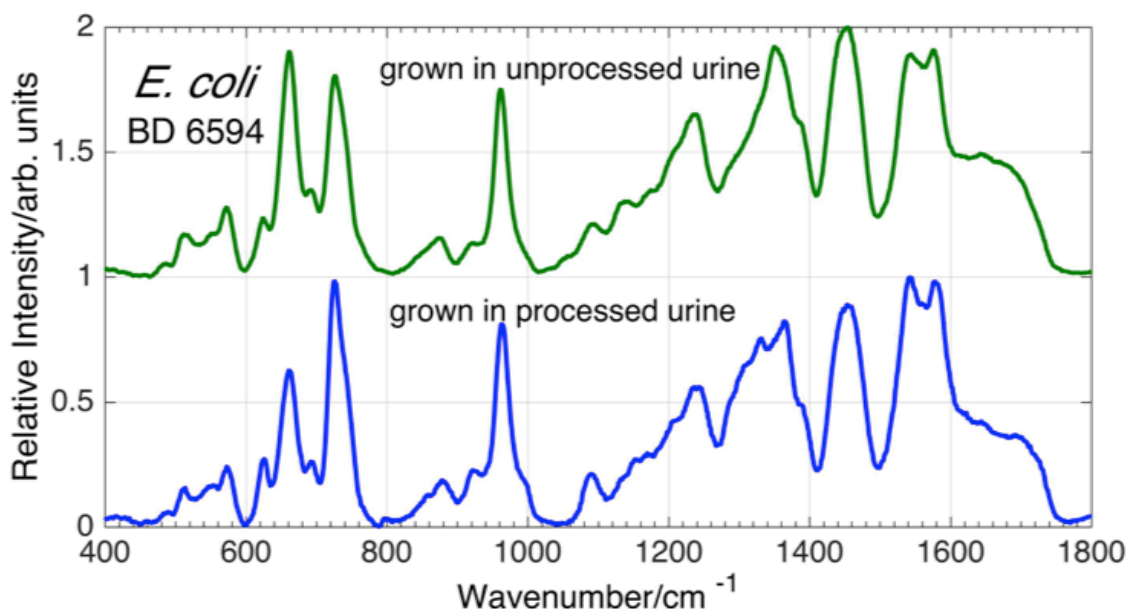


Figure 2-9 SERS spectra of different growths of *E. coli* BD6594 grown and enriched from unprocessed and processed urine.

However, when twenty SERS spectra of these bacteria grown in unprocessed urine were converted into barcode and inputted as unknowns into the PLS-DA classification model (Figure 2-8) developed with the spectra for the twelve strains of bacteria grown in processed urine, the classification correctly predict *E. coli* BD6594 as the most probable bacterial strain for all twenty spectra shown in Figure 2-10. The entire procedure from enriching bacteria grown in unprocessed urine to correctly classify is accomplished in ~ 50 minutes. Thus with this successful identification and with the previously determined drug susceptibility for this strain, our rapid spectroscopic diagnostic platform would

allow the physician to know which antibiotics would be effective for this patient's UTI condition within one hour. Such a result would have taken more than 48 hours via the gold standard, cell growth procedures.

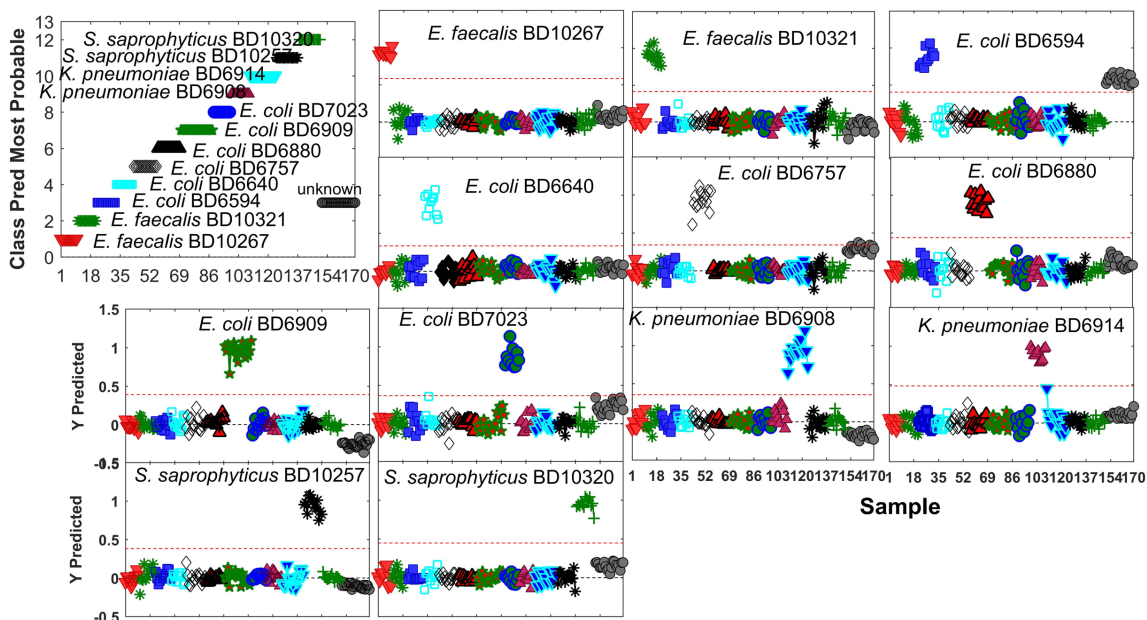


Figure 2-10 Using the PLS-DA model constructed with SERS spectra of twelve UTI bacterial strain grown in processed urine, a set of twenty spectra of an unknown bacterial strain grown in unprocessed urine is correctly identified as *E. coli* BD6594.

2.7 - Conclusion

The results shown in this chapter demonstrate the capability of the SERS platform to be a rapid (< 1 hour), growth-free technique for diagnosis of UTI, and when combined with an *a priori* developed library of antimicrobial susceptibility profile for each strain, our SERS platform can provide strain-specific identification at clinically relevant infection levels which is crucial for determining the best antibiotic treatment for the patient. UTI diagnosis with strain identification and antibiotic specificity at 10^5 cfu/mL

level can be achieved in less than an hour via the SERS platform accurately, characterized by >95% sensitivity and >99% specificity even in this relatively small library of 12 UTI clinical UTI bacterial isolates. The SERS spectra of these bacterial strains grown in urine are shown to be primarily due to purine components: adenine, hypoxanthine, xanthine, guanine, AMP, uric acid and guanosine. The species and strain specific SERS signatures are due to different amount of these purine components secreted by the bacterial cells to the surrounding extracellular region instead of cell wall components as reported in many literatures previously. The observation of purine metabolite as main molecule contributing to the SERS spectra in these UTI clinical isolates is consistent with our previous report regarding SERS spectrum from vegetative bacteria⁸⁸. The differences in relative contributions of these purine metabolites giving rise to the SERS strain specificity are resulted from the absence or presence of specific enzymes in the purine degradation pathway as previously reported.⁸⁸

While these proof-of-principle results shows promise for developing a low-cost, rapid optical approach for antibiotic-specific, strain-specific UTI diagnosis, several challenges needed to be addressed before clinical adoption. These challenges including development of a low cost or reusable device for bacterial cell enrichment and separation from other solid urine matters. The prototype filtration system needs to be rebuilt for each sample to avoid cross contamination. Also more bacterial strains with antibiotic susceptibility profile pre-determined are needed to be added to the SERS library to ensure sufficient range of potential UTI pathogens. In summary, the results discussed in this

chapter demonstrate the potential of a SERS based technology to be developed into a rapid, growth-free, low-cost UTI diagnostic with strain specificity.

2.8 - Extended study: Time evolution of UTI bacteria SERS signature

Figure 2-6 shows that purine metabolites secreted by the bacterial cells to the surrounding extracellular region are the molecular basis for the species and strain SERS specificity of the UTI causative bacteria. Therefore it would not be surprising that the relative contribution of different purine metabolites could have a post-washing time dependence, since the bacterial starvation response is a multicomponent dynamic process. For the SERS UTI diagnostic perspective it's also important to know how these changes of relative contribution affect the spectroscopic features that allows the distinction between different bacterial strains. In other words, the timing at when the SERS spectra are acquired will be important post sample washing if there are time-dependent spectral features change. On the other hand, these time-dependent spectral feature changes can serve as additional identification of the bacterial strain. All the previously discussed UTI clinical isolate spectra were acquired at the same post-washing time (20 min).

Figure 2-11 and Figure 2-12 show the SERS spectra as function of time post washing of two of the twelve UTI *E. coli* strains, *E. coli* BD6880 and *E. coli* BD7023. In both bacterial strains the SERS spectral features appear as early as 10 minutes post washing, but in both strains the contribution of guanine continue to increase as evident by the relative ratio between the $\sim 725\text{ cm}^{-1}$ and the $\sim 665\text{ cm}^{-1}$ band, corresponds to the unique peak of hypoxanthine and guanine respectively. As shown in the bar plot in

Figure 2-6, the main difference that allow distinction between these two strains is the difference in the relative contribution of guanine (0.07 and 0.21, respectively).

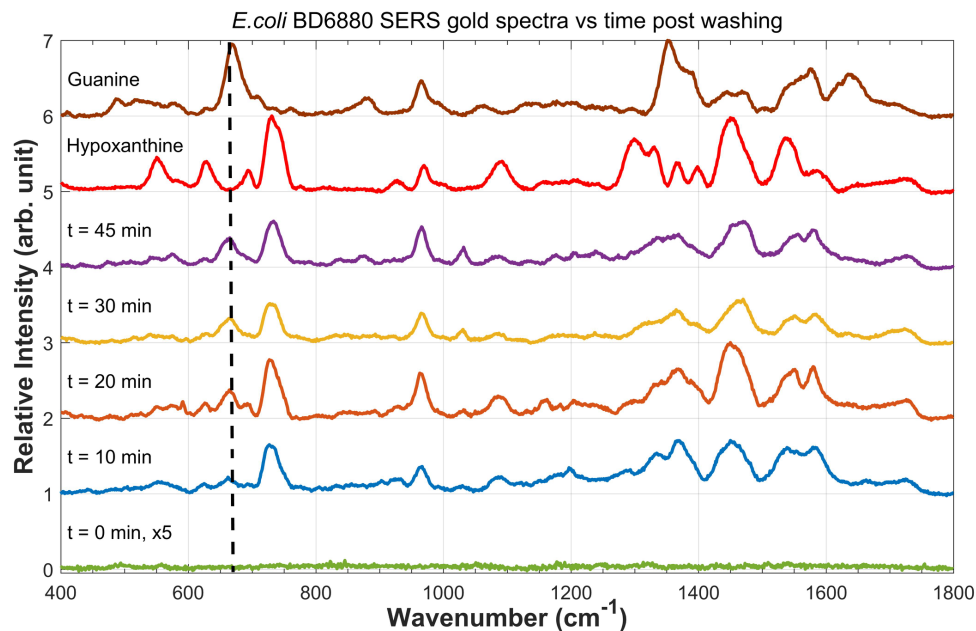


Figure 2-11 SERS spectra of *E. coli* BD6880 as a function of time post washing. The increasing contribution of guanine evident from the increasing intensity of the ~ 665 cm⁻¹ band is indicated by the vertical dash line.

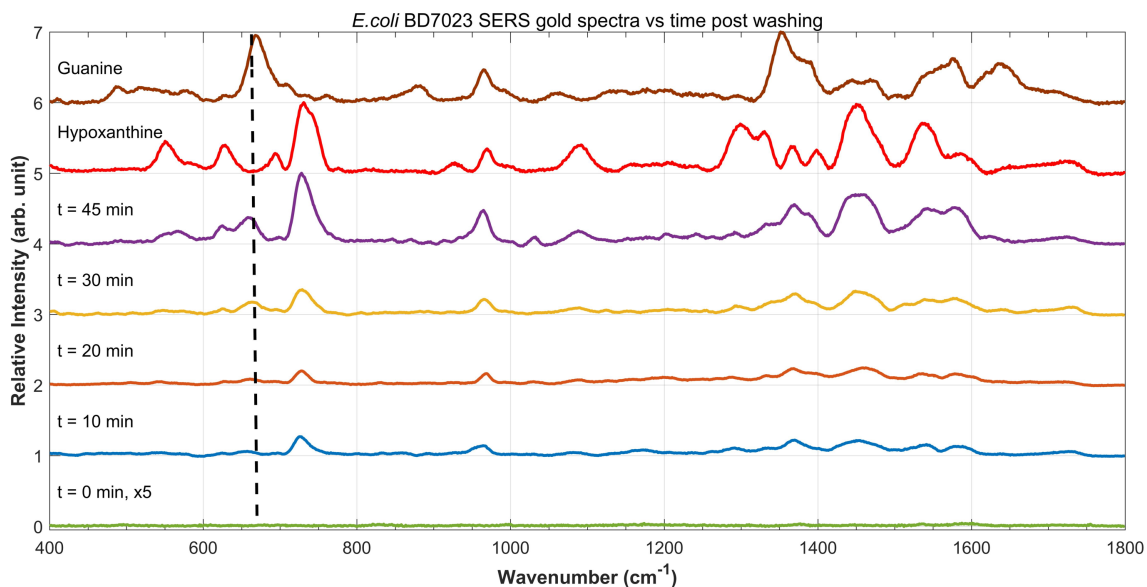


Figure 2-12 SERS spectra of *E. coli* BD67023 as a function of time post washing. The increasing contribution of guanine evident from the increasing intensity of the ~ 665 cm⁻¹ band is indicated by the vertical dash line.

3. SERS Diagnostic Platform: Sexually Transmitted Disease

3.1 - Chlamydia and Gonorrhea – the Silent Killer

Sexually transmitted diseases (STDs) continue to be a significant cause of morbidity in the US with ~ \$15.9 billion spent annually on healthcare costs related to their diagnosis and treatment.⁵⁴ Chlamydia, the most common sexually transmitted disease (STD) in the US, is caused by infection from the Gram-negative bacterium *C. trachomatis*.⁵⁵ More than 1.5 million cases of Chlamydia were reported to the Center for Disease Control and Prevention (CDC) in 2015, an increase of nearly 6% over 2014, with twice as many cases reported for woman than men. Recent CDC data also demonstrate an increase of reported Chlamydia infections in Europe, rising from 191,000 in 2004 to 385,000 in 2013.⁵⁶ About 1 in 15 sexually active young women in the US between the ages of 14 and 19 have already been infected once with chlamydia.⁵⁷ Although most patients with chlamydia are asymptomatic, and hence these numbers may underrepresent the prevalence in the population,⁵⁸ long-term, untreated chlamydia infection can lead to severe consequences such as pelvic inflammatory disease, a major cause of infertility, ectopic pregnancies and chronic pelvic pain in women.^{57,59} Chlamydia has been shown to increase the risk of HIV transmission and infection^{60,61} and perinatal transmission may result in conjunctivitis, pharyngitis and pneumonia in newborns.^{62, 63} In addition, *C. trachomatis* is the cause of trachoma, a major cause of preventable blindness in developing countries in Asia and Africa.^{64,65}

The *C. trachomatis* organism is an obligate intracellular Gram-negative bacterium requiring an epithelium host cell to complete its life cycle.⁶⁶ It lacks the enzymes for

many biosynthetic and metabolic pathways, including ATP production and degradation, and consequently, must rely on the infected host for many nutrients and energy.⁶⁷ This bacterium has a complex bi-phasic developmental cycle which involves a metabolically-active and noninfectious form called reticulated body (RB) and a metabolically-inactive but infectious form called an elementary body (EB). Following invasion of epithelial cells, the EBs are converted to RBs, the intracellular replicating form of this organism. Approximately 20 hours after infection and after multiple divisions by binary fission, the RB starts to differentiate into the EB developmental stage and 48-72 hours later the infectious EBs are released to initiate new rounds of infection.⁷⁰ Like other Gram-negative bacteria, the *C. trachomatis* cell membrane is comprised of an outer and an inner membrane separated by a peptidoglycan layer. However, uniquely to *C. trachomatis* is the presence of an unusually thin peptidoglycan layer that normally filled up the space between the outer and the inner membrane in other Gram-negative bacteria. Instead, a protein layer, termed major outer membrane protein (MOMP) is present in that space. MOMP is a highly disulfide cross-linked protein that provides additional structural reinforcement against osmotic pressure effects^{68,69,70} and also acts as an anchor for many “accessory” protein such as those for antigen recognition and entry to host cell.^{70,71,72,73}

Gonorrhea is the second most commonly reported STD in the US, with ~400,000 cases reported in 2015 and results from infection by the Gram-negative bacterium *N. gonorrhoeae*. After decades of decreasing reported rates had reached an all-time low in 2011, the prevalence of gonorrhea in the US has shown a steady increase in the last five years.⁵⁵ Patients with gonorrhea are often asymptomatic until complications arise such as

pelvic inflammatory disease, ectopic pregnancy and infertility. Untreated gonorrhea can also lead to disseminated gonococcal infection (DGI) when *N. gonorrhoeae* spreads to the blood or other parts of the body.^{74,75} In addition, as also found for *C. trachomatis*, gonococcal infections have been shown to facilitate the transmission of HIV infection.⁷⁶ The emergence and spread of multi-drug resistant *N. gonorrhoeae* strains is an increasingly recognized problem for effective treatment of gonorrhea.^{55,77} Furthermore, ~30% of patients infected with *N. gonorrhoeae* are co-infected with *C. trachomatis*.⁷⁸ Consequently, patients treated for gonococcal infection are often routinely treated with an antibiotic regimen that is effective against *C. trachomatis* infection as well.⁷⁹

3.2 – Current Chlamydia and Gonorrhea Diagnostic Methods

Direct detection of *C. trachomatis* and *N. gonorrhoeae* can be achieved by culture and non-culture methods. Cell culture method, long the reference standard for chlamydia and gonorrhea diagnosis, requires specialized culture medium and culture conditions, skilled staff for the technically-demanding procedures and is very slow (≥ 72 hours), making it virtually impossible for routine and point-of-care diagnostics.^{80,81} Similarly, *N. gonorrhoeae* is also a fastidious organism requiring enriched media in a CO₂ atmosphere for lab cultured growth for ≥ 48 hours. Alternatively, non-culture methods include enzyme immunoassay (EIA) which detects the chlamydial lipopolysaccharide or the major outer membrane protein (MOMP), and direct fluorescent antibody stain (DFA) are available and had largely replaced the cell culture method as standard diagnostic methods for chlamydia and for gonorrhea.^{81,82,83} Nucleic acid amplification tests (NAAT) are the

current best technology recommended by the CDC for the detection of chlamydia and gonorrhea.⁸¹ NAAT is a growth-free diagnostic offering sensitivity and specificity comparable to culturing with a faster turnaround time.⁸⁴ However, the susceptibility to cross-contamination from exogenous genetic material, cost, inability to distinguish bacterial viability (i.e. live vs. dead cells), the presence of inhibitory factors and the need for experienced technicians in laboratory settings, which necessitates a second clinical visit for some patients, are limitations for the NAAT approach.^{58,85,86} Given the asymptomatic nature of many chlamydia and gonorrhea infections, screening is recognized as the most effective approach for reducing the societal and personal impact of these diseases.^{81,84} Thus, the development of alternative, low-cost, easy-to-use, rapid, point-of-care approaches for the detection and simultaneously differentiate *C. trachomatis* and *N. gonorrhoeae* in clinical setting and in a useful timeframe (\leq one hour) for narrow spectrum antibiotic drug prescription remains a critical strategy for improving reproductive and sexual health worldwide.

Here, we report for the first time on the potential ability of SERS to provide rapid, growth-free, detection and identification of the Chlamydia and gonorrhea etiological agents, *C. trachomatis* (EBs) and *N. gonorrhoeae*. The SERS spectra of these bacterial cells are studied as a function of nanoparticle metal (Ag and Au), sample concentration and time from sample enrichment. The molecular and biochemical origins of the SERS vibrational signatures of these two Gram-negative microorganisms are found to be very different reflecting their significantly distinct bacterial lifestyles. These results will be compared and contrasted to our previous SERS studies, and in terms of our fundamental

understanding of the interaction of bacterial cells and metal nanoparticles. The prospects for the development of a SERS based platform for rapid (< one hour), low-cost STD diagnostic are promising given the data presented here.

3.3 – Materials and Methods

SERS active substrate All SERS spectra reported here were obtained using *in-situ* grown, aggregated Au or Ag nanoparticle covered SiO₂ substrates previously developed in our laboratory.³⁴ Details concerning the production and description of these SERS active chips, and the characterization of their performance for providing reproducible SERS spectra of bacteria have been described in previously.^{34,43,44,47,48,49,50,87,88,89} These nanostructured substrates result from a two-stage reduction of a metal ion doped sol-gel, producing small (2 – 15 particles) aggregates of monodispersed ~80 -100 nm Au or Ag nanoparticles covering the outer layer of ~1 mm² SiO₂ substrate. The SEM images of the aggregated Au or Ag nanoparticles on the SiO₂ substrate are shown in Figure 3-1 and Figure 2-2.

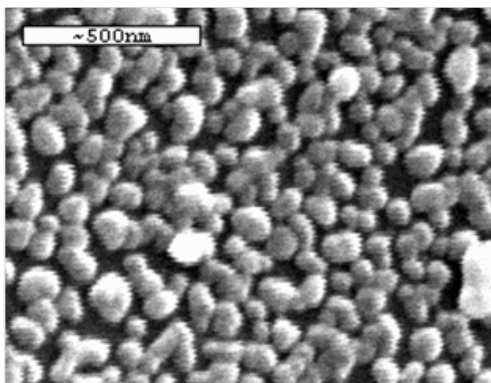


Figure 3-1 SEM image of the aggregated Ag nanoparticles-covered SiO₂ substrate.

In vitro* cultivation of *C. trachomatis *C. trachomatis* D/UW-3/CX (VR-885) was obtained from American Type Culture Collection (ATCC®, Manassas, VA). The McCoy cell line, CRL-1696, (ATCC®) was used as the host cell. McCoy cells are grown in minimal essential medium (MEM) containing 10% fetal bovine serum (ATCC®) in a humidified incubator at 37 °C and 5% CO₂ until 90%-100% confluent. After the McCoy cells are infected a special maintenance medium is prepared with the following ingredients: 90 mL DMEM (Life Technologies®), 10 mL fetal bovine serum (ATCC®) and 1 µg/mL cycloheximide (Sigma®). Addition of cycloheximide inhibits the growth the host cell and allows nutrients to be directed to the proliferating *C. trachomatis* cells. The procedure for *C. trachomatis in vitro* cultivation and harvest is described in Appendix 8.4. The harvest *C. trachomatis* are aliquoted and stored in Hank Balanced Salt Solution (HBSS) at -80 °C.

Processing *C. trachomatis* cells for SERS spectral acquisition To prepare *C. trachomatis* for SERS spectra acquisition, an aliquot (100 µL) is removed from -80 °C sample supply and quickly thawed at room temperature (< 30 seconds). The sample is then centrifuged at x23,000g (Eppendorf®) for 4 minutes at 4 °C and the HBSS supernatant is removed after centrifugation. The pellet at the bottom, which mainly consists of *C. trachomatis* EBs and a small amount of RBs, is washed four times with 10 µL ice-cold deionized water each time. Between washes the sample is centrifuged at x 23,000g (Eppendorf ®) for 4 minutes at 4°C. The chlamydial EB has a layer of disulfide-bonded protein at its membrane as compare to other Gram negative bacteria,^{68,69} while the RB has fragile cell membrane and will not be able to withstand the osmotic pressure

from pure water. Therefore the RB will be lysed and removed during the washing process, leaving only EBs behind. After the last wash, the pellet is dispersed in 5 μ L ice-cold deionized water by pipetting and vortexing. For acquisition of SERS spectra, 1 μ L sample is added to the SERS active substrate and air-dried for 5-10 minutes.

Processing *N. gonorrhoeae* cells for SERS spectral acquisition *N. gonorrhoeae* (FA1090) is obtained from ATCC[®]. The agar medium is chocolate II agar plate with IsoVitaleX[®] enrichment and is commercially available (BD[®]). The cultivation and harvest procedure for this bacterial strain is described in Appendix 8.3. To prepare the bacterial cells for SERS spectra acquisition, the harvested bacteria are placed in a 2 mL micro-centrifuge tube containing 0.5 mL ice-cold deionized water immediately after being stripped off from the plate. The bacteria are washed four times with 0.5 mL ice-cold water and centrifuged at x4500g at 4 °C between each wash. After last wash the bacteria pellet is dispersed in about 50 μ L ice-cold water by vortexing. The amount of bacteria in this 50 μ L sample is determined to be $\sim 10^7$ ifu/mL by serial dilution and overnight culture. 1 μ L sample is added to the SERS active substrate and air-dried for \sim 5 minutes before spectral acquisition.

SERS spectral acquisition and data processing All SERS spectra reported here were acquired with an RM-2000 Renishaw Raman microscope employing a 50x (infinity-corrected, 0.75 numerical aperture) objective and 785 nm excitation. Incident laser powers of \sim 3.3 mw and \sim 10 seconds of illumination time were used to obtain the reported bacterial SERS spectra. Typically ten spectra per sample were obtained for each experimentally reported spectrum. Spectral acquisition took less than 10 min. The

illuminated Raman excitation field of view was $\sim 30 \mu\text{m} \times 6 \mu\text{m}$. The 520 cm^{-1} band of a silicon wafer was used for frequency calibration. Peak frequency precision is $\pm 0.5 \text{ cm}^{-1}$. The acquired spectra are averaged and baseline corrected with GRAMS® (Thermo®). The SERS spectra are normalized and plotted via MATLAB® and the spectra are vertically offset for clarity.

3.4 – Results and Discussion

Differentiation of *C. trachomatis* and *N. gonorrhoeae* by vibrational signatures on gold and silver SERS active substrates

SERS spectra of *C. trachomatis* and *N. gonorrhoeae* on the gold and silver nanoparticle covered SiO_2 SERS substrates excited at 785 nm are shown in Figure 3-2.

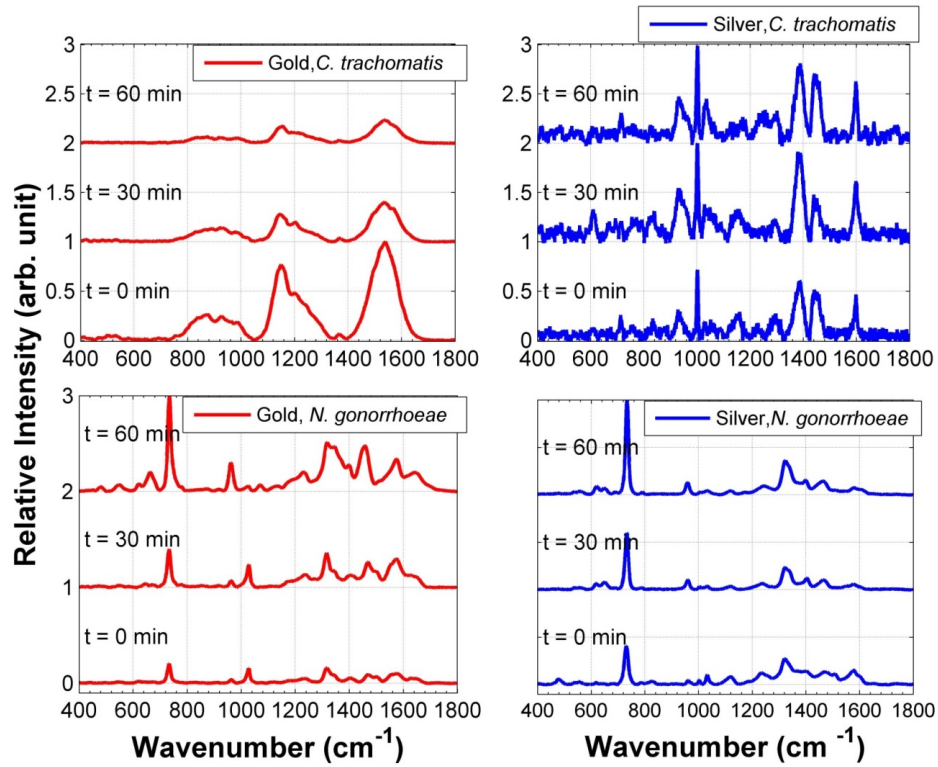


Figure 3-2 Compare *C. trachomatis* (top) and *N. gonorrhoeae* (bottom) SERS spectra on the gold and the silver substrate.

Three important points are illustrated in this figure. Firstly, *N. gonorrhoeae* and *C. trachomatis* can be clearly distinguished from each other through their spectral features on the gold and silver SERS active substrates right after sample washing ($t = 0$ min). This means these two bacteria can be distinguished as soon as a washed sample is placed on the substrate and a SERS spectrum is acquired on either the gold or the silver substrate. Secondly, this figure shows that the SERS spectra of the same bacteria can be quite different on different metal substrates. For example, the SERS gold spectrum of *C. trachomatis* is dramatically different from its SERS silver spectrum, and the overall intensity and S/N ratio for the silver spectrum is much weaker than the gold spectrum. On the gold spectrum three broad vibrational features center around $\sim 1550\text{ cm}^{-1}$, $\sim 1200\text{ cm}^{-1}$ and $\sim 900\text{ cm}^{-1}$ are observed. These three broad features are not observed on the silver spectrum; instead discreet, narrower vibrational bands are seen. On the other hand, the SERS gold and silver spectrum of *N. gonorrhoeae* is relatively similar. The overall signal intensity for the gold and for the silver spectra are also similar. Thirdly, *N. gonorrhoeae* and *C. trachomatis* display different time-dependent signal intensity and spectral feature changes on both metal substrates, which can be used as additional revenue to distinguish these two bacteria. On the gold substrate *C. trachomatis* shows a decrease of overall signal intensity by 80% over the course of one hour while on the silver the signal intensity remains relatively constant. On the other hand, prominent spectral feature changes can be seen on both the gold and the silver spectra for *N. gonorrhoeae*, example by the disappearance of the $\sim 1030\text{ cm}^{-1}$ band at $t = 60$ min spectra and the blue shift from 733 cm^{-1} to 736 cm^{-1} . These time-dependent signal intensity and spectral features

changes will be discussed below. Figure 3-2 powerfully demonstrates the prospect of the SERS methodology as a label-free, growth-free, rapid diagnostic method with potential in-clinic use when combining a portable instrument and an effective bacterial cell isolation and enrichment procedure from patient samples. Consequently, a physician can arrive to a diagnostic decision in ~40 min, with most of this time is spent on sample preparation in the current prototype procedure. In contrast the current non-culture genotype-based techniques required ~2-4 hours sample preparation time in laboratory setting before obtaining results.^{55,56,57,58} Moreover, the physician will also be able to distinguish a chlamydia infection from a gonorrhea infection through comparison of the SERS gold and silver spectral features from one isolated bacterial cell sample. This is valuable because up to 40% patients infected with chlamydia are also infected with gonorrhea, and the current diagnostic methods require the test for gonorrhea to be performed before test for chlamydia to avoid cross-contamination and false negative.^{55,58}

The sensitivities for *C. trachomatis* and *N. gonorrhoeae* on the gold and silver substrates are shown in Figure S-7-2 and Figure S-7-3, respectively. Serial dilution on washed bacteria sample was performed to determine the sensitivity. Quantitation of bacterial cells in undiluted sample was determined through serial dilution and overnight cell culture growth and colony counting. For *C. trachomatis* the lowest concentration of EBs to yield a SERS signal on the gold and silver substrates was determined to be ~ 5×10^4 ifu/mL and ~ 10^2 ifu/mL, respectively. For comparison, the chlamydial loads determined by genotype-based techniques in first-void urine specimens in infected patient range from ~ 10^1 to 10^5 EB/mL, and ~ 10^4 EB/mL for vulvo-vaginal swabs as reported in

clinical studies.^{90,91} Therefore the sensitivity of our SERS substrates for the chlamydial EB falls within the range of typical EB concentration found in patient samples. For *N. gonorrhoeae* the lowest concentration to yield a SERS signal on the gold and silver substrate is $\sim 10^6$ cfu/mL. For comparison, *N. gonorrhoeae* loads found in urine in infected patient range from $\sim 10^4$ - 10^6 in these studies.^{92,93} Thus, our SERS sensitivity for *N. gonorrhoeae* is at the upper limit of the clinical concentration. However $\sim 10^6$ is the concentration of enriched bacteria, and with effective enrichment procedure such concentrations can be achieved as demonstrated above for the UTI samples.

In summary, we have demonstrated the advantages of ease-to-use, multiplexing-capability, specificity and sensitivity with our SERS methodology for potentially point-of-care diagnostic of *C. trachomatis* and *N. gonorrhoea*, the causative agent for the two most common sexually transmitted diseases worldwide. The ability to distinguish these two bacteria using differences in the vibrational features on gold and silver SERS substrates is shown. In the next section we will discuss the molecular origins of these vibrational features as well as the observed spectral feature changes. Understanding molecular mechanism behind these is crucial not only to explain the SERS observations, but also to demonstrate the potential of SERS to be a powerful bioanalytical probe for understanding dynamic biological activity of these bacteria at the molecular level.

The identities of the molecules contributing to the SERS spectra

The location (i.e. extracellular vs. intracellular) of the molecules contributing to the SERS spectrum provides information on the identity of possible molecular candidates

that are responsible for the observed SERS signal. To understand where these SERS molecular contributors are for the *N. gonorrhoeae* SERS spectrum, we compared the SRES spectrum on the gold and the silver substrate acquired from the cells and from the supernatant surrounding the cells. The sample are centrifuged at $t = 0$ min (immediately after washing), 30 min and 60 min post-washing and a portion of the supernatant is removed from the bacterial cells. The supernatant SERS spectra are compared to the cell spectra acquired at the same time point.

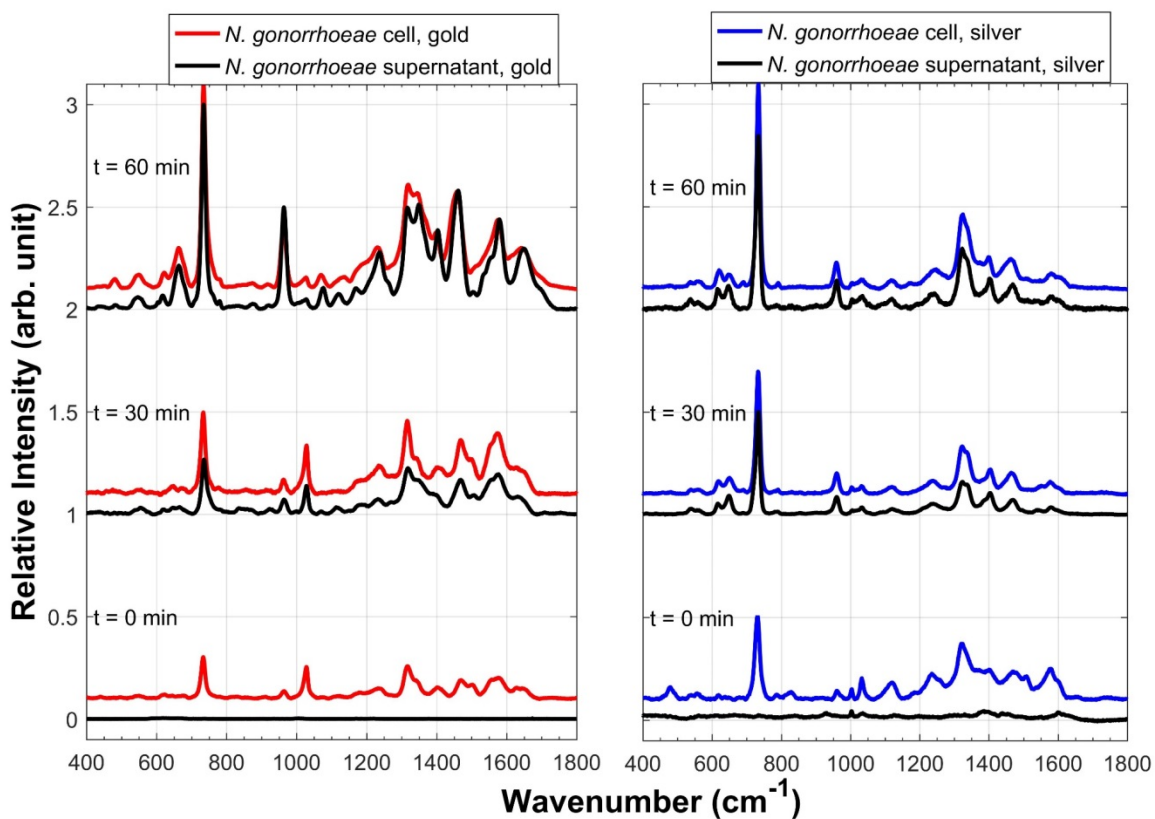


Figure 3-3 Gold and silver SERS spectra comparing the signal from *N. gonorrhoeae* cell and from the unfiltered supernatant fluid around the cell as a function of time post sample processing.

As shown in Figure 3-3, initially ($t = 0$ min) the molecules contributing to the *N. gonorrhoeae* spectra are located on the bacterial cell. At $t = 30$ min spectral features start

to appear in the SERS spectra of the supernatant. This implies that molecules are beginning to be secreted into the supernatant and providing the SERS spectrum of *N. gonorrhoeae*. At $t = 60$ min molecules contributing to the SERS spectrum are located on both in the supernatant and on the cell spectra, but the change of the spectral features, notably the disappearance of the $\sim 1030\text{ cm}^{-1}$ band and the blue-shift 733 cm^{-1} to 735 cm^{-1} , indicates that a different set of molecules are dominating the SERS spectrum at $t = 60$ minutes, as compare to $t = 30$ minutes. The observation that SERS spectra are dominated by molecules secreted by bacterial cells has been previously reported by the Ziegler lab,^{34,47,48,49,50,87,88,89} Bacterial SERS spectra have been attributed to seven purine metabolites secreted by the bacteria to the surrounding as a response to the stress or starvation conditions. Best-fitting the observed bacterial spectra to a linear combination of these purine molecular component spectra^{44,88,89} is used to determine the relative contribution of these seven purine metabolites in each bacterial spectra. In this STD study we use the same best-fit calculation method to decipher the identity and relative contribution of the key SERS molecular contributor for each time point and for the gold and the silver SERS spectrum, as shown in Figure 3-4. Two purine metabolites, adenine and guanine, and a third molecule, nicotinamide adenine dinucleotide (NAD), are identified from the *N. gonorrhoeae* spectra. Their relative contribution at each time point and on the gold and the silver substrate are demonstrated graphically in Figure 3-4 as well as numerically in Table 3-1. The normalized SERS spectra of adenine, guanine and NAD used for the calculation are shown in Figure S-7-7. We note that there's no distinction between the oxidized NAD form and the reduced NADH form, therefore we

denoted this component as NAD/NADH in the figure. The disappearances of the ~ 1030 cm^{-1} band as well the blue-shifts of the 733 cm^{-1} is attributed to the change of relative contribution of NAD/NADH after 60 minutes post washing. *N. gonorrhoeae* is the first bacterial species that we have encountered that shows NAD/NADH vibrational features in addition to purine metabolites. It is also the first species we reported to display a time-dependent change of spectral features due to change of relative contribution of the key SERS molecular contributors. Our next discussion will focus on why NAD/NADH appears at the earliest times but seemingly disappears from the SERS spectrum at later times and the possible molecular origin of this molecule.

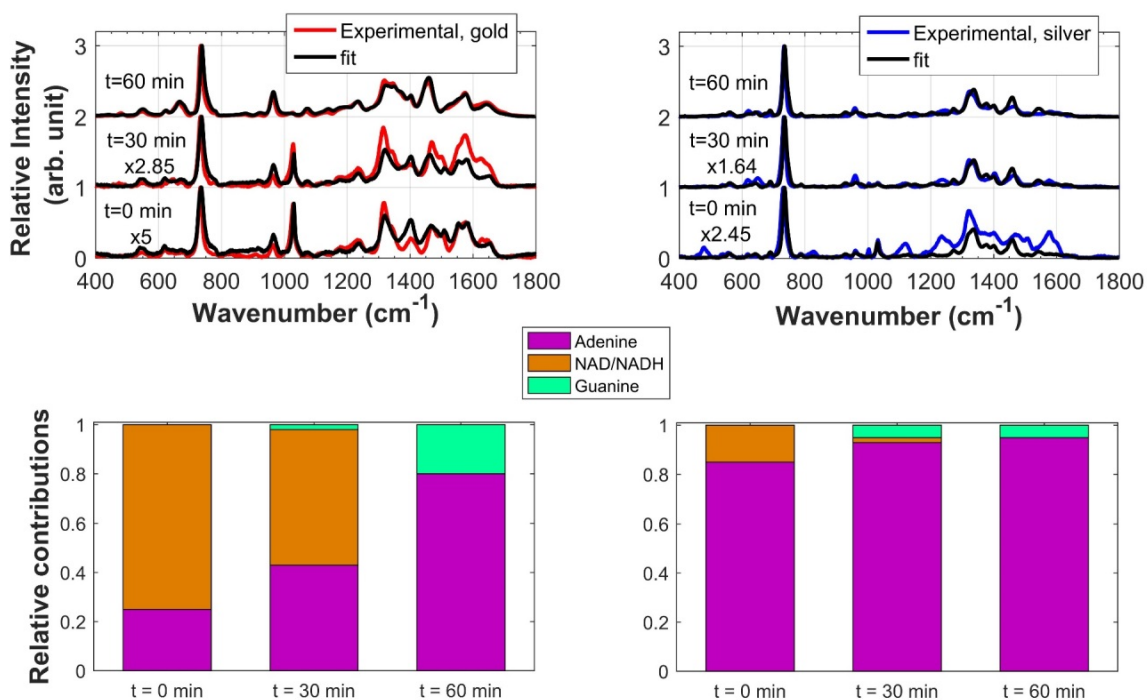


Figure 3-4 The gold and silver SERS spectra of *N. gonorrhoeae* as a function of time post washing are shown with their best-fit calculated by a linear combination of three purine components: adenine, nicotinamide adenine dinucleotide (NAD/NADH) and guanine.

	time (min)	adenine	guanine	NAD/NADH
On gold	0	0.25	0	0.75
	30	0.43	0.02	0.55
	60	0.8	0.2	0
On silver	0	0.85	0	0.15
	30	0.93	0.05	0.02
	60	0.95	0.05	0

Table 3-1 Contribution of purine metabolite to gold and silver *N. gonorrhoeae* spectra at each time point determined by linear combination of the normalized component spectra.

To understand the disappearance of NAD/NADH at the later time point ($t = 60$ min), a *N. gonorrhoeae* sample which had been left at room temperature for 60 minute following an initial wash with ice-cold water was washed with ice-cold water again and a SERS spectrum of the bacteria cells was obtained, as shown in Figure 3-5 (left). We see the re-appearance of NAD/NADH spectrum and the spectral features are nearly identical to the *N. gonorrhoeae* on gold spectrum at $t = 0$ min. This observation shows that NAD/NADH molecules are bound to the bacterial cell membrane and therefore should be seen in spectra of *N. gonorrhoeae* at all the time points. The NAD/NADH features seem to disappear from the $t = 60$ min because their features are masked by the more intense adenine and guanine SERS bands. Adenine and guanine are excreted to the surrounding supernatant as response to the low nutrient condition, therefore when the bacteria cell are dried onto the SERS substrate these molecules are close to the surface of the gold nanoparticles than NAD/NADH, which are bound to the cell membrane. In addition, both adenine and guanine have greater Raman cross-sections on the gold and silver SERS

substrates than NAD/NADH as shown in Figure S-7-8. Therefore the spectral features from NAD/NADH are not evident when the SERS spectrum is dominated by adenine and guanine at $t = 60$ min. When adenine and guanine are washed away at $t = 60$ min, the NAD/NADH features reappear. This re-washing experiment also ensures that the NAD/NADH observed in the *N. gonorrhoeae* spectra are from these molecules bound to the cell membrane instead of being due to remaining material from the growth plate since the IsoVitaleX® supplement to the agar plate contains NAD. The appearance of NAD/NADH is unique to *N. gonorrhoeae*, at least in this limited comparison between Gram-positive *S. aureus* Newman and three Gram-negative *E. coli* clinical isolates⁸⁹ shown in Figure 3-5 (right). All the bacteria strains are grown on chocolate agar plates with IsoVitaleX® (BD) supplement. This shows the presence of NAD/NADH is a unique property of *N. gonorrhoeae* cell membranes.

NAD/NADH is a co-substrate for many membrane-bound enzymes that are critical for the growth of *N. gonorrhoeae* in the human body. Examples are NADH dehydrogenase (EC 1.6.99.3) and NAD(P)H oxidase (EC 1.6.99.1), which are enzymes that defend the bacteria against reactive oxygen species (O_2^-) in the mucosal surface environment and from the host local inflammatory response.^{94,95} The observed bounded NAD/NADH are the co-substrates for these enzymes. In addition, it's also known that *in vitro* growth of *N. gonorrhoeae* requires two essential growth factors in addition to standard bacterial growth medium: lysed red blood cells and NAD. The lysed red blood cells serve as the primary source of iron which is an essential metal for many enzymes. However, the oxidation state of iron is Fe^{3+} (hence the “chocolate” color of the agar plate)

which can form insoluble $\text{Fe}(\text{OH})_3$ under physiological condition. Therefore Fe^{3+} ion must be converted into Fe^{2+} which is soluble under physiological condition, and NAD/NADH can serve as the electron donor Fe^{3+} ion.^{96,97} Thus the observed NAD/NADH signal could be the co-substrate for the enzyme that catalyzed the reduction of Fe^{3+} . In the absence of an iron source some of the NAD/NADH may be released from the enzyme therefore explaining the presence of NAD/NADH features in the supernatant at $t = 30$ min. In summary, Figure 3-4 demonstrates the potential of our SERS methodology not only as a disease diagnostic platform but also a powerful bioanalytical tool for studying enzymatic processes at the outer cell membrane region of bacterial cells when the bacteria are placed in a low-nutrient environment.

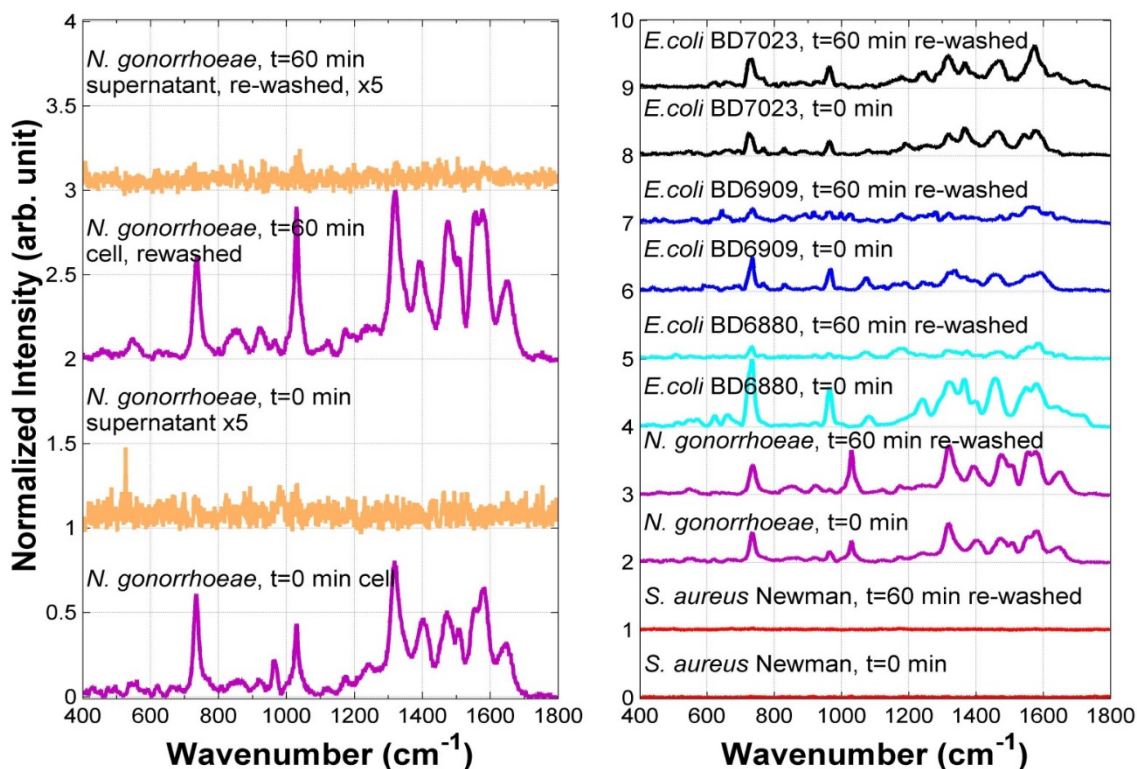


Figure 3-5 (Left) Comparing the gold SERS spectra from *N. gonorrhoeae* from the cell and from the supernatant at $t = 0$ min (initial wash) and after re-washing at $t = 60$ min further show that the NAD/NADH molecules are bound to the bacteria cell membrane.

(Right) Comparing gold SERS spectra at $t = 0$ min from the cell of *S. aureus* Newman (Gram-positive), *N. gonorrhoeae* (Gram-negative) and three *E. coli* (Gram-negative) strains grown on chocolate agar plat with IsoVitaleX® show that the appearance of NAD/NADH features is unique to *N. gonorrhoeae* only. All bacteria cells are re-washed with ice-cold water after left at room temperature 60 minutes and the NAD/NADH features re-appear only on *N. gonorrhoeae*.

On the other hand, comparing the SERS spectra from *C. trachomatis* cells with the spectra from the supernatant as shown in Figure 3-6 reveals that the molecules contributing to the SERS spectra are located on the cell but not in the supernatant. Furthermore, monitoring the supernatant spectra as a function of time post-washing shows that these SERS contributors are always on the cell immediately after washing up to an hour post washing on both metal SERS substrates as shown in Figure S-7-4. This means the molecules contributing to the *C. trachomatis* spectra are securely anchored onto the cell membrane. This observation is thus consistent with the origin of these

molecules to be the bacterial cell membrane component or the ‘accessory’ molecules connected to the cell membrane.

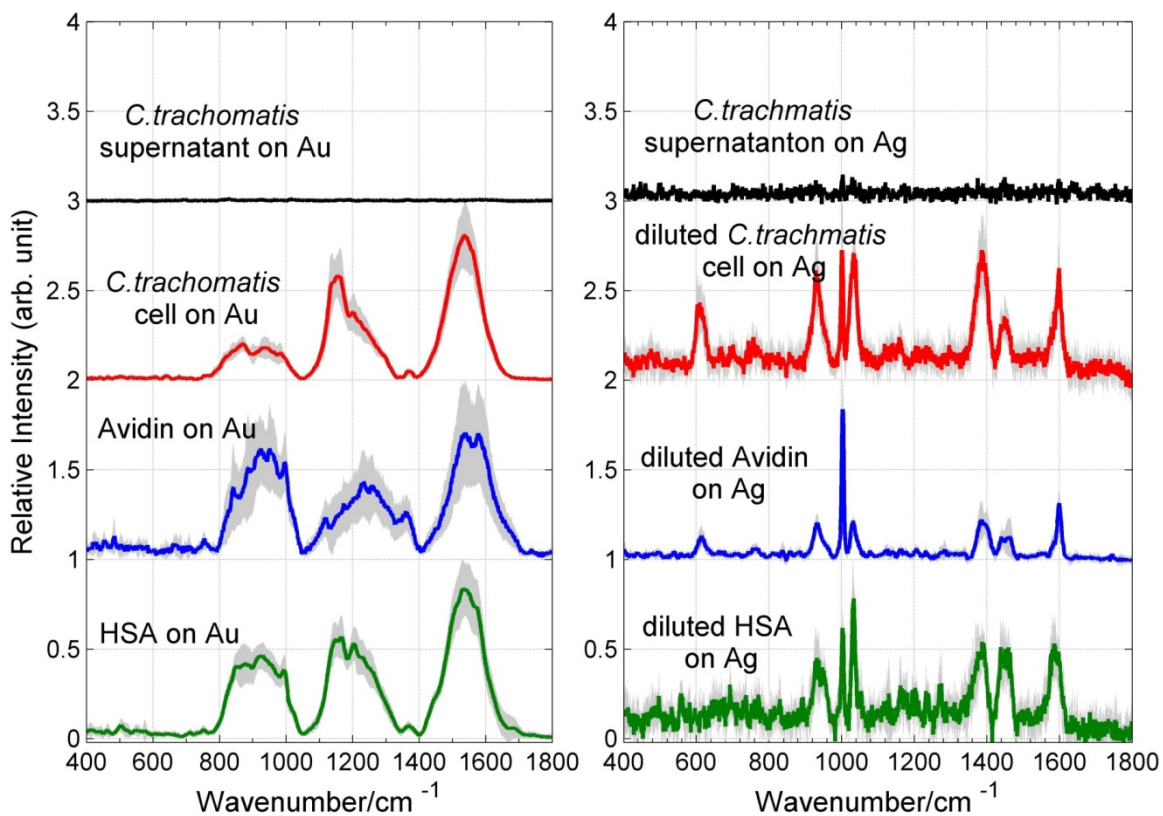


Figure 3-6 Comparing the SERS gold and silver spectra from *C. trachomatis* cell with the spectra from the supernatant reveal that the molecule contributing the spectra locates only on the cells. Compare with spectra from HSA and avidin show that protein molecules on the cell membrane are the major contributor to the SERS spectra of *C. trachomatis*.

In order to determine the molecular origins of these *C. trachomatis* signal we first consider the structure of *C. trachomatis* cell membrane. As mentioned previously, unique to *C. trachomatis* is the presence of MOMP that fill up the space in between the outer and the inner cell membrane in addition to an unusually thin peptidoglycan layer. MOMP is a highly disulfide cross-linked protein that serves as an anchor for many “accessory” proteins such as those for antigen recognition and entry to host cell.^{71,72,73} Thus, we hypothesize that the main contributors to our *C. trachomatis* SERS spectra are protein

molecules on the *C. trachomatis* cell membrane. Because it's very difficult and costly to isolate each of the protein components of the *C. trachomatis* membrane to acquire SERS spectra at this preliminary stage, we use commercially available protein molecules as models instead. Human serum albumin (HSA) and avidin from chicken egg white (avidin) are selected as protein model compounds. HSA, a three-domain protein consist of mostly alpha helices, is selected because HSA is a model protein molecule used in studying metal-protein interactions in literature.^{133,134,135} Avidin is chosen because it has similar size (i.e. molecular weight) as HSA but is consists of mainly beta-sheets. Both proteins are available commercially as lyophilized powder. Solutions of both proteins are freshly prepared in deionized water prior to each SERS experiment. For the gold substrate the protein solution concentration is 100 μM . However, we found that on the silver substrate lower protein concentration (1 μM or less) yields greater SERS intensities and larger S/N ratios. Therefore for the silver substrate the protein solution concentration is 10 nM. Comparison of the SERS spectra of the two proteins and *C. trachomatis* cell spectra are shown in Figure 3-6. We can clearly see the similarity between the *C. trachomatis* cell and the two protein SERS spectra, indicating that the main SERS molecular contributors of *C. trachomatis* spectra are protein molecules on both nanostructure metals. However, *C. trachomatis* can still be distinguished from the two proteins on both metals. For example, the difference in relative peak intensity ratio between the three broad features on the gold spectra, as well as the presence/absence and the peak intensity of the $\sim 610\text{ cm}^{-1}$ band on the silver substrate can be used to distinguish these samples.

The three vibrational features (center around $\sim 900\text{ cm}^{-1}$, $\sim 1200\text{ cm}^{-1}$ and $\sim 1550\text{ cm}^{-1}$) on the gold spectra for *C. trachomatis* and the proteins are very broad ($\sim 150\text{ cm}^{-1}$), suggesting that these features are due highly inhomogeneous molecular systems as might be expected for protein aggregates. To investigate this hypothesis we acquired dynamic light scattering spectra of the same HSA solution that show these broad SERS features, and the results (see Chapter 4) had lead us to conclude that these broad features are in fact due to protein aggregates created during the solution preparation process. More specifically, these protein aggregates are formed when their tertiary structure is perturbed due to the mechanical stress occurring when the protein solution is repetitively and vigorously pipetted.^{98,99,100,101} For *C. trachomatis*, this is happens when the centrifuged bacterial cells are re-suspended in water after each centrifugation step during the washing process. The re-suspension is achieved by pipetting to disperse the cell pellet which causes aggregation of the protein molecules on the outer layer of the cell membrane. This can also explain the decrease of overall signal intensity on *C. trachomatis* as a function of time post washing. Following the last washing step, the tertiary structures of the proteins at the outer layer are perturbed by pipetting and aggregations are formed. However, when the sample is left undisturbed over time these protein molecules may re-arrange themselves back to their native tertiary structure, therefore the aggregated protein signal (i.e. the three broad features on gold spectrum) intensity decreases as a function of time. On the other hand, on the silver substrate, these broad aggregated protein vibrational features are not observed. Instead, discreet, more typically shaped vibrational features can be seen. The assignments for these bands on the silver substrate are listed in Table 3-2.

These features can be attributed to individual amino acids and molecular moieties, for example phenylalanine, tryptophan, the C-S stretch and CO₂⁻ and CH₂ bending vibrational modes. We attribute this metal dependence of the protein signal to the more strongly perturbative nature of silver nanoparticles interacting with proteins.

Band frequency on <i>Ct</i> silver SERS spectrum	Band assignment ^{102, 103, 104, 105, 106, 107, 108, 109, 110, 111*}
610	v(CS) P _H -T
936	v(C-COO ⁻)
1004	Phe (v ₁₂)
1035	In-plane C-H deformation of mono-substituted benzene ring**
1385	v(COO ⁻)
1450	δ(CH ₂)
1600	Trp ^{w1} , Tyr, and/or Phe (v _{8a})

Table 3-2 Band Assignment for Silver *C. trachomatis* SERS spectrum.
* References of the band assignments

From the results shown in Figure 3-4 and Figure 3-6 we can how the SERS results reflect the different “lifestyles” of these two STD causing bacteria. All bacterial strains studied in the Ziegler lab previously^{34,43,44,47,48,49,50,87,88,89} had shown purine metabolites as main contributors to their SERS spectra. We generalized that bacteria release purine metabolites as a rapid response to low nutrient conditions, and their purine metabolism KEGG pathway for purine degradation can be used as guideline to predict what purine molecule will be produced.⁸⁸ For example, the KEGG pathway for purine metabolism of *N. gonorrhoeae* is shown in Figure 3-7, and from the pathway we can see the bacteria can produce adenine and guanine when nucleotides are degraded. This matches our SERS observation in Figure 3-4 which is just a linear combination of these two purine free bases and NAD/NADH. However, *C. trachomatis* is an exception to all previously observed SERS spectra. It shows membrane protein components instead of purine

metabolites as main contributor to the SERS spectra. *C. trachomatis* is an obligate intracellular pathogen which solely depends on the host cell for nutrient and energy supply,^{112,113} and its KEGG purine degradation pathway reflects its parasitic lifestyle. As shown in Figure 3-7 *C. trachomatis* lacks all enzymes for the appearance of AMP, GMP and IMP, the key molecules to the purine degradation pathway. Furthermore, this species lacks the necessary enzymes for the degradation of these nucleotides to the free purine bases. This means *C. trachomatis* are unable to produce the purine metabolites through its KEGG degradation pathway, therefore no purine metabolites are observed from its SERS spectra.

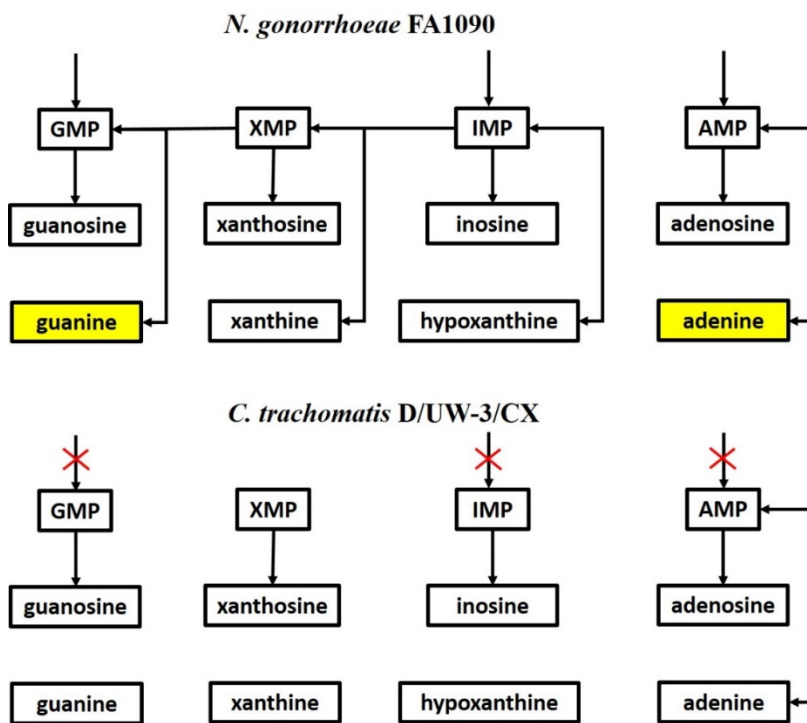


Figure 3-7 Comparing the KEGG purine degradation pathway for *C. trachomatis* and *N. gonorrhoeae*.

3.5 - Conclusion and Future work

As a proof of concept for the development of SERS as a rapid STD diagnostic, the results discussed in this chapter demonstrate the potential of our SERS-based platform for label-free, growth-free, whole-cell diagnostic tool for rapid detection and differentiation of *C. trachomatis* and *N. gonorrhoeae*, which are responsible for the two most common underdiagnosed STDs that affect millions people and result in billions dollar healthcare cost annually. By compare and contrast the unique SERS vibrational signatures on our gold and silver substrates, we were able to distinguish these two bacteria based on their vibrational features. When combine with a portable instrument and an effective bacterial cell enrichment procedure, potentially the physician can obtain the rest in the clinical setting in ~40 min. We are able to decipher the main SERS molecular contributors to the observed SERS spectra and demonstrate the ability of our SERS-based platform as a novel analytical probe for studying metabolic activity near extracellular region. Our SERS-based platform can provide a rapid, ease-to-use, specific diagnostic methodology without the need of slow and technically-demanding cell growth or sample labeling.

The details regarding the protein aggregation that was first observed in the *C. trachomatis* spectra are discussed in Chapter 4. The possible molecular origin of the broad spectral features on the gold substrate that seem ubiquitous across multiple protein samples will also be discussed in the subsequent chapter. Future work on this project will be directed toward expanding our SERS reference library with more STD related bacterial strains to test this methodology for strain specificity. Another important aspect

will be to work on an effective enrichment procedure to isolate bacterial cells from patient samples at clinically relevant concentrations.

4. The SERS Vibrational Signature of Proteins

4.1 - Introduction to SERS study of proteins

Protein stability in aqueous solution is an increasingly important issue particularly in the pharmaceutical field as the number of therapeutic protein drugs has development increased dramatically over the past two decades.¹¹⁴ Protein drugs provide critical treatments in numerous health conditions and diseases (e.g. diabetes, cancer, cardiovascular disease, autoimmune disease). However if the protein drug molecule is not stable in aqueous solution and forms aggregates, its biological activity and thus its therapeutic value diminishes.¹¹⁵ Moreover, accumulation of these aggregated proteins in body tissues can cause damage to the human body. Therefore it's important to monitor the state of protein structure in aqueous solution for both treatment efficacy and human health concerns.

Vibrational spectroscopies such as IR and Raman spectroscopy are valuable tools for analysis of protein structure. Since the vibrational frequencies depend molecular structure, IR and Raman spectroscopy can provide a good estimate of the secondary structures of proteins in aqueous solution. The composition of secondary structures in a particular protein molecule may be determined by inspection of the frequencies of amide bands. Nine normal modes (A, B, and I-VII in the order of decreasing frequency) are allowed for amide bond of proteins. Table 4-1 lists the frequency and vibrational

assignments of the amide bands relevant to protein structure analysis by IR and Raman spectroscopy. Among them Amide I, II and III are the most recognizable amide bands in the spectrum when excited by visible light and therefore are frequently employed for determination of the secondary structures of protein molecules.^{116,117} Table 4-2 lists the typical frequencies of Amide I, II and III in different secondary structures. Additionally, the precise vibrational frequencies of the disulfide bridge (500-550 cm⁻¹ region) and aromatic amino acid residues tryptophan (Trp), tyrosine (Tyr), phenylalanine (Phe) and histidine (His) are useful for probing the local chemical environments around these amino acid residues and hence the microenvironment inside the protein molecule.¹¹⁶ Thus IR and Raman are popular tools for studying the kinetic of protein aggregation formation.^{122, 118, 119, 120} Information provided by IR and Raman spectroscopy are complimentary to each other since some vibrational modes are IR-active and some are Raman-active, however a disadvantage of IR relative to Raman is the strong absorption of water at ~1650 cm⁻¹ which is at the frequency of the Amide I band. In contrast, water is a relatively weak Raman scatter and especially so for SERS. Water bands typically do not appear in SERS spectra of aqueous solutions.

Name	Frequency (cm ⁻¹)	Vibrational motion	Reference
Amide A	3270 - 3310	>95% N-H stretch, part of a Fermi resonance doublet	121,122
Amide B	3030 - 3100	Intramolecular H-bonded N-H stretch, part of a Fermi resonance doublet, weaker than Amide A	121, 123
Amide I	~ 1650	80% C=O stretching	116,117
Amide II	~ 1550	60% N-H bend, 40% C-N stretch	116,117
Amide III	1200 - 1400	40% C-N stretch, 30% N-H stretch	116,117

Table 4-1 The frequency and vibrational assignment of Amide A, B and I-III relevant to the protein structural analysis by IR and Raman spectroscopy.

Conformation	α -helix	Antiparallel β sheet	Parallel β sheet	Turn	Unordered
Amide I (cm^{-1})	1650 - 1657	1612-1640 1670-1690 (weak)	1626-1640	1655-1675 1680-1696	1640-1651
Amide II	Centered on $\sim 1550 \text{ cm}^{-1}$, weak band and cannot be observed in the absence of resonance excitation. Not affected by side-chain vibrations.				
Amide III (cm^{-1})	1270-1330	1229-1235		1243-1253	

Table 4-2 Frequencies of Amide I, II and III bands for different secondary structures.^{116,117}

The SERS spectra of proteins were previously discussed in Chapter 4 in order to understand the molecular origins of the SERS spectrum of *C. trachomatis* cells on gold nanostructured substrates. The similarity between the SERS gold and silver spectra of the bacterial cells and two proteins, human serum albumin (HSA) and avidin, lead to the conclusion that the main molecular contributor to the SERS spectra of *C. trachomatis* were the cell membrane proteins (Figure 3-6). The SERS spectra of these proteins and the *C. trachomatis* on gold were characterized by three broad spectral features centered around 1550 cm^{-1} , 1150 cm^{-1} and 850 cm^{-1} while their silver SERS spectra display narrower vibrational bands assigned to vibrational motions of C-H, C-S, COO^- and aromatic amino acid residues Phe, Trp and Tyr (Table 3-2). The broad spectral features on the gold SERS spectrum were shown to be attributable to aggregated protein molecules created during the sample preparation process. This chapter will describe the discovery process that leads to this conclusion in greater detail as well as providing additional explanation of why the gold and silver SERS spectral features of the same protein molecule are dramatically different. In addition to the SERS results, the presence of aggregated protein will be confirmed by dynamic light scattering (DLS) measurements.

4.2 - Materials and Methods

SERS active substrate The SERS spectra reported here are obtained using *in-situ* grown, aggregated Au or Ag nanoparticle covered SiO₂ substrate described extensively in the previous two chapters and prior publications from our laboratory.^{34,44,47,48,49,50,87,88,89} For SERS spectral acquisitions, 1 μ L of the protein solution was added to the SERS substrate (gold or silver) and allowed to air dry (~5 minutes) at room temperature.

Protein solution preparation All protein molecules used in the study are obtained from Sigma® as lyophilized powder and used directly. The lyophilized powder are stored at 4 °C or -20 °C according to manufacturer's instruction. Unless otherwise indicated the concentration of protein solution used for SERS gold experiment is 50 μ M and for SERS silver experiment is < 1 μ M. The solutions are prepared by adding the solvent (water, saline, phosphate buffered saline (PBS)) to the lyophilized powder in 2 mL micro-centrifuge tube. Rehydration of the lyophilized powder is accomplished by pipetting or inverting the micro-centrifuge tube. No sonication or vortex is used. All solutions are freshly prepared within one hour prior to the experiment and left at room temperature after preparation.

SERS spectra acquisition SERS gold and silver spectra are acquired with an RM-2000 Renishaw Raman microscope with 50x objective. A 785 nm excitation with incident laser power of ~3.3 mW over ~ 30 μ m x 6 μ m illuminated Raman excitation field of view and 10 seconds illumination time are used to obtain the protein SERS spectra. Ten spectra per sample are obtained. The peak frequency precision is ± 0.5 cm⁻¹.

SERS spectra processing and baseline correction The acquired SERS spectra are averaged and baseline corrected with GRAMS®. The SERS spectra are normalized and plotted with MATLAB® (release R2016) and displayed vertically offset for clarity.

In Figure 4-3 where the “generic” broad spectral features on the gold SERS spectrum are removed to show the weaker, narrower bands, the broad spectral features are treated as baseline and removed by the MATLAB function *msbackadj*. *Msbackadj* corrects baseline of signal with peaks that can't be satisfactorily removed without altering the peaks via the more traditional polynomial fittings procedure of baseline corrections.¹²⁴ The quality of baseline removal by *msbackadj* is monitored by overlapping the original SERS spectrum and the calculated baseline and the optimal parameters for *msbackadj* function are selected during this process.

Dynamic Light Scattering Measurements (DLS) The presence of protein aggregates in the solution upon vigorous agitation was identified and confirmed by making simultaneous SERS and a DLS measurements of the same protein solutions. The DLS measurements are performed on a DynaPro NanoStar 499DPN (Wyatt Institute®) at fixed 90° scattering angle. A 658 nm laser is used to illuminate the sample, and 10 measurements with 5 seconds acquisition time for each measurement are obtained and averaged per sample. The hydrodynamic radius of the protein aggregates are estimated from the autocorrelation function and the relative amount of mass (%mass) at each radius is shown when plotting %mass against radius.

HSA was chosen as model protein molecule for this SERS and DLS experiment given its ubiquitous presence in human body fluids. Three HSA solutions are prepared in

three different solvent systems: water, PBS and 10% glycerol. Therefore the effects of ionic strength and viscosity, which are known to play an important role in protein aggregation formation,^{132,133} can be examined simultaneously by SERS and by DLS. Each solvent is double-filtered by a 0.22 micron syringe filter before protein solution preparation and the concentration of HSA is 1 mg/mL. The HSA solution is prepared by slowly adding 1 mL of the solvent drop-wise to 1 mg lyophilized protein powder in a 2 mL borosilicate glass container. Then the solution is left undisturbed for one hour at room temperature to allow thorough rehydration.

During the SERS and DLS experiments, a long gel-loading pipet tip (Corning®) is used to avoid bubbles during HSA solution preparation. Immediately preceding SERS and DLS measurements the glass container is gently inverted to ensure solution homogeneity. Extreme caution is taken to avoid any bubble formation during this inversion. 1 μ L of the HSA solution is loaded onto a gold SERS substrate. Then 4 μ L of the same HSA solution is added to a micro-cuvette (Wyatt Institute®) to perform the DLS measurement. Then the HSA solution is agitated by vigorous pipetting. The solution is left still for 5 minutes to allow the bubbles to float to the top, and using a long gel-loading pipette tip 1 μ L and 4 μ L of the solution is obtained from the bottom of the container for SERS and DLS measurement respectively. To ensure the changes of %mass before and after agitation are not due to the presence of bubbles, DLS measurements are repeated on the same solution 15 minutes after agitation to confirm the result.

4.3 – Results and Discussion

4.3.1 - SERS spectra of proteins on gold and silver substrates

Five different proteins, apo-transferrin, avidin, HSA, insulin and ubiquitin, were studied by SERS. The Ribbon representation of their tertiary structures are shown in Figure 4-1. These five protein molecules are of different molecular weights and secondary structures which can be used to study the effect of size and shape, respectively, on the SERS spectral features. For example HSA (alpha-helical), avidin (beta-sheet) and transferrin (mix) are of similar size but have different secondary structures, while HSA and insulin have similar secondary structure but differ in size (see Figure 4-1). The effect of monomer vs multi-mer (avidin vs ubiquitin and HSA vs insulin) are also included in this protein group.

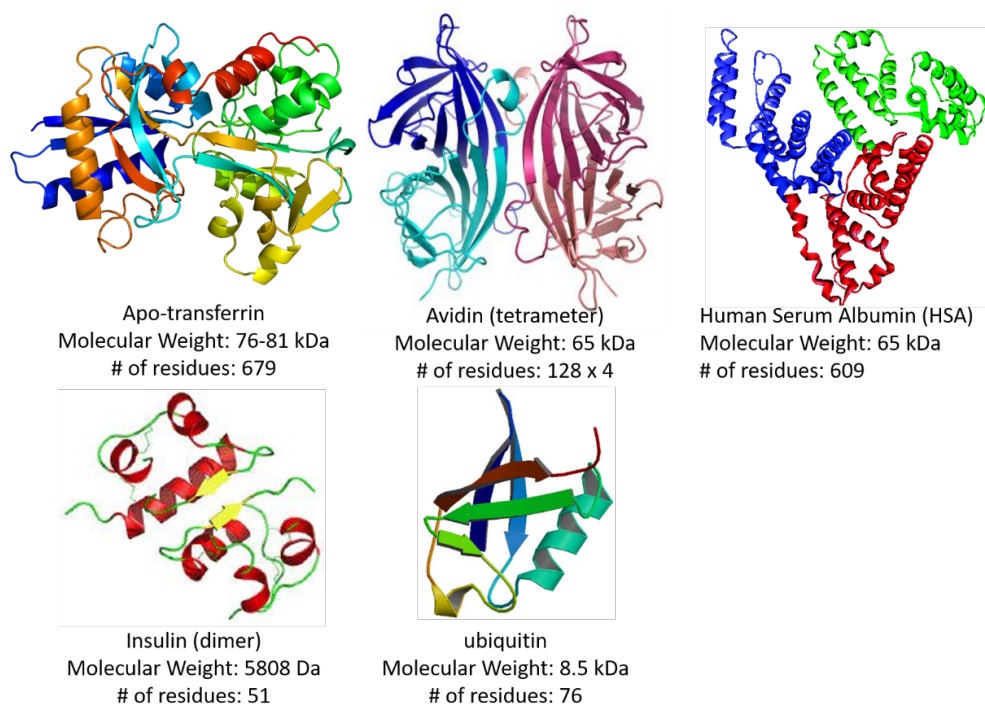


Figure 4-1 Ribbon diagram representing the tertiary structures of five protein molecules studied by SERS. These five protein molecules has different tertiary and secondary structures, molecular weight, and number of amino acid residues.

However despite the difference in size and shape, Figure 4-2 shows the SERS spectra of these five proteins on the gold and the silver substrate exhibit very similar SERS spectral features. All of these proteins show the three characteristic broad spectral features on the gold substrate and narrow bands on the silver substrate. However, each protein molecule can still be distinguished from each other on both the gold and silver substrate resulting from the difference in relative band intensities. This figure shows that the size and shape of the protein does not cause dramatic differences on the SERS spectra. However, closer inspection of protein SERS spectra on gold substrates reveals that weak but recognizable narrow vibrational features can be seen after the three broad bands are removed through baseline correction as shown in Figure 4-3. The optimized baseline determine by *msbackadj* in comparing with the original SERS spectrum are shown in Figure 4-4. The most important point from this figure is that each protein shows a different signature on the baselined gold spectrum. However these same protein spectra on the silver substrates differ mainly by the relative intensity of the common vibrational bands. In addition, most of the silver spectral bands, such as the 936 cm^{-1} , 1004 cm^{-1} , 1035 cm^{-1} , 1385 cm^{-1} , 1450 cm^{-1} and 1600 cm^{-1} are observed in the baselined gold substrate spectra and shared in all four proteins. The assignment for these silver bands has been given in Table 3-2. The contribution from the disulfide bond stretch (vS-S) from $\sim 500\text{-}550\text{ cm}^{-1}$ region¹⁰⁴ are visible for each protein on the baselined gold spectrum but not visible on the silver spectra. However, the $\sim 615\text{ cm}^{-1}$ band which was assigned to C-S stretch,¹⁰² is present in the gold baselined spectra of insulin and avidin but very weak in HSA and apo-transferrin.

In conclusion, all five studied proteins, regardless of size and shape, show similar SERS spectral features on gold and silver nanostructured substrates. However, weaker and narrower bands unique to each protein can be seen on the gold spectrum after the broad spectral features are removed. In addition, most of the silver spectral bands except the 615 cm^{-1} band are observed in the baselined gold spectrum. The molecular mechanism that causes the presence of the broad protein spectral features on the gold substrates is not evident for proteins on the silver substrate. Thus the silver spectrum of the protein is dramatically different from its corresponding SERS spectrum on gold. The observation of very similar SERS spectral features for all five protein molecules despite the large difference in size and shape of these molecules is surprising, given the well-established ability of Raman spectroscopy to distinguish protein secondary and tertiary structures. Moreover, the three broad spectral bands on the gold substrate have not been previously reported for any of the five proteins studied here. The origin of these broad SERS spectral features and the mechanism of their formation on gold SERS spectrum will be discussed below. Since HSA is the most the abundant protein in humans, the studies described in the next two sections will focus on HSA.

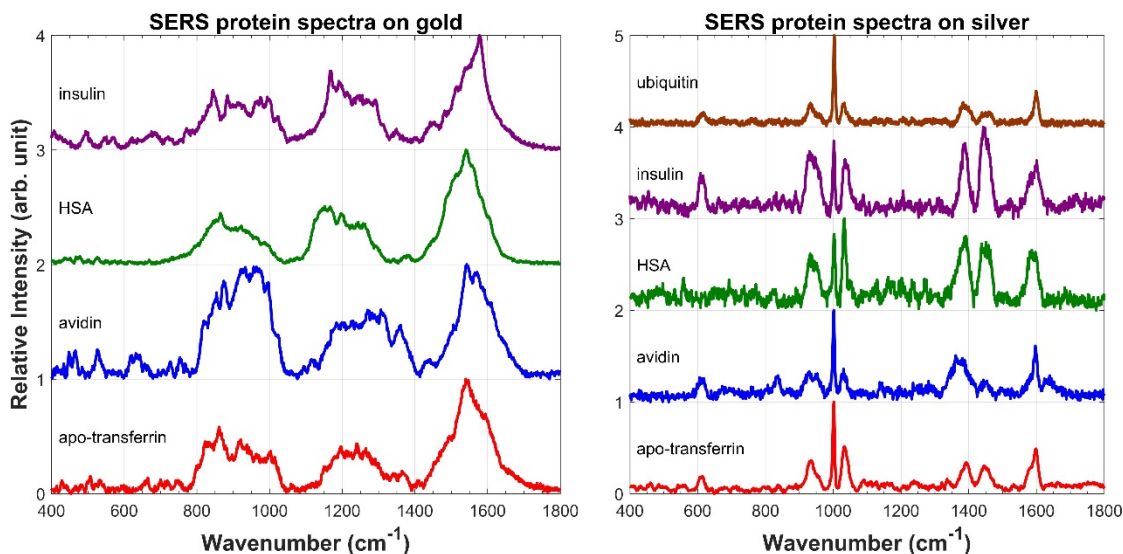


Figure 4-2 SERS spectra of various protein molecule solutions in water on the gold substrate (left) and the silver substrate (right). On the gold substrate all protein molecules display three broad spectral features center around 1550 cm^{-1} , 1200 cm^{-1} and 900 cm^{-1} , but each protein can still be distinguished from each other from the relative intensity of the three broad features. On the silver substrate all protein display similar, narrower spectral bands but each protein can still be distinguished based on the difference in relative peak intensity.

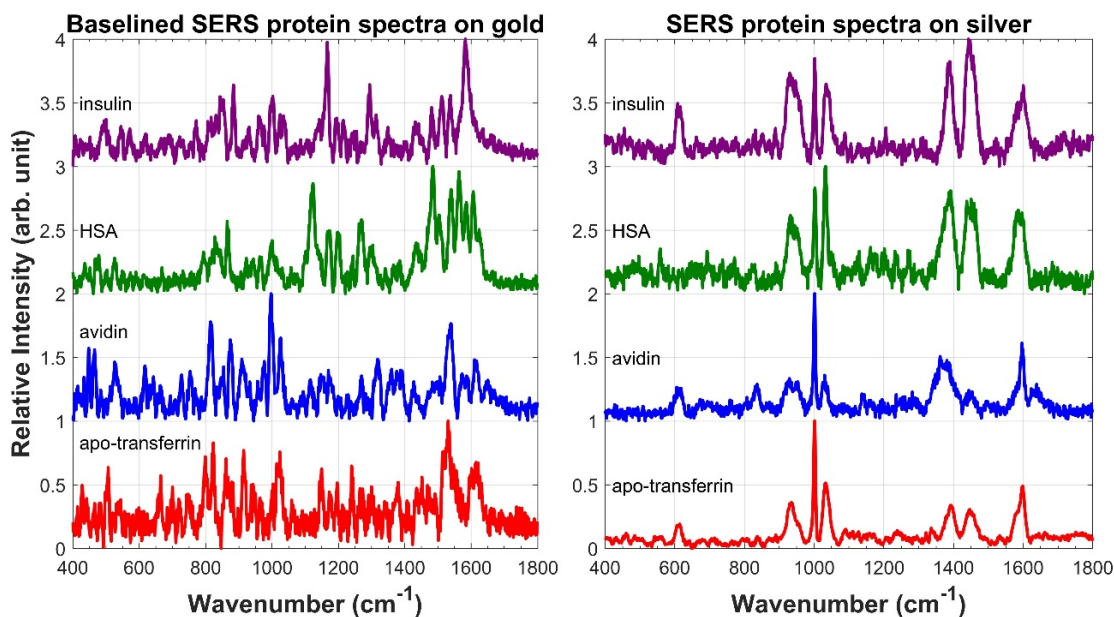


Figure 4-3 After removing the three broad spectral features by MATLAB function *msbackadj* distinct, narrower spectral features can be seen for each of the four protein molecules on the gold substrate. Each protein shows different gold spectral features, but many common bands can be found among them. Comparing with their silver SERS spectra (right) show that almost all silver spectral features (with exception to the $\sim 610 \text{ cm}^{-1}$ features) can be seen on the baseline gold spectra.

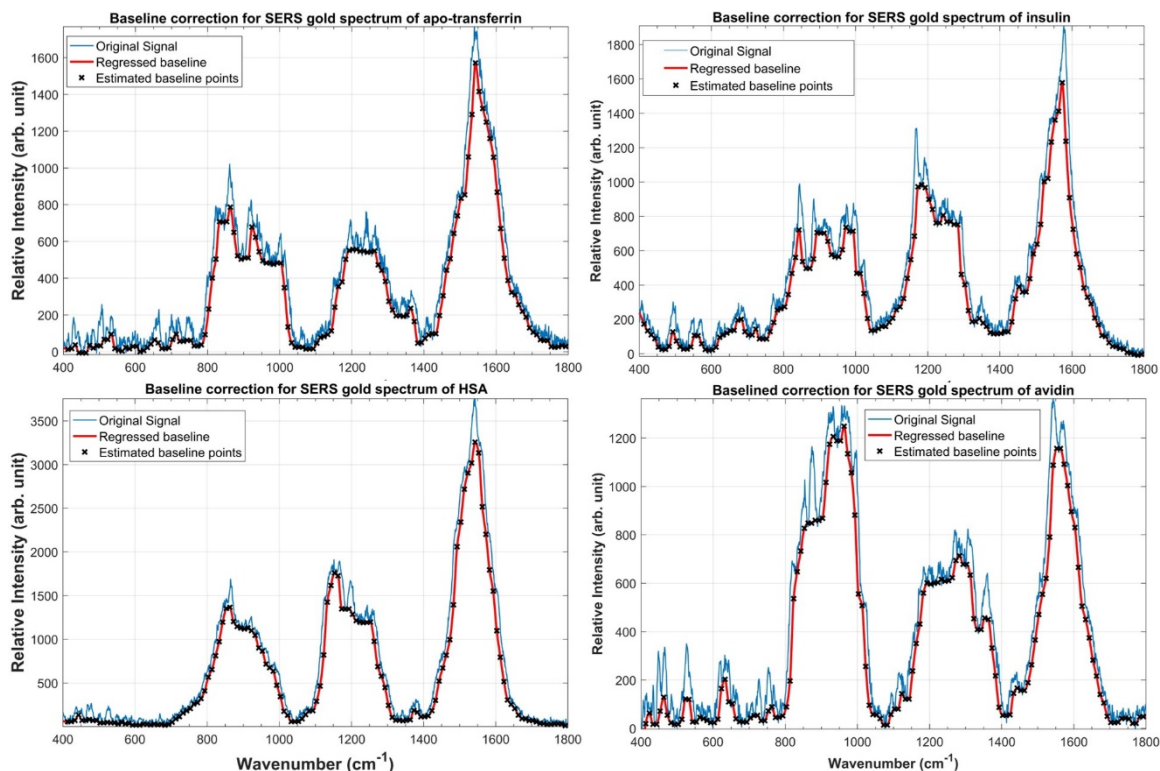


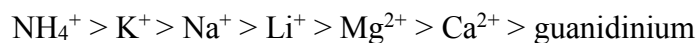
Figure 4-4 The optimized baseline determined by MATLAB function *msbackadj* is shown with the original spectrum.

4.3.2 - Perturbing the SERS Protein Spectra

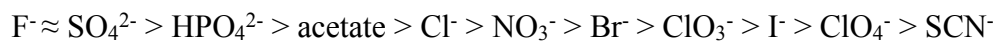
Effects of ions and ionic strength

Ions have complex effects on the structural stability of proteins in solution. Ions can modulate the strength of electrostatic interactions by interacting with unpaired charged side chains on the protein surface, both within the protein and between protein molecules. Binding of multivalent ions can cross-link charged residues between two protein surfaces and leading to protein stabilization^{125,126} (salting-in effects), whereas intramolecular charge-charge interactions disrupt the conformational stability (salting-out effects).¹²⁷ The net effect of salt on protein stability is thus a delicate equilibrium balance between intermolecular protein-salt-protein interactions and intramolecular protein-salt

interactions. The ability of ions to salt-out or salt-in proteins are classified by the Hofmeister series, first work out by Franz Hofmeister in 1827. He discovered a series of salts that had consistent solubility effects on chicken egg protein mixtures, which was extended to the stability of their secondary and tertiary structures in the salt solution as discovered later. The Hofmeister series ranks ions in the order of their ability to stabilize protein structure in aqueous solution.¹²⁸ The Hofmeister series for cations is,



Anions usually have a larger impact on protein solubility than cations and the corresponding series is,



Although some controversy about the mechanism of ion effects still persists, the Hofmeister series is commonly exploited in protein precipitation and purification procedures. For example the highest ranking cation and anion in the series $(\text{NH}_4)_2\text{SO}_4$ is used extensively for bulk protein precipitation from a cellular lysate mixture. At sufficiently high salt concentrations the protein components precipitated out. By increasing ammonium sulfate concentration stepwise the precipitated protein components in the mixture is recovered between each step.

In this section, the effects of cations and anions as well as ion strength to the broad SERS spectral features on the gold substrate are described. Particularly, the perturbation of SERS spectra of HSA on gold by 100 μM of Na^+ , K^+ cations and Cl^- , NO_3^- anions are explored. All these ions are early members of the Hofmeister series and thus expected to destabilize the protein structure in solution. In addition to these four ions,

the effect of Ag^+ (in the form of AgNO_3) is studied on the gold substrate. As shown in Chapter 4, the same protein displays very different SERS spectral features on gold and silver nanostructured SERS substrates (Figure 4-2) and thus adding Ag^+ ions to the protein may help to understand the origin of such sharp differences.

Figure 4-5 shows the SERS spectra of HSA in 100 μM of KCl , NaCl , NaNO_3 and AgNO_3 on the gold substrate. These are compared to the HSA SERS spectrum in pure water as a reference at the bottom of this figure. Except for HSA in AgNO_3 which shows only a weak SERS spectrum with few bands, the HSA SERS spectra in the other three salt solutions display the three characteristic broad bands on the gold substrate. Also the differences between the HSA SERS spectrum in these three salts is relatively small and mostly due to differences in relative peak intensities. For example, note the relative intensity of the 1150 cm^{-1} band in Figure 4-5. Thus, the broad spectral features on the gold substrate are largely not affected by protein size, shape or the presence of ionic species. Moreover, the broad SERS features of HSA on gold don't seem to be affected by the concentration of salt as shown in Figure 4-6. Relatively few spectral changes are observed for the HSA SERS spectrum on gold as the NaCl concentration ranges from 1 μM to 100 μM . However given that Na^+ , K^+ , Cl^- and NO_3^- are earlier members of the Hofmeister series and thus tend to destabilize the protein structure in solution, one may conclude that the observed broad gold spectral features are related to the destabilized protein structure. One simple test of this hypothesis is to study the protein SERS spectral changes upon dilution. Also comparing the dilution dependence of both the gold and silver SERS spectrum of the same protein may help to understand the mechanism that

causes the very different spectral features observed on these two substrates.

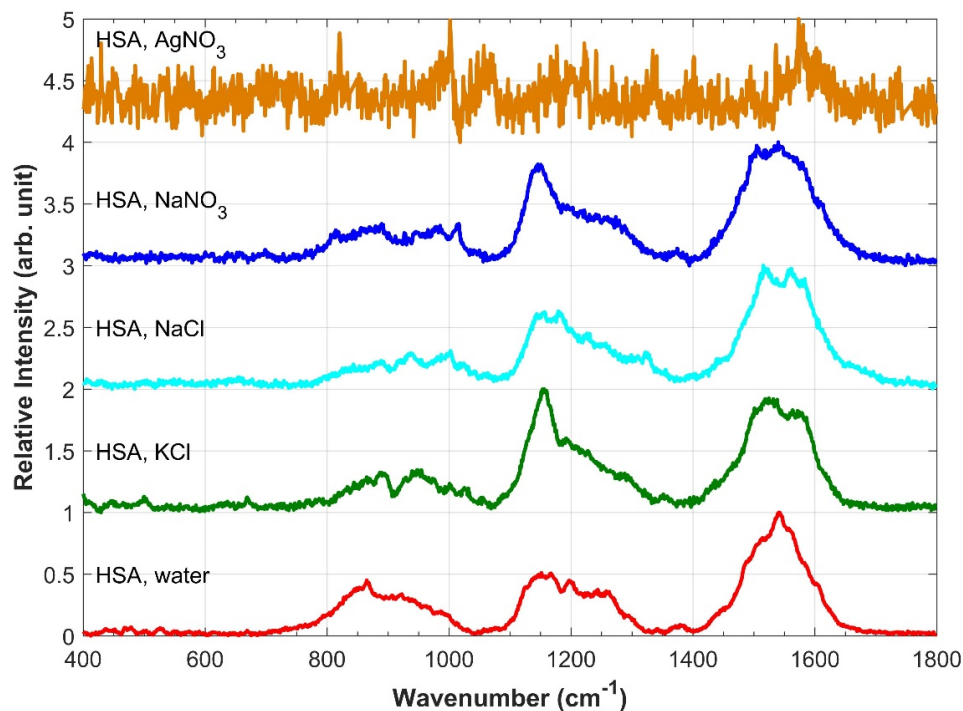


Figure 4-5 SERS gold spectra of HSA in 100 μM salt solutions: silver nitrate (AgNO₃), sodium chloride (NaCl), potassium chloride (KCl) and in water as reference. The three broad gold spectral features are observed in all the salts except in silver nitrate.

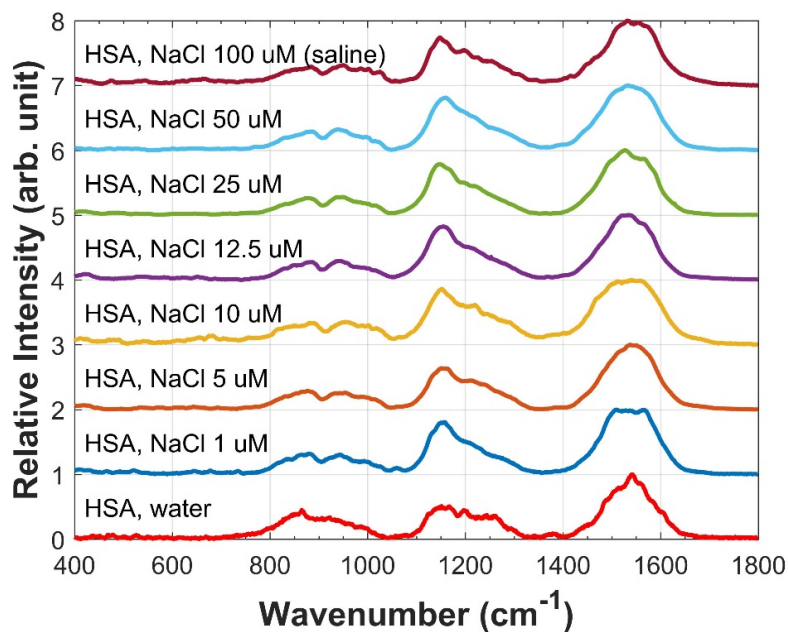


Figure 4-6 SERS gold spectra of HSA in NaCl of different concentration to study the effect of ion strength to the three spectral features. SERS spectra of HSA in water is shown at the bottom.

The effect of protein concentration on SERS gold and silver spectral features

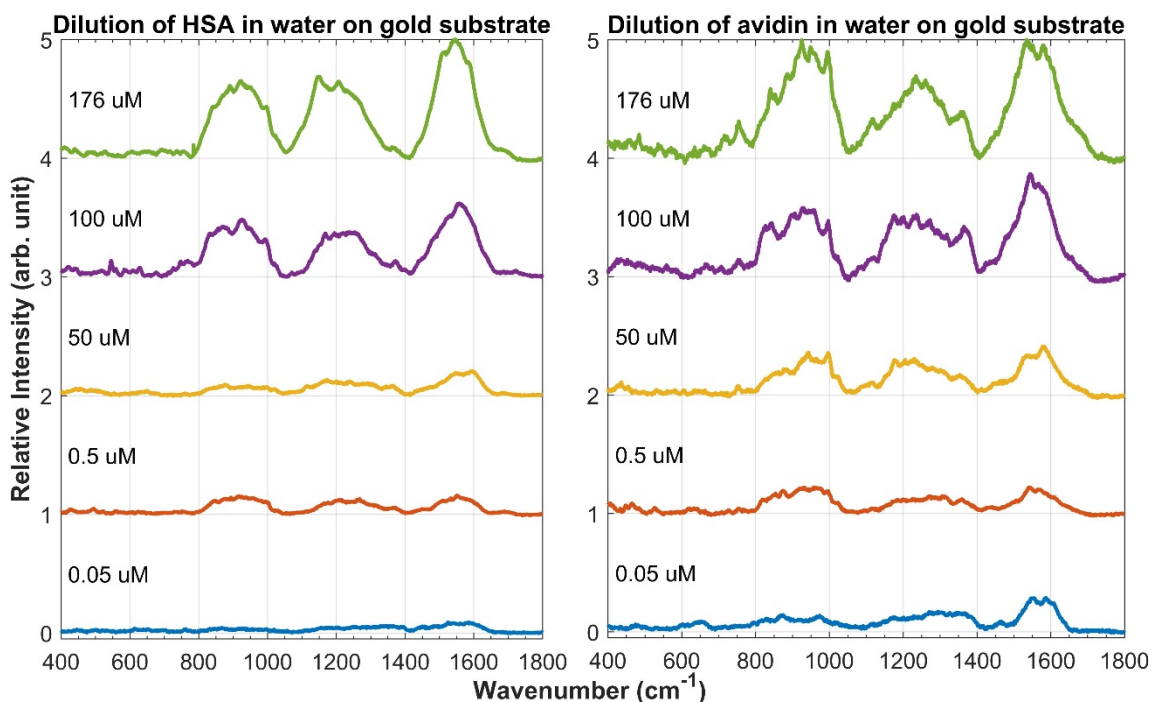


Figure 4-7 Dilution of HSA and avidin, two protein molecules of similar size but having alpha-helix and beta-sheet respectively, as main secondary structure on the gold SERS substrate. The three broad spectral features intensity decrease with dilution in water.

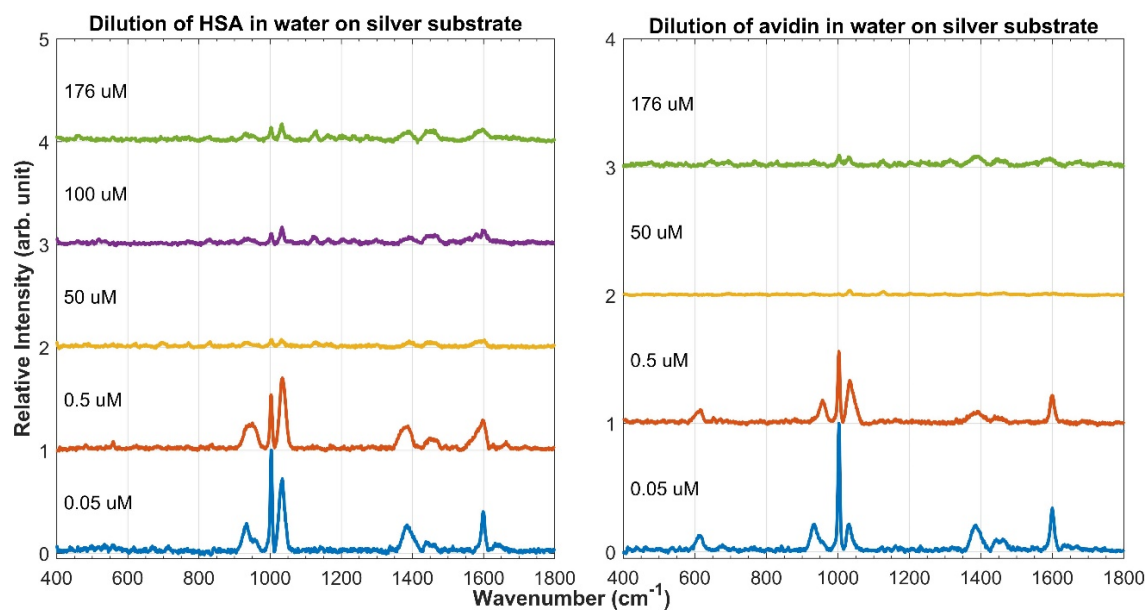


Figure 4-8 Dilution of HSA and avidin in water on the silver SERS substrate. The intensity and the S/N ratio of the SERS spectral features of both protein molecules on the silver substrate increase with dilution.

Figure 4-7 shows the dilutions of the aqueous solutions of HSA and avidin, two protein molecules of similar sizes but different secondary structures, on the gold substrate. The three broad spectral features are evident for both proteins. What's more important is that there are few changes of the relative peak intensities and narrow, fine spectral feature on the broad spectral features as a function of dilution. In other words, dilution only causes the decrease of overall spectral intensity due to the lower molecular concentration, but the chemical species that cause the three broad spectral features remain intact during dilution. A good hypothesis of such chemical species is protein aggregates in the solution created during the solution preparation process, since the protein structural changes during aggregation formation are both irreversible and thermodynamically stable.¹²⁹ Therefore if protein aggregation is the cause of the broad spectral features, dilution will not cause major structural change on these aggregation and will only result in decrease of the overall signal intensity.¹³⁰

Furthermore, Figure 4-8 shows that the dilution of HSA and avidin display different behaviors on the silver substrate compare to the gold substrate. The three broad spectral features disappear on the silver substrate and the narrower bands attributed to amino acid residues (Table 3-2) appear. Interestingly, the intensity and signal-to-noise ratio of these narrow bands increase with dilution. The appearance of spectral features from individual amino acid is attributed to the known strong interactions of the silver nanoparticles with the protein molecules.^{131, 132, 133, 134} Treuel *et al.* demonstrated via SERS that there are strong interaction between sulfur-containing groups (serine, cysteine and methionine) in bovine serum albumin (BSA) and uncoated silver nanoparticle.¹³⁵ This

is consistent with our protein silver SERS spectrum on Figure 4-8. The $\sim 615\text{ cm}^{-1}$ band which is assigned to C-S stretch becomes evident for avidin at lower concentration. In the same study¹³⁵ it's also shown via circular dichroism that BSA loses its α -helix features when interacting with the silver nanoparticles. In other words, silver nanoparticles have the ability to denature protein molecules. These silver nanoparticles-protein interactions are the cause of the cytotoxicity of silver nanoparticles *in vivo* and have been known and exploited as an antimicrobial agent. For example, silver staining is a common technique to visualize the protein bands on polyacrylamide gel after electrophoresis, and an aqueous solution of 1% silver nitrate is used to prevent bacterial conjunctivitis in newborn babies. Based on these observation, we attribute the dramatically different spectral features of the same protein on gold and silver substrates are due to the strong interactions between the protein and the silver nanoparticles which disrupt the aggregated protein molecules and allow the observation of features from individual amino acids on the silver substrate. The reason why the silver SERS signal intensity increases upon dilution is because dilution lowers the ratio between protein aggregates and silver nanoparticles, i.e. more silver nanoparticles are available to interact on a per aggregate basis, resulting in better SERS signals on the silver substrate upon dilution.

This dilution experiment suggests that protein aggregates may be the chemical species that cause the broad spectral features observed on the gold substrate. Also discussed in this section, the reason for the difference between the gold and the silver protein spectral features is attributed to the more perturbative nature of the silver nanoparticles. However, additional evidence is needed to confirm the presence of protein

aggregation as well as understand how the aggregates are form. In the next section, dynamic light scattering (DLS) in conjunction with our SERS measurements will be described in the next section to confirm the presence of aggregates. The comparison between the SERS and DLS results will not only allow the understanding of the unique gold SERS spectral features but also adds SERS to the list of rapid, ease-to-use optical technique for protein aggregates studies.

4.3.3 - Origin of the Protein SERS Signature

In this section the results from dynamic light scattering (DLS) will be compared in conjunction with the gold SERS spectrum of HSA to confirm the hypothesis that the three broad spectral bands observed on the SERS spectrum are caused by protein aggregates in the solution. The question of how these protein aggregates are formed in the solution will also be addressed. Three solvent systems are chosen to be studied by SERS and by DLS: water, PBS and 10% glycerol. Thus the effects of ionic strength^{125, 126} and viscosity¹³⁶ which are known to play important roles in protein aggregation formation will be studied simultaneously by SERS and by DLS.

DLS is a powerful technique to determine the size distribution of small particles suspended in solution. DLS measures the intensity fluctuation of scattered light resulting from the Brownian motion of small particles (<250 nm) in solution. Since the distances between molecules in solution are constantly changing, the scattered light from one molecule can undergoes either constructive or destructive interference with the scattered light from its neighboring molecule and information can be obtained about the time scale

of movement of the scatters. The dynamic information of the particles is derived from an autocorrelation of the changing intensity recorded in the experiment. An exponential decay of the autocorrelation function will thus indicate the particle is in motion, and the rate of motion is related its diffusion coefficient. Since the diffusion coefficient is inversely related to the radius for small spherical particles, the autocorrelation function will thus provide an estimation of the hydrodynamic radius of the molecule, or the radius of an equivalent hard sphere diffusing at the same rate as the molecule under observation, in solution.

Protein aggregation can be induced by a wide variety of conditions, such as temperature, pH, freezing and/or thawing and mechanical stress such stirring, pipetting and shaking.^{98,99} Since in our previous SERS protein experiments the solutions are prepared at constant temperature and our efforts with varying salt and ionic strength of the solution doesn't cause significant change of the gold SERS spectral features of the protein, this experiment will focus on the effect of mechanical stress on the induction of protein aggregation.

The shearing stress during agitation, such as stirring, pipetting and shaking, are known to induce protein aggregation.^{98, 137} In addition, agitation can cause cavitation, or the formation of voids or bubbles within the protein solution which rapidly collapse and sends shock waves that can perturb the tertiary structure of the protein.¹³⁸ HSA solutions were initially prepared at 1 mg/mL concentrations as gently as possible to minimize aggregation formation. Then aggregates are induced by vigorous pipetting to generate both shearing stress and cavitation. Simultaneous comparison of the SERS and DLS

measurement before and after pipetting confirms our previous hypothesis that the protein SERS spectral features on gold are caused by protein aggregation in the solution (See Figure 4-9). This is evidenced by the increase in % mass of particles with larger radius after agitation which is coincident with the increase of the overall signal SERS intensity. The magnitude of increase in % mass for larger particles is roughly correlated to the increase in SERS signal intensity, with 10% glycerol shows the greatest increase. In addition, narrower bands such as the $\sim 1000\text{ cm}^{-1}$ and $\sim 1030\text{ cm}^{-1}$ begin to appear on the SERS spectra for the un-perturbed protein solution. This observation is in agreement with results shown in Figure 4-3 that after the broad spectral features are removed the contribution from individual amino acid residues appear.

From these SERS and DLS experiments the molecular origin of the broad protein SERS on gold spectral features that are observed for all proteins we have studied are established to result from protein aggregation, which is probably created by agitation during the protein solution preparation process. We note that these protein aggregates are not affected by the presence of ions or ionic strength (Figure 4-5 and Figure 4-6) with the exception of silver nitrate. This is probably because silver ions can bind to and interact strongly with the protein aggregates thus allowing the appearance of vibrational features from individual amino acid residues to appear in the SERS spectrum.

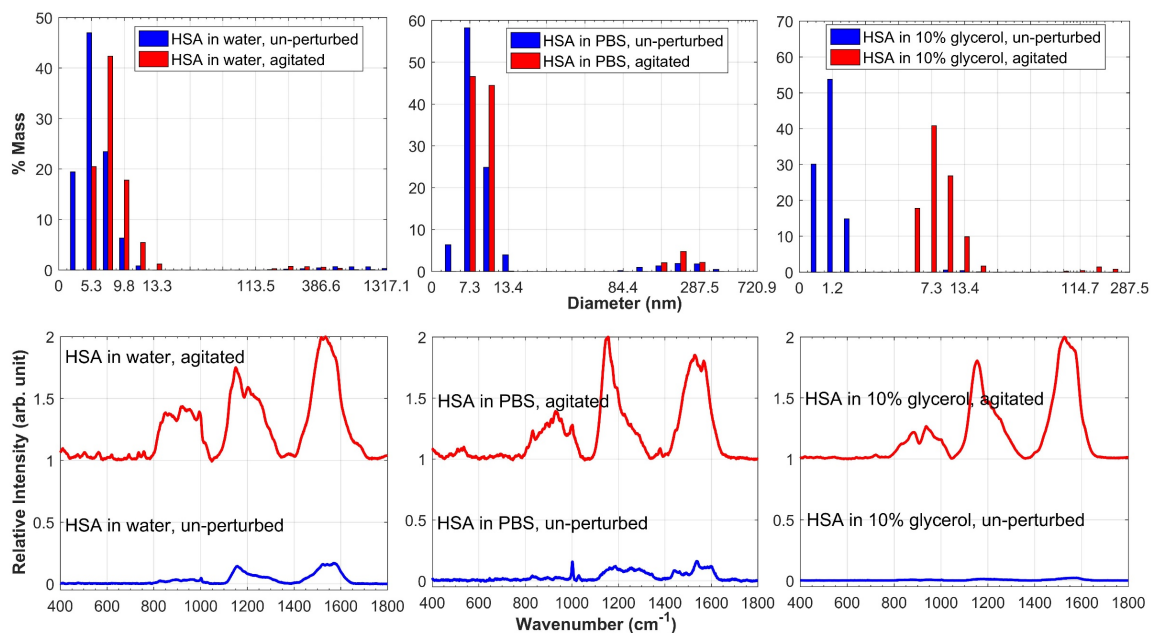


Figure 4-9 Simultaneous comparisons between SERS (bottom) and DLS (top) measurements of HSA solution in three solvent systems before and after agitation confirm the molecular origin of the three broad spectral features on the gold SERS spectrum of HSA as protein aggregation in the solutions.

4.4 - Conclusion

The results demonstrated in this chapter shows that protein aggregation can be observed by our SERS method. Previous literature reports of proteins SERS studies have been focused on the observation and identification of features from individual amino acid residues by utilizing the strong interaction between the protein molecules and silver nanoparticles. Few previous protein SERS studies reports have employed gold nanoparticles and, as far as we are aware of, the ubiquitous characteristic broad protein aggregation gold spectral features we observe have not been reported in prior studies. Since protein aggregation has significant impacts in many areas such as in understanding disease progression in Alzheimer's and Parkinson's Diseases, and in therapeutic

development where the stability of a protein drug is paramount to patient safety and treatment efficacy, the ability of SERS to observe characteristic signatures of protein aggregations offers a new and powerful bioanalytical probe. More importantly, since it has been shown that the SERS vibrational signature of protein aggregates are universal regardless of the size and the secondary and tertiary structure of the protein, ionic strength and solution viscosity, SERS would be a valuable and ease-to-use tool for identifying the presence of protein aggregates under complex conditions such as those in body fluids and during disease progression. An essential remaining question is how does protein aggregation result in the three broad vibrational features observed on gold substrates. Understanding the underlying molecular origins of this robust protein aggregate structure will be of great value because it will reveal the mechanism of protein aggregation and such knowledge may help understanding protein-misfolding more generally especially in the context of human diseases.

5. SERS Diagnostic Platform: Cancer Cell Detection

5.1 - Basis of Metabolomic-based Cancer Identification

Cancer is responsible for nearly 1 in 6 death globally in 2015 and an increase of 70% new cases is expected in the next two decades.¹³⁹ For all cancer types, early diagnosis is crucial for effective treatment, higher survival rate and improved quality of life. Therefore screening tests to identify cancer cells are paramount for early diagnosis of cancer. Given that cancer is a highly complex disease and screening tests are to be applied to a large population, such tests must be cost-effective, multiplexing, ease-to-use,

sensitive and specific.^{139, 140}

Metabolomics or the analysis of the complete metabolites from a cell, organ or organism focus on quantifying the concentrations of low-molecular weight metabolite molecules that can be detected by various analytical methods.¹⁴¹ Metabolomics analysis is particularly useful for identifying biochemical pathways that are perturbed in a particular pathological process, such as tumorigenesis.¹⁴² Metabolomic analysis has been successfully employed in the field of cancer biology.¹⁴¹ Cell metabolism is known to be altered in tumor cells. The first tumor-specific metabolic alternation was reported in 1930s by Warburg, who demonstrated that cancer cells rely on an increased dependence on glycolysis, a metabolic pathway normally used by anaerobic organisms for ATP generation, even in the presence of sufficient oxygen.^{143,144} This switch from oxidative phosphorylation to glycolysis has been considered as a main hallmark of a cancer cell.^{143, 145} Other biological capabilities acquired during tumorigenesis process have been discovered and attributed as indicators for cancer as described by Weinberg *et al.*¹⁴² including sustained growth signaling, evaded growth suppressor, resistance to apoptosis, replicative immortality, angiogenesis and activated invasion and metastasis. Mutations occur during tumorigenesis at the “upstream” genomics and proteomics, i.e., genetic or enzymatic activity/concentration changes, are reflected in the “downstream” change in cellular metabolism. However, measurements of the change in the overall metabolite concentration is a much more sensitive approach than measuring the change in gene expression or enzymatic activity/concentration, because changes in the metabolic flux (the rate of change of total amount of material passes through a given metabolic pathway)

have a significant impact on the overall metabolite concentrations.¹⁴⁶

5.2 - Current Analytical Techniques for Cancer Metabolomic Study and Introduction of SERS-based Cancer Identification

Metabolomics analysis of cancer cells is a powerful approach to identify biomarkers to use for diagnostics, treatment efficacy evaluation and identification of novel therapeutic targets.^{141,147} Currently nuclear magnetic resonance (NMR) and mass spectrometry (MS) are the two dominant experimental methodologies for this purpose. Examples of metabolic biomarkers of tumors identified by NMR or MS approaches include alanine,¹⁴⁸ saturated lipids,¹⁴⁹ glycine,¹⁵⁰ lactate,¹⁵¹ and nucleotides.¹⁵² NMR, particularly MRI, is used extensively for metabolomic study in intact human tissues.¹⁵³ The non-invasive nature of NMR is valuable for *in vivo* monitoring of tumor progression. However, the disadvantage of NMR-based approaches is that only limited types of molecules can be identified in a simple one-dimensional spectrum. Co-resonance between two metabolite molecules can make quantification of metabolite concentrations difficult as well.¹⁴¹ On the other hand, MS-based approaches are used extensively for a full-spectrum proteomic and metabolomics analyses with good sensitivity.¹⁴¹ MS-based approaches can be further classified based on the sample separation method (GC-MS, LC-MS, HPLC-MS, etc.) and the type of ionization used (ESI, MALDI-TOF, etc.).¹⁴⁸ The metabolites are separated at the initial chromatographic stage first and then separated based on their mass to charge (m/z) ratio. MS-based approaches are far more sensitive than NMR-based approaches and more metabolite molecules can be identified from a

single measurement. However, the major problem is that not all metabolites can be readily ionized which potentially bias the metabolite identification result and limit the ability for quantitative measurements. Moreover, the presence of ions in the sample significantly impacts the ionization process and this problem is particularly prominent when the metabolite concentration in the sample is low.¹⁵⁰ Additional treatment is required to remove ion sources from the sample, which usually involves extensive dialysis or solid-phase extraction. Finally, the hardware requirement and the high maintenance expense makes MS-based approaches less affordable to be used in a large scale in clinical settings.

The advantages of SERS as rapid, label-free, sensitive and specific approach for disease diagnosis has been described in details in the previous chapters. The use of a SERS-based methodology for detection and identification of cancer has been investigated particularly over the last decade.^{154, 155, 156, 157, 158, 159, 160} The attributes of speed, ease-of-use, sensitivity and specificity makes SERS an attractive analytical approach that could be used for real-time cancer diagnostics. Most of the previous SERS-based approaches for cancer identification center on the use of antibody-labeled metal nanoparticles that bind to cancer cell surface biomarkers and subsequently allow specific cellular imaging due to the bright SERS reporter molecules. The advantages of this approach are the high sensitivity and specificity associated with the selectivity of the antibody. However, this imaging approach is dependent on the identification of unique antigens that are over-expressed on the cancer cell surface and the successful production of antibody-conjugated nanoparticles with SERS reporter molecules. Alternatively, SERS spectra of

in vitro cultured cancer cell or blood plasma from cancer patient have been examined and shown to offer vibrational signatures that, when couple with multivariate data analysis techniques, can distinguish cancer and normal cells.^{161, 162, 163, 164} In these reports the identities of molecules contributed to the SERS vibrational feature that allows the distinction between cancer and normal cells are assigned to anomalous cell surface features or alternated level of nucleic acids, proteins, saccharides or lipids in the blood plasma. It's interesting to note that in most of these studies a vibrational band of anomalous intensity around $\sim 725\text{ cm}^{-1}$, which is attributed to adenine or to the C-N bond of quaternary ammonium groups in the membrane lipid bilayer components,^{161,162,163,164} is reported.

In this early stage of expanding the SERS methodology as a label-free cancer cell detection and identification diagnostic platform, this work will demonstrate, at least phenomenologically, the ability of SERS to distinguish *in vitro* grown non-tumorigenic and cancer cells based on their unique SERS vibrational signatures as well as their time-dependent spectral dependence that can be used as an additional characteristic to identify cancer cells. We will also identify the main molecules contributing to these spectra which give rise to the ability to distinguish cancer and non-tumorigenic cells via SERS, as well try to understand the biochemical origins of these SERS molecular contributors.

5.3 - Materials and Methods

SERS active substrate The SERS substrates used in this study are the gold SERS active substrate synthesized in our laboratories and described in details in the previous

chapters. 1 μL cell samples in Dulbecco's phosphate buffered saline (DPBS, Life Technologies®) is added to the substrate and air-dried before spectral acquisition.

Cancer/non-tumorigenic cell lines Two epithelial cell lines, MCF10A (M1) and MCF10ACA1h (M3) representing non-tumorigenic mammary gland cells and invasive breast cancer cells respectively, are generously provided by Dr. Douglas Faller at the Evans Center for Interdisciplinary Biomedical Research at Boston University School of Medicine (BUSM). The M1/M3 combination is a breast cancer cell line model system for studying the mechanism of aberrant epigenetic DNA methylation pattern.¹⁶⁵ The advantage of using the M1/M3 cell system to demonstrate the ability of the SERS cancer diagnostic platform is both cell lines were derived from a common genetic background (MCF10A) and the genetic/epigenetic alternation on M3 compare to M1 is a good representation of the gradual progression from non-tumorigenic to carcinogenic state *in vivo*. In addition, both M1 and M3 cells will be cultured using the same growth medium formulation, therefore the possibility of observed SERS vibrational signature difference due to two cell lines being cultured in different growth media is eliminated.

The general procedure for cell culture is summarized in Section 8.5 while details regarding specific cell lines are discussed below. All cell lines are grown in triplicate in a humidified 37 °C incubator with 5% CO₂ by adhering to the surface of a TTP® tissue culture flask (T25, Corning®). The surface area is 25 cm² which corresponds to $\sim 10^5$ cells/mL as determined by cell counting with hemocytometer at $\sim 90\%$ confluence (i.e. 90% area of the flask surface are covered by cell monolayer), and the working volume (i.e. the volume of growth medium to be added to a cell monolayer) for the T25 flask is 5

mL. Cell growth was monitored daily via an inverted microscope and the growth medium was refreshed every two to three days. Only cells after at least two passages were used in these experiment to ensure robustness.

Specific cell culture instruction for M1 and M3 cells

Reagent: both M1 and M3 cells are grown with the same reagent with the following composition. DMEM-F12, Dulbecco's Modified Eagle Medium: Nutrient Mixture F-12. HEPES, 4-(2-hydroxyethyl)-1-piperazineethanesulfonic acid. DDwater, sterilized and double-filtered water by 0.22 micron syringe filter.

Medium	Final concentration	Stock concentration	Vol needed for 100 mL medium
DMEM-F12 medium (Life Technologies®, with HEPES)			95 mL
Filter the below items together, then add to DMEM-F12			
Heat-inactivated horse (equine) serum (ATCC®)	5%		5 mL
Cholera Toxin (Fisher®, 1 mg)	100 ng/mL	1 mg/mL (Add 1 mL Ddwater) store at -20 °C, 10 µL/tube	10 µL
Epithelial growth factor (Life Technologies®, 100 µg)	20 ng/mL	50 µg/mL (Add 2 mL Ddwater) store at -20 °C, 40 µL/tube	40 µL
Hydrocortisone (Sigma®, powder)	0.5 µg/mL	500 µg/mL (measure 10 mg + 1 mL 100% ethanol + 19 mL DMEM-F12) store at – 20 °C, 100 µL/tube	100 µL
Insulin solution (Sigma®, 10 mg/mL)	10 ng/mL	10 mg/mL (Store at 4 °C, 100 µL/tube)	100 µL

Harvest Time: 72 hours for M1 cell, 48 hours for M3 cell.

Sample Handling Each of the three T25 flasks was harvested individually using trypsin-EDTA following the procedure described in Section 8.5. The harvested cells are spun down at 1000g for 5 minutes before transferring the cell pellet to a 2.0 mL micro-centrifuge tube. Cells in each micro-centrifuge tube are washed four times with 1 mL of DPBS at room temperature. After the last wash, all supernatant is removed and 5-10 μ L DPBS is added to the tube without disturbing the cell pellet. The cells are left at room temperature and SERS spectra are acquired as a function of time post washing.

SERS spectrum acquisition and Data processing All SERS spectra are acquired with an RM-2000 Renishaw® Raman microscope employing a 50x (infinity-corrected, 0.75 numerical aperture) objective and 785 nm excitation. Incident laser powers of \sim 0.45 mW and \sim 10 seconds of illumination time are used to obtain the reported bacterial SERS spectra. The illuminated Raman excitation field of view is \sim 30 μ m x 2.5 μ m. Ten SERS spectra per culture flask are acquired and data from all three flasks (30 spectra) are inspected to ensure robustness within the same flask and reproducibility between different flasks. Then the ten spectra with highest S/N ratio are selected and averaged. The averaged spectrum is baseline corrected and plotted in a spectral region from 400 – 1800 cm^{-1} with MATLAB®.

5.4 - Results and Discussions

Time-dependent SERS spectral feature change is the key to distinguish non-tumorigenic and cancer cells

The SERS spectra as a function of time post-washing for non-tumorigenic mammary gland epithelial cell (M1, red) and for invasive breast cancer cells (M3, blue) are shown in Figure 5-1. The M1 and the M3 cells can be distinguished immediately after washing ($t = 0$ min) in which the M1 cells shows broad and weak spectral features that resembles an aggregated protein spectrum (Chapter 4), but the M3 cells shows narrower bands such as the 736 cm^{-1} , 965 cm^{-1} and 1030 cm^{-1} . Within 30 minutes the M1 cells begin to show stronger SERS signal and very distinct vibrational bands with the most intense band centered around 735 cm^{-1} . However, a notable time-dependent red-shift of this band from 733 cm^{-1} to 725 cm^{-1} are observed on the M1 cells after 30 minutes. This red-shift from 735 cm^{-1} to 725 cm^{-1} is accompanied by a slight decrease of the overall intensity. On the contrary the M3 cells show no such red-shift of its most intense band as demonstrated in the zoom-on view on the right, and the overall intensity increases with time. Also SERS signals intensities from the M3 cells are considerably stronger than the M1 cells after 30 minutes as evidenced from the signal-to-noise ratio. Both cells show a decrease of the 1030 cm^{-1} band intensity after ~ 60 minutes. These vibrational bands have been previously reported in our bacteria SERS spectra (Chapter 2 and Chapter 3) and have been assigned to features from purine metabolites. The 1030 cm^{-1} band has been determined to be due to nicotinamide adenine dinucleotide as described on our *N. gonorrhoeae* spectrum (Figure 3-4). As discussed in Chapter 3 since the oxidized and

reduced form of nicotinamide adenine dinucleotide can't be distinguished from their SERS spectra, we will denote as NAD/NADH.

To determine the relative contribution of each molecular component to the M1 and M3 spectra we will use the best-fit method discussed in Chapter 2. The best fits are shown in Figure 5-2 and the contributions are shown as bar graph on the top. Almost all spectral features in each spectrum are captured by its best-fit with minor difference in relative intensity. It's evident from the bar graph that the red-shift of the $\sim 733\text{ cm}^{-1}$ to $\sim 725\text{ cm}^{-1}$ band on the M1 cell spectra corresponds to the change of ATP to hypoxanthine as the largest molecular contributor to the SERS spectrum. On the other hand, the contribution of each molecular component to the M3 SERS spectra remain relatively constant throughout the experiment, with adenine and ATP making the largest and second largest contribution to each spectrum. Hence no time-dependent shift of the most intense band is observed on the M3 spectra. We noted that the consistent discrepancy between the M3 experimental spectra and best-fits of the 735-to-965 cm^{-1} band ratio, and this discrepancy has been attributed to the local acidic pH environment near the cell surface (See The contribution from NAD/NADH decreases with time in both cell lines as evidenced by the decreasing intensity of the 1030 cm^{-1} band.

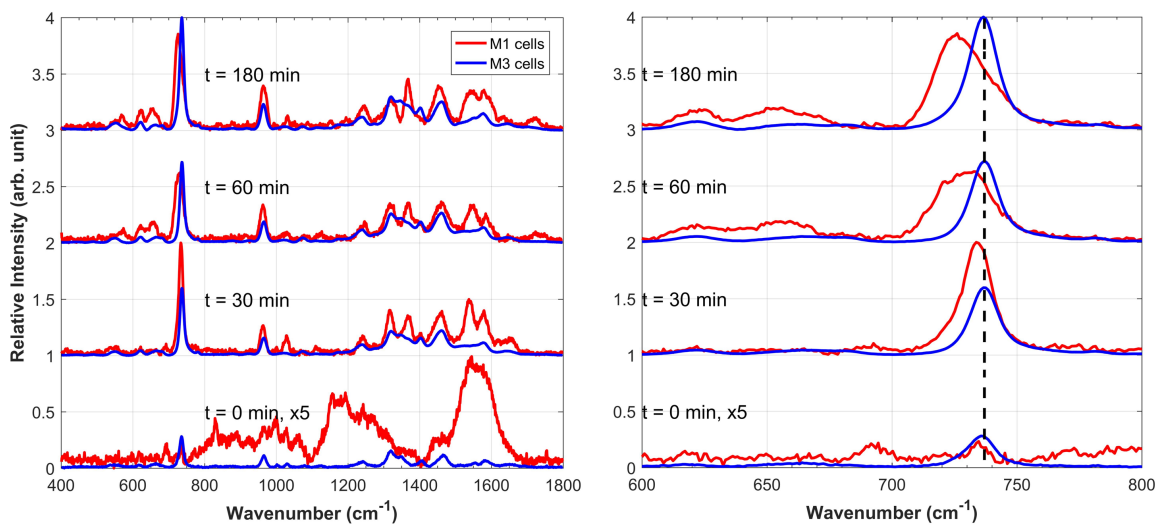


Figure 5-1 Side-by-side comparison of the SERS spectra of non-tumorigenic M1 cells (red) and invasive breast cancer cell M3 (blue) as function of time post-washing. The time-dependent red-shift of the 733 cm^{-1} band on M1 cells is contrasted with the M3 cells which show no red-shift in the zoom-in view on the right.

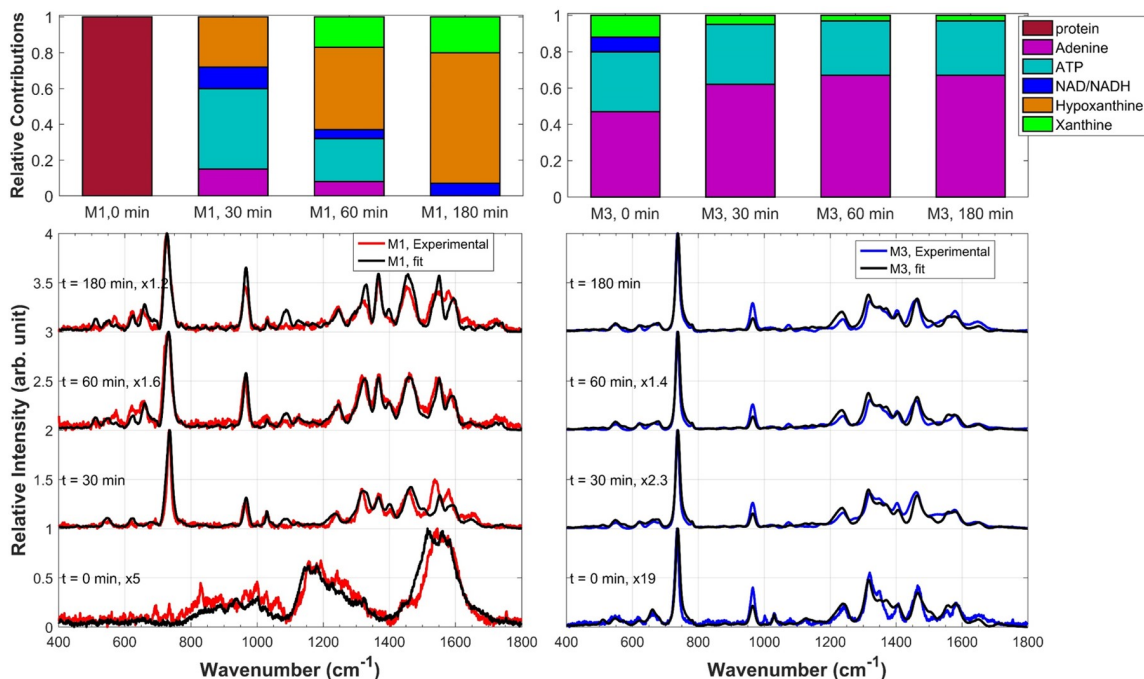


Figure 5-2 Best fits (black) resulting from linear combination of SERS spectra of four purines, NAD/NADH and protein for M1 and M3 cells at each time point are shown. The relative contributions of each molecular components are shown as bar graph on the top.

Although a larger database of cancer/normal cell combinations is needed to confirm the generality of this dynamical SERS effect, Figure 5-1 and Figure 5-2 demonstrate the new possibility of using a SERS platform to distinguish non-tumorigenic and cancer cells. From the data presented in Figure 5-1 it can be seen that two key SERS phenomena are the basis for distinction between non-tumorigenic and cancer cells. The first is that non-tumorigenic cells exhibit weak and broad spectrum which resemble features from protein aggregations (Chapter 4) initially after washing while the cancer cells always show relatively stronger and narrower spectral features. The second is that non-tumorigenic cells exhibit a time-dependent red-shift of the most intense band from centered on $\sim 733\text{ cm}^{-1}$ to $\sim 725\text{ cm}^{-1}$ while the cancer cells don't exhibit such time-dependent shifts. This red-shift corresponds to a change of ATP to hypoxanthine as the largest contributor to the SERS spectra. This time-dependent change occurs within 60 minutes post sample washing. Thus, monitoring SERS spectra of cells isolated from a biopsy sample for up to one hour after washing SERS can provide evidence of a distinction between cancer and normal cells without the need for antibody labeling.

In the next section, the possible biochemical origin of the presence of these purine metabolites is discussed. Specifically, the appearance of these purine metabolites as well as the observed time-dependent spectral change is related to the known purinergic signaling cascade that occurs at near-cell membrane extracellular region.

Extracellular purine molecules are purinergic signaling molecules

The action of purine and purine nucleosides/nucleotides as extracellular signaling molecules has long been recognized and appreciated. Burnstock *et al.* first described the

release of extracellular ATP as transmitter between non-adrenergic inhibitory nerves.¹⁶⁶ Burnstock's hypothesis was initially met with skepticism primarily because as the key energy source molecule, it seem unlikely for such important molecule to be present extracellularly for cell signaling purpose. Nevertheless, three decades later, following cloning and characterization of the ATP receptors expressed on cell membrane, purinergic signaling has been a well-established concept and has been applied to cancer research as well.¹⁶⁷ The role of extracellular ATP and adenosine, and purinergic signaling cascade in tumorigenesis progress has been extensively studied.^{168, 169, 170} Purines can be released by any cell types to the extracellular region,¹⁷¹ but the concentration of extracellular purines increase dramatically from nano-and pico-molar to micro-molar level when cells are under stress condition such as damage, inflammation, hypoxic and apoptosis.^{172, 173, 174} Thus it seems possible for the presence of extracellular purine molecules at concentrations detectable by SERS when the cells are placed in a nutrient-depleted environment which pose immense stress to the cells. Figure 5-3 summarized the typical routes of ATP release to near-cell membrane extracellular regions.

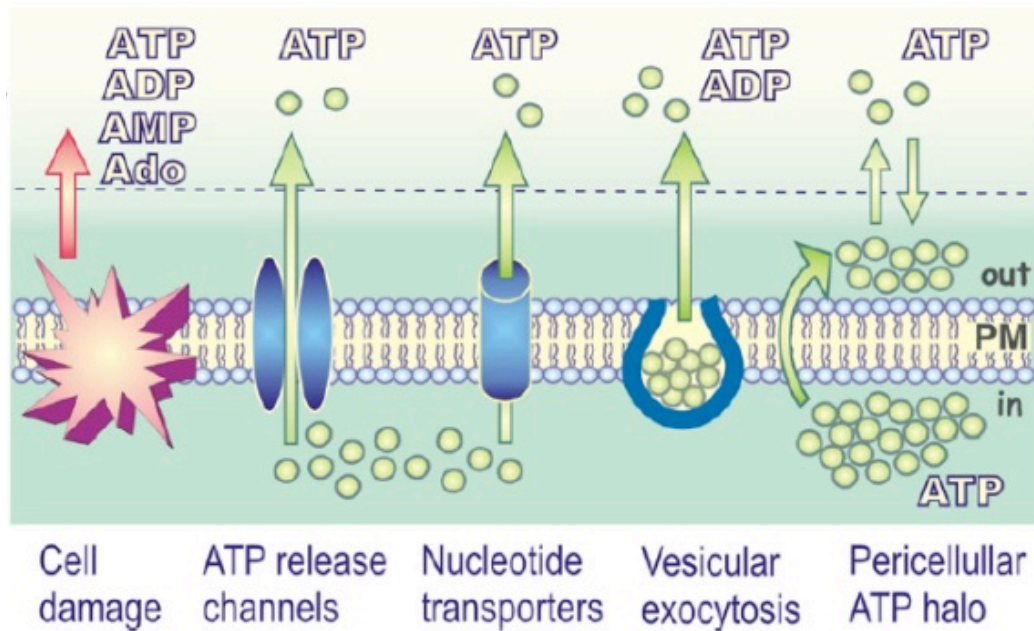


Figure 5-3 Summary of the non-lytic mechanism for release of ATP to extracellular region.¹⁷⁵

Since ATP and adenosine are powerful cell growth stimuli, their activity and extracellular concentrations are regulated by a series of ecto-nucleotidase on the cell outer membrane by either directing the import of these two molecules back to the cytoplasm or by subsequent conversion to purine bases such as hypoxanthine.¹⁷⁵ The inactivation mechanism of purinergic signaling cascade by the actions of ecto-nucleotidase is illustrated in Figure 5-4. Thus it seems possible that time-dependent ATP-to-hypoxanthine shift observed on the non-tumorigenic M1 cell (Figure 5-2) reflect this normal inactivation process when ATP are converted to hypoxanthine and subsequently xanthine. Furthermore, it can be anticipated that in cancer cells this inactivation mechanism is mutated or non-functioning,^{168, 169, 170} therefore the M3 cells are able to maintain relatively constant extracellular [ATP] concentration as evident from the bar graph on Figure 5-2. Hence the M3 cells can sustain constant growth signaling, one of the six hallmarks of cancer as described by Weinberg.¹⁴²

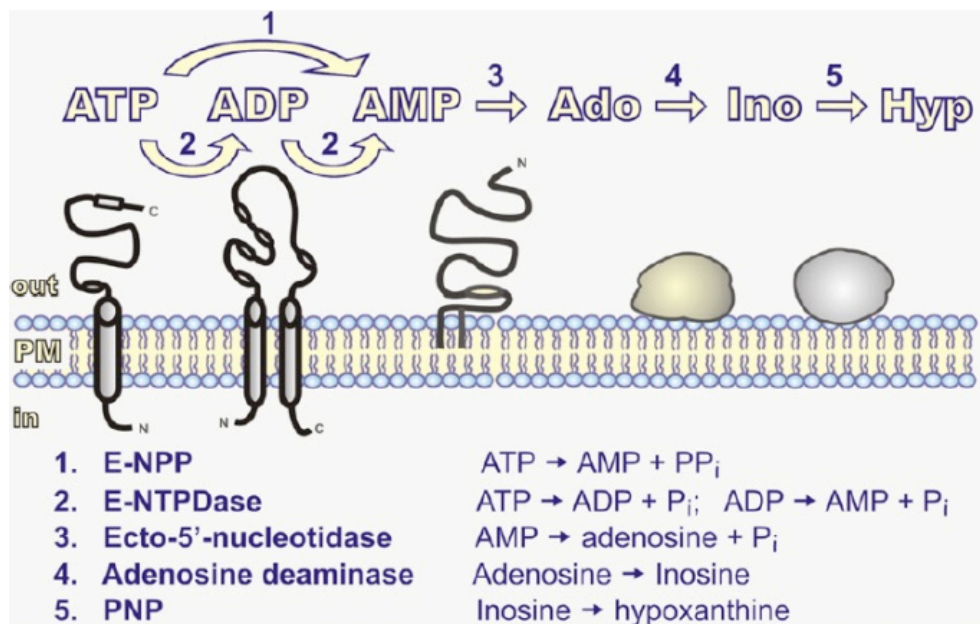


Figure 5-4 The inactivation mechanism of ATP purinergic signaling cascade by membrane-bound nucleotide converting-ectoenzymes.¹⁷⁵

5.5 - Conclusion and Future work

The results described in this chapter demonstrates the ability of the SERS platform to distinguish *in vitro* grown cancer and normal cell lines as well as the potential of SERS as novel bioanalytical probe for studying the purinergic signaling processes occurring at near cell membrane extracellular region. Two cell lines, non-tumorigenic mammary gland epithelial (M1) cells and invasive breast cancer (M3) cells, are studied using the gold substrate. These cells show similar spectral features as the bacterial spectra reported previously in our laboratories, and the main molecular contributor to the SERS spectra of these cell lines are found to be four purines, adenine, ATP hypoxanthine, and xanthine, and nicotinamide adenine dinucleotide (NAD/NADH). However several distinct SERS characteristics are found to be unique to these non-tumorigenic/cancer cells. These

includes the presence of the $\sim 1030\text{ cm}^{-1}$ band which is associated with the presence of NAD/NADH known to be elevated in cancer cells¹⁷⁶ and had only been previously observed on the fastidious bacterial species *N. gonorrhoeae*, and the decreasing contribution of NAD/NADH as a function of time post-washing. The most unique SERS characteristic to these normal/cancer cell lines are the red-shift of the most intense band from $\sim 733\text{ cm}^{-1}$ to $\sim 725\text{ cm}^{-1}$ which had not been observed previously in any of our bacterial SERS spectra or reported in the literature. This red-shift is due to the change of ATP to hypoxanthine as the largest SERS molecular contributor as a function of time post-washing. This time-dependent change is related to the conversion of ATP to hypoxanthine by the action of a series membrane-bound nucleotide converting-ectoenzymes. Moreover, this ATP-to-hypoxanthine time-dependent change is the most important SERS characteristic to distinguish non-tumorigenic M1 cells and cancerous M3 cells. The M1 cells display this ATP-to-hypoxanthine time-dependent change within 60 minutes post washing while the M3 cells don't show such a time-dependent change. By monitoring the SERS spectra of a sample for up to one hour after washing our SERS platform could provide a distinction between the M1 and M3 cells. The biochemical origin of these purine molecules is proposed to result from the molecules involved in extracellular cell signaling pathways. The purinergic signaling cascade is activated in cells are under stressful condition, and by placing the cells in a nutrient-depleted environment the cascade is activated and the concentration of extracellular purines increase dramatically. Since purine molecules especially ATP and adenosine are potent growth factor, their concentrations are regulated by series of ecto-nucleotidase on cell

membrane which can inactivate them by converting them to hypoxanthine and subsequently other free purine bases. Therefore it's possible the time-dependent ATP-to-hypoxanthine change observed on the SERS spectra of the M1 cells reflects this inactivation process, while in M3 cells the inactivation mechanism of the purinergic signaling cascade is defected or non-functioning and thus no such time-dependent change is observed. The results in this chapter demonstrate at least phenomenologically the ability of SERS to detect and identify *in vitro* grown cancer cells as well as the potential of the SERS platform for studying cancer metabolomics.

6. Conclusion

The results described here demonstrate the potential of SERS of living cells as a molecular disease diagnostic platform and as a probe for studying metabolomic activities that take place at near-cell extracellular region. When compounded with appropriate sample preparation and enrichment procedure, multivariate classification model for unknown prediction and portable instrument, SERS could provide rapid (<1 hour), sensitive and specific diagnostic of bacterial infections in body fluid and cancer cell identification without the requirement for the slow cell growth step. The basis of the use of SERS for rapid diagnostic is the multiplexing capability which allows simultaneous identification of different purine metabolites from the same spectrum. With the exception of *C. trachomatis* in which aggregated proteins are found to be key contributor to their SERS spectra, purine metabolites release to extracellular regions by the bacteria as response to starvation are the key SERS biomarker and serve as basis for strain

identification in unknown sample. In cancer cells, these purine are found to be release by the cells to extracellular as part of purinergic signaling cascade. The spectral differences on the gold and the silver SERS substrate of the same molecules as well as the time-dependent changes provides additional basis for bacteria and cancer cell identification. The ability of SERS to observe protein aggregates extends the applicability of SERS platform beyond disease diagnostics as a novel, powerful bioanalytical probe for the dynamic of protein structure in solution, which may be of value in protein therapeutic research for both safety and treatment efficacy reasons.

7. Supplementary Figures and Information

7.1 – SERS Diagnostic Platform: Urinary Tract Infection

Antibiotic	<i>E. coli</i>	<i>E. coli</i>	<i>E. coli</i>	<i>E. coli</i>	<i>E. coli</i>	<i>E. coli</i>	<i>K. pneu</i>	<i>K. pneu</i>
	BD 6594	BD 6640	BD 6757	BD 6880	BD 6909	BD 7023	BD 6908	BD 6914
Gentamicin	S	S	S	S	S	S	S	S
Tobramycin	S	S	S	S	S	S	S	S
Ertapenem	S	S	S	S	S	S	S	S
Meropenem	S	S	S	S	S	S	S	S
Cefazolin	S	S	R	S	S	S	S	S
Cefuroxime	S	S	S	S	S	S	S	S
Cefoxitin	S	S	R	S	S	S	S	S
Ceftazidime	S	S	S	S	S	S	S	S
Cefotaxime	S	S	S	S	S	S	S	S
Cefepime	S	S	S	S	S	S	S	S
Aztreonam	S	S	S	S	S	S	S	S
Ampicillin	S	S	S	S	S	R	R	R
Amox/Clav	S	S	S	S	S	S	S	S
Amp/Sulbactam	S	S	S	S	S	S	S	R
Ticar/Clav	S	S	S	S	S	S	S	S
Pip/Tazo	S	S	S	S	S	S	S	S
SXT	S	S	R	S	S	S	S	S
Nitofurantoïn	S	S	R	S	S	S	R	S
Ciprofloxacin	S	S	S	S	S	S	S	S
Levofloxacin	S	S	S	S	S	S	S	S

^a *Escherichia coli* (*E. coli*), *Klebsiella pneumoniae* (*K. pneu*)

^bS = susceptible, R = resistant

Table S-7-1 Gram-negative UTI Clinical Isolates ^{a,b}

Antibiotic	<i>S. sapro</i> BD 10257	<i>S. sapro</i> BD 10320	<i>E. faecalis</i> BD 10267	<i>E. faecalis</i> BD 10321
Gentamicin	S	S	R	R
Cefazolin	R	R	R	R
Cefoxitin	R	R	R	R
Ampicillin	R	R	S	S
Amp/Sulbactam	R	R		
Pip/Tazo	S	S	S	S
SXT	S	S	R	R
Nitofurantoin	S	S	S	S
Streptomycin			R	R
Levofloxacin	S	S	R	R
Penicillin G	R	R	S	R
Oxacillin	R	R	R	R
Vancomycin	S	S	R	R
Clindamycin	S	S	R	R
Erythromycin	R	S	R	R
Linezolid	S	S	S	S
Moxifloxacin	S	S	R	R
Rifampin	S	S	R	I
Minocycline	S	S	S	S
Tetracycline	S	S	S	S
Daptomycin	S	S	S	S

^a *Staphylococcus saprophyticus* (*S. sapro*), *Enterococcus faecalis* (*E. faecalis*)

^bS = susceptible, R = resistant, I = indeterminate

Table S-7-2 Gram-positive Clinical Isolates ^{a, b}

		Actual →												Class	Strain
		1	2	3	4	5	6	7	8	9	10	11	12		
Predicted →	1	10	0	0	0	0	0	0	0	0	0	0	0	1	<i>E. faecalis</i> BD 10267
	2	0	11	0	0	0	0	0	0	0	0	0	0	2	<i>E. faecalis</i> BD 10321
	3	0	0	9	0	1	0	0	1	0	0	0	0	3	<i>E. coli</i> BD 6594
	4	0	0	0	10	0	0	0	0	0	0	0	0	4	<i>E. coli</i> BD 6640
	5	0	0	0	0	13	0	0	0	0	0	0	0	5	<i>E. coli</i> BD 6757
	6	0	0	0	0	0	13	0	0	0	0	0	0	6	<i>E. coli</i> BD 6880
	7	0	0	0	0	0	0	19	0	0	1	0	0	7	<i>E. coli</i> BD 6909
	8	0	0	2	0	0	0	0	9	0	0	0	0	8	<i>E. coli</i> BD 7023
	9	0	0	0	0	0	0	0	0	10	1	0	0	9	<i>K. pneumoniae</i> BD 6908
	10	0	0	0	0	0	0	0	0	1	13	0	0	10	<i>K. pneumoniae</i> BD 6914
	11	0	0	0	0	0	0	0	0	0	0	13	0	11	<i>S. saprophyticus</i> BD10257
	12	0	0	0	0	0	0	0	0	0	0	0	13	12	<i>S. saprophyticus</i> BD10320

Table S-7-3 PLS-DA classification confusion table results for the cross validation model treatment of the SERS spectra of 12 UTI causative clinical isolates.

Modeled class	Sensitivity	Specificity	Class. err.
<i>E. faecalis</i> BD 10267	100.	100.	0.0
<i>E. faecalis</i> BD 10321	98.7	99.4	1.9
<i>E. coli</i> BD 6594	83.5	98.4	7.2
<i>E. coli</i> BD 6640	99.0	99.3	0.3
<i>E. coli</i> BD 6757	92.9	100.	3.5
<i>E. coli</i> BD 6880	100.	100.	0.0
<i>E. coli</i> BD 6909	100.	99.5	0.2
<i>E. coli</i> BD 7023	83.3	97.9	9.4
<i>K. pneumoniae</i> BD 6908	100	99.3	0.4
<i>K. pneumoniae</i> BD 6914	92.7	97.5	4.8
<i>S. saprophyticus</i> BD 10257	100.	100.	0.0
<i>S. saprophyticus</i> BD 10320	100.	100	0.0
Average	95.8	99.3	2.3

Table S-7-4 PLS-DA classification sensitivity and specificity for twelve UTI bacteria SERS spectra.

Bacterial strain	ad	hx	xan	gu	ua	AMP	gs
<i>E. faecalis</i> BD 10267	0.70	0.0	0.0	0.0	0.08	0.08	0.14
<i>E. faecalis</i> BD 10321	0.69	0.08	0.0	0.0	0.0	0.08	0.15
<i>E. coli</i> BD 6594	0.07	0.55	0.20	0.18	0.0	0.0	0.0
<i>E. coli</i> BD 6640	0.0	0.56	0.29	0.15	0.0	0.0	0.0
<i>E. coli</i> BD 6757	0.08	0.30	0.15	0.29	0.12	0.0	0.06
<i>E. coli</i> BD 6880	0.03	0.53	0.31	0.07	0.06	0.0	0.0
<i>E. coli</i> BD 6909	0.0	0.63	0.18	0.18	0.01	0.0	0.0
<i>E. coli</i> BD 7023	0.05	0.53	0.21	0.21	0.0	0.0	0.0
<i>K. pneumoniae</i> BD 6908	0.0	0.28	0.0	0.0	0.0	0.0	0.72
<i>K. pneumoniae</i> BD 6914	0.0	0.21	0.0	0.0	0.0	0.0	0.79
<i>S. saprophyticus</i> BD 10257	0.44	0.05	0.13	0.10	0.23	0.0	0.05
<i>S. saprophyticus</i> BD 10320	0.76	0.08	0.0	0.08	0.0	0.08	0.0

ad = adenine, hx = hypoxanthine, xan = xanthine, gu = guanine, ua = uric acid, AMP, gs = guanosine

Table S-7-5 Relative contribution of purine components to UTI bacteria SERS spectra

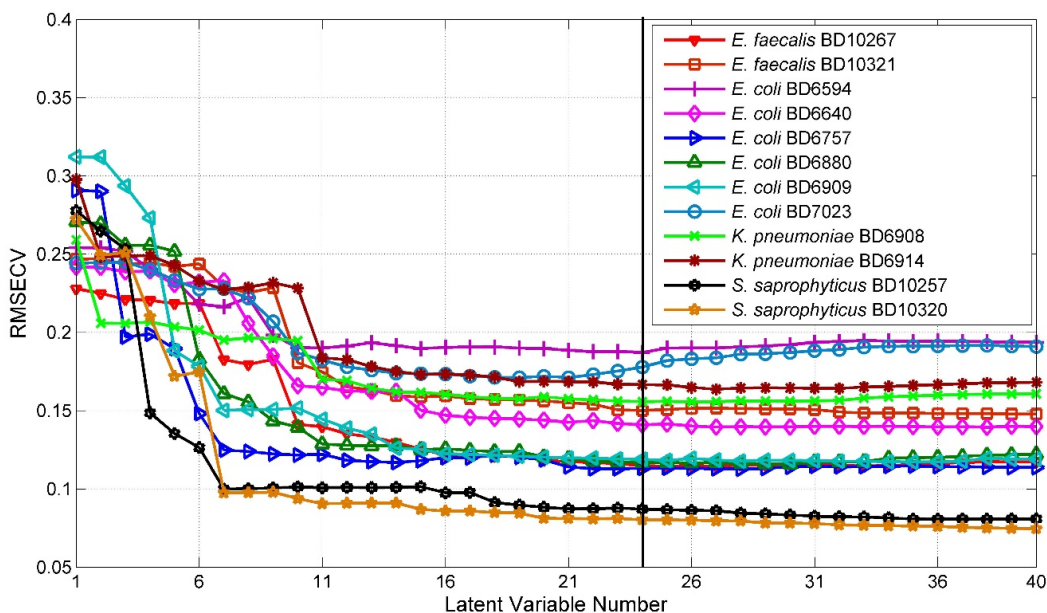


Figure S-7-1 Plot of the PLS-DA classification cross validation root mean square error (RMSECV) as a function of the number of latent variables (LV) selected. 24 LVs was selected for this treatment because this number corresponded to a minimum in the RMSECV.

7.2 - SERS Diagnostic Platform: Sexually Transmitted Disease

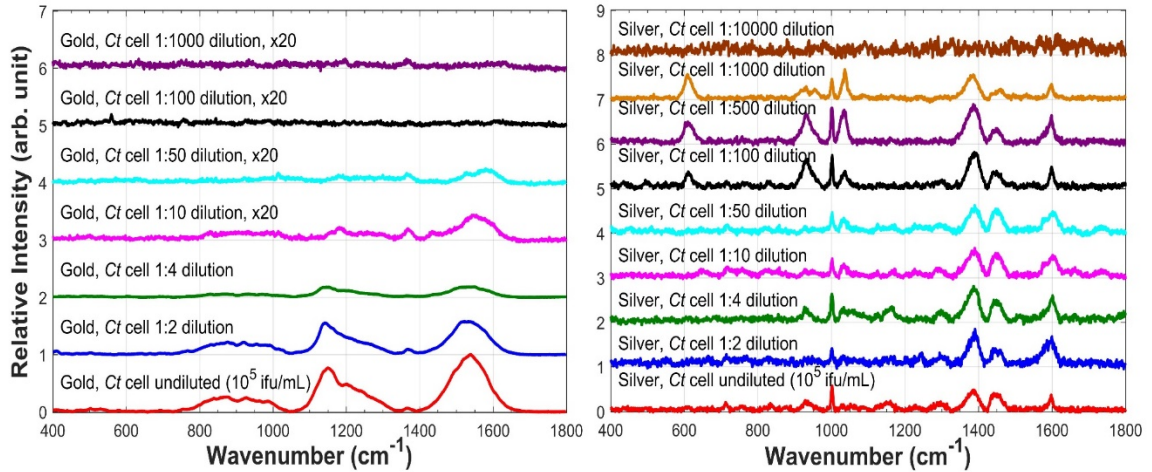


Figure S-7-2 Sensitivity of *C. trachomatis* (*Ct*) on gold and silver SERS substrate at $t = 0$ min (right after sample processing). The initial concentration of elementary body is determined by titer to be $\sim 10^5$ ifu/mL. The lowest concentration of EB to yield SERS signal on gold is determined to be $\sim 5 \times 10^4$ ifu/mL and $\sim 10^2$ ifu/mL on silver.

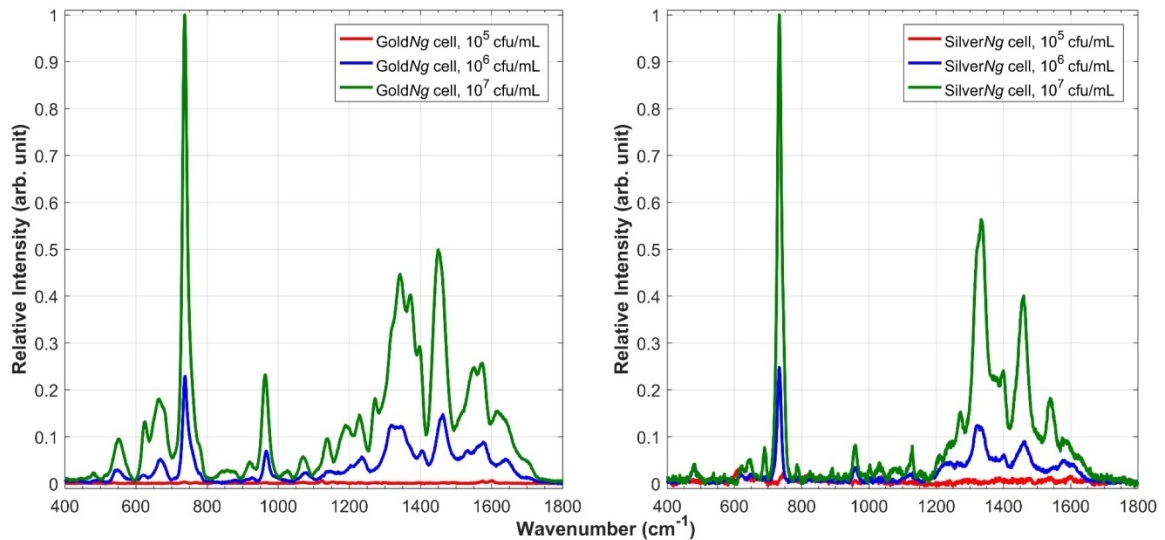


Figure S-7-3 Sensitivity of *N. gonorrhoeae* (*Ng*) on gold and silver SERS substrate at $t = 60$ minutes post sample processing. The initial concentration of *Ng* is determined by serial dilution and overnight cell culture to be $\sim 10^7$ cfu/mL. The lowest concentration of bacterial cell to yield SERS signal is $\sim 10^6$ cfu/mL on both metals.

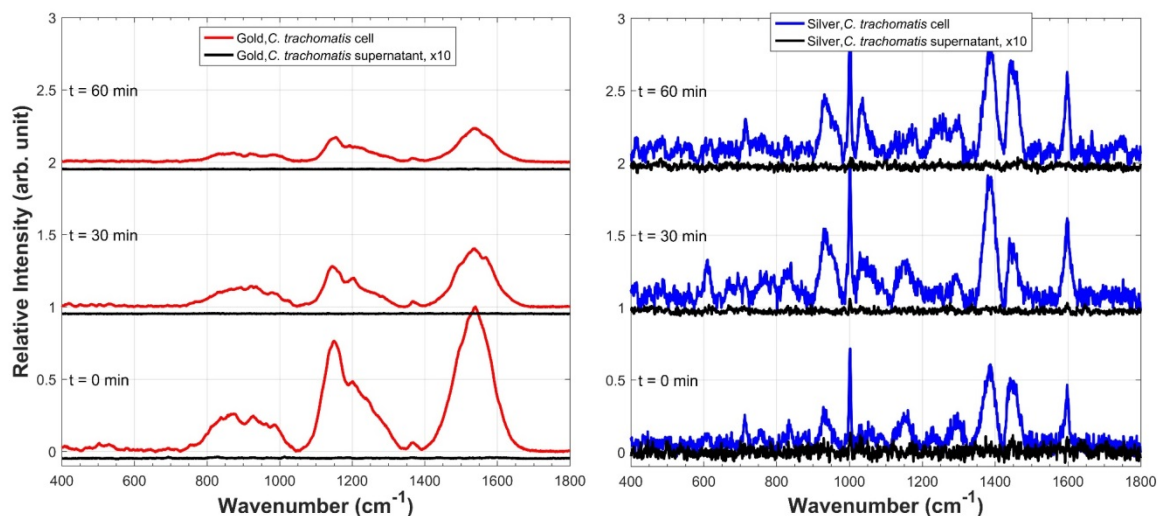


Figure S-7-4 Gold and silver SERS spectra comparing the signal from *C. trachomatis* cell and from the unfiltered supernatant fluid around the cell as a function of time post sample processing. On both metals the SERS molecular contributors are always found on the cell, hinting the identity of the SERS molecular contributors to be of cell membrane components.

7.3 - SERS Diagnostic Platform: Cancer Cell Detection

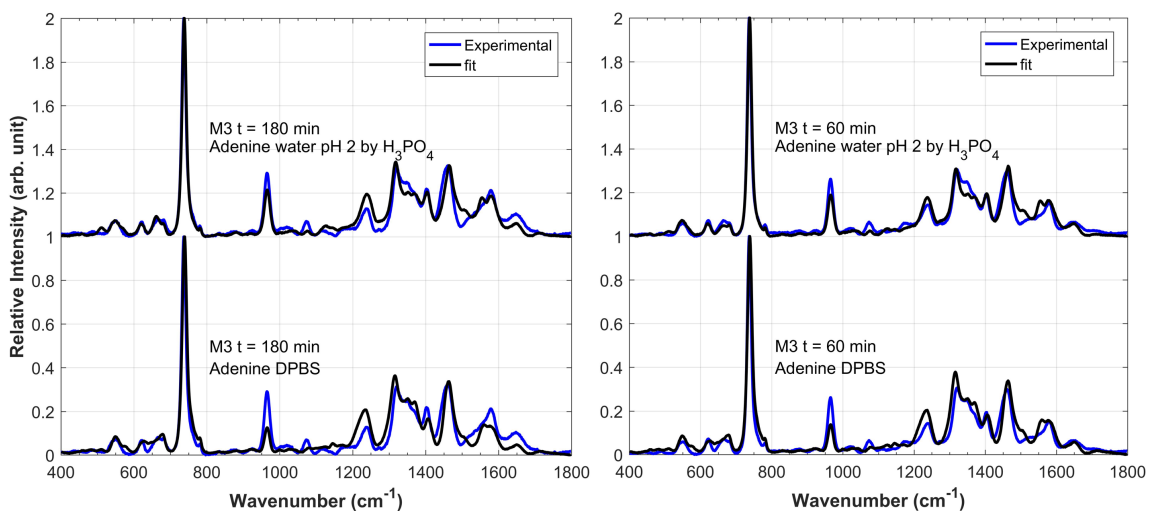


Figure S-7-5 SERS spectral features are strongly affected by the local pH environment on the M3 cells. Comparing the best-fits calculated using adenine in DPBS (pH 7.0 – 7.6) vs adenine at acidic pH as compared to the experimental data for the M3 60 minutes and 180 minutes spectra show improvements on the 735-to-965 cm^{-1} ratio as well as the features from 1300-1400 cm^{-1} region.

M1 cells (non-tumorigenic)						
Time point	protein	adenine	ATP	NAD/NADH	hypoxanthine	xanthine
t = 0 min	1.00	0.00	0.00	0.00	0.00	0.00
t = 30 min	0.00	0.15	0.45	0.12	0.28	0.00
t = 60 min	0.00	0.08	0.24	0.05	0.46	0.17
t = 180 min	0.00	0.00	0.00	0.07	0.73	0.20
M3 cells (cancer)						
t = 0 min	0.00	0.47	0.33	0.08	0.00	0.12
t = 30 min	0.00	0.62	0.33	0.00	0.00	0.05
t = 60 min	0.00	0.67	0.30	0.00	0.00	0.03
t = 180 min	0.00	0.67	0.30	0.00	0.00	0.03

Table S-7-6 Relative contribution of molecular components to M1 and M3 SERS spectra at each time point.

7.4 - Modeling compound SERS spectra

In water

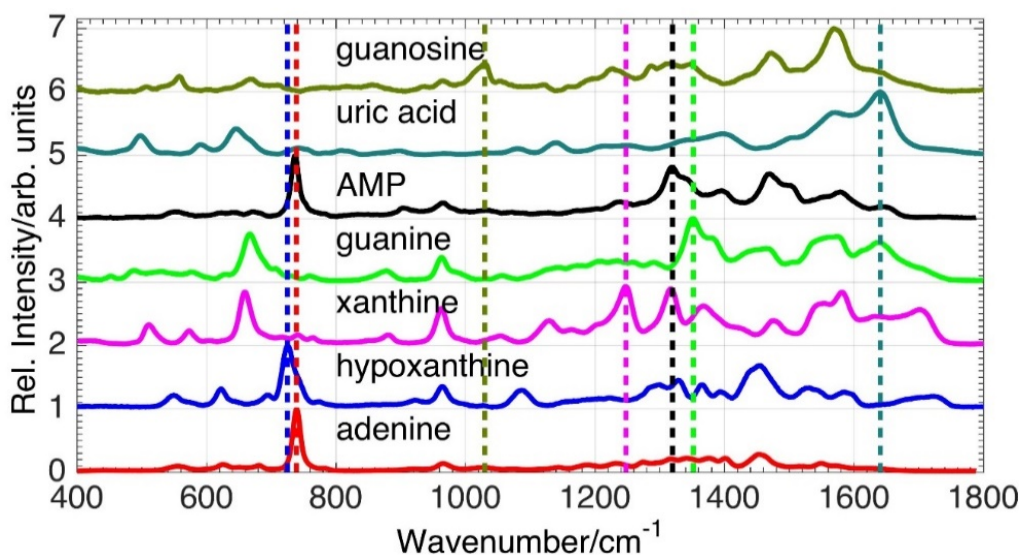


Figure S-7-6 Normalized SERS spectra on gold substrate for seven purine compounds found contributing to the twelve UTI bacterial spectra. The vertical dash line correspond to a unique peak in the SERS spectrum of each purine that help to identify this molecular contribution to the bacterial SERS spectrum.

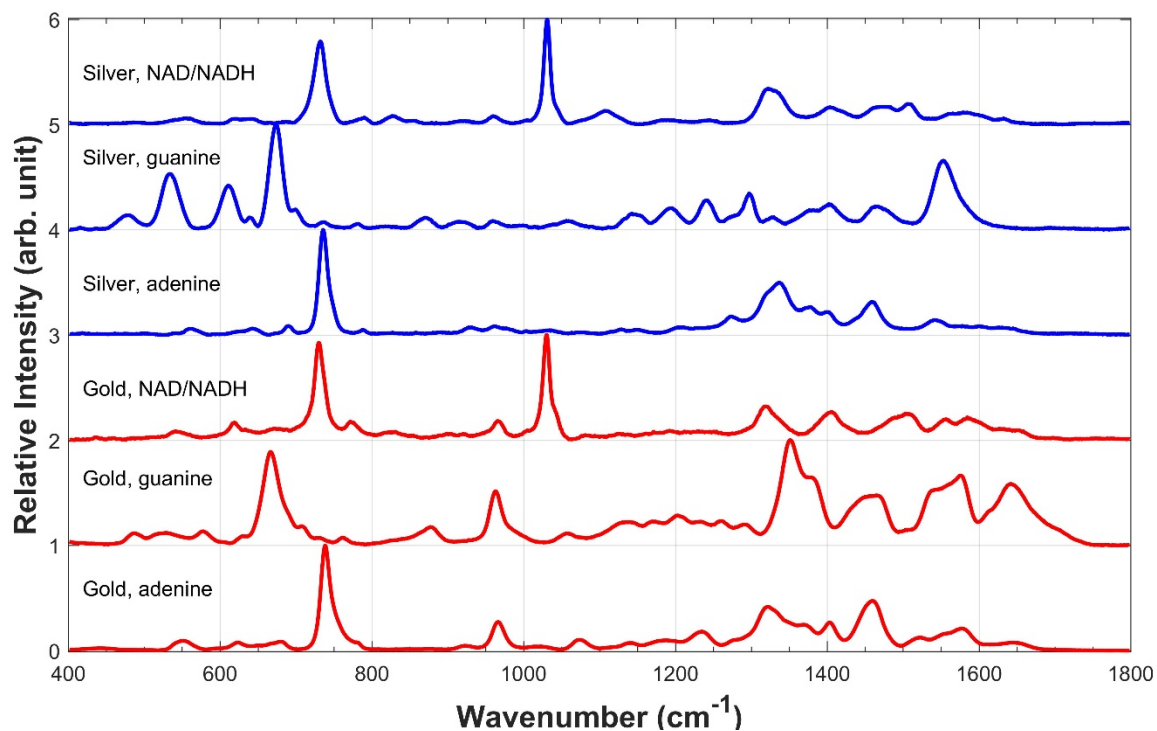


Figure S-7-7 Normalized SERS gold (red) and silver (blue) spectra of the three purine molecules found to be the components of the SERS spectra of *N. gonorrhoeae*.

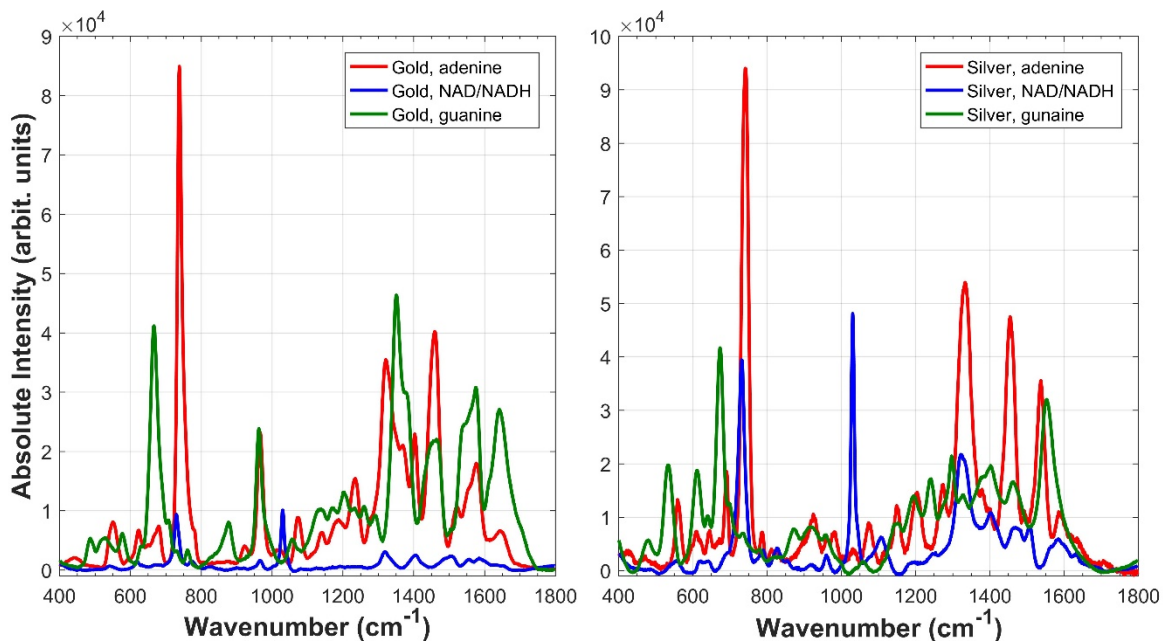


Figure S-7-8 The absolute intensity of adenine, NAD/NADH and guanine found in *N. gonorrhoeae* spectra are shown here on the gold and the silver substrate.

In DPBS

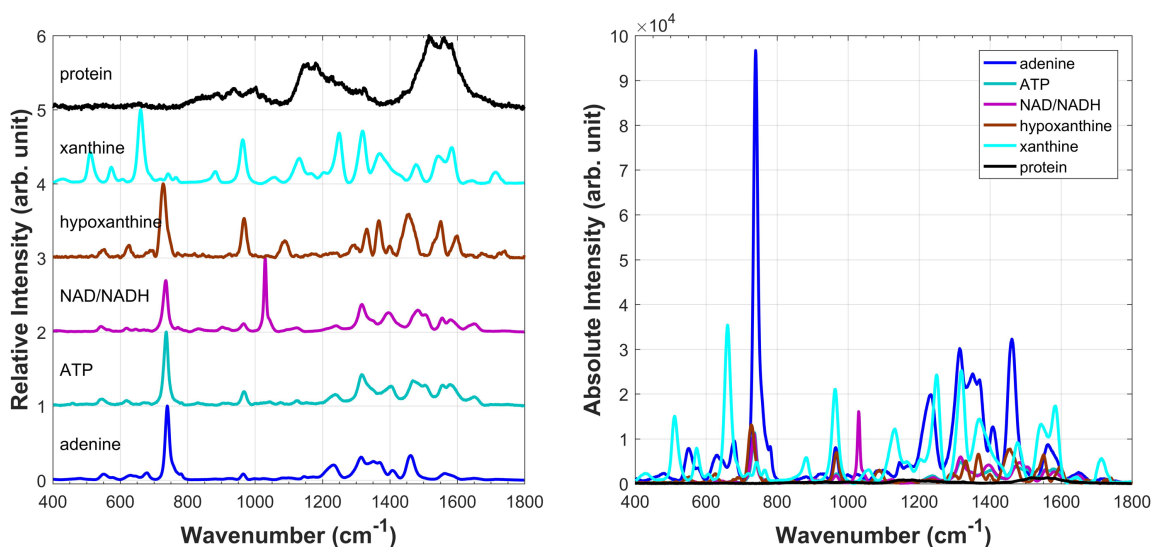


Figure S-7-9 Normalized (left) and baselined (right) SERS spectra on gold substrate of molecular components (four purines, protein and NAD/NADH) found contributing to the SERS spectra of M1 and M3 cells.

8. Appendix

8.1 - General laboratory cultivation guideline for vegetative bacteria

Agar medium most bacteria can be cultured easily on trypticase soy agar, nutrient agar, or LB agar from frozen culture. It's recommended the agar medium to be prepared according to manufacture instruction fresh before bacterial culture and stored at 4 °C for no more than one week. The bacteria should be plated and allowed to grow on the agar plate overnight at 37 °C.

Broth medium common broth media for bacterial culture include trypticase soy broth (TSB), nutrient broth (NB) or Luria broth (LB) unless otherwise specified. It's recommended the broth medium to be prepared in sterile 100 mL flask and autoclaved at 121 °C for 30 minutes before use. The prepared broth medium can be stored at 4 °C for

up to two weeks. 10-20 mL broth medium in sterile test tube covered by aluminum foil is used to culture bacteria that have been grown on the agar medium. One to two bacteria colonies are aseptically removed from the agar plate by sterile loop and add to the medium. The medium should be incubated overnight at 37 °C. After that 10-20 µL overnight growth is inoculate into 10-20 mL fresh broth medium and incubate at 37°C for 5-6 hours or until specific optical density ($OD_{600\text{ nm}}$) is reached. This allows the bacteria population to reach vegetative state during which they are most metabolically active. The optimal duration of incubation should be determined for each strain vial serial dilution (see next section).

Frozen sample preparation skim milk is used as medium to prepare frozen bacterial sample. The skim milk should be prepared fresh and stored at 4 °C for up to one week. Cryogenic tubes (Corning®, 1.5 mL) should be sterilized at 121 °C before used. After the bacteria have grown to vegetative state, the broth medium is spin down at 10,000 rpm for 5 minutes to collect all bacterial cells. The cell pellet is re-suspend in 1 mL skim milk in the cryogenic tube and vortex vigorously to ensure bacterial cells are well-mix with skim milk. The cryogenic tube is stored at -80 °C or vapor phase of liquid nitrogen.

8.2 - Quantitation of Bacterial Cells by Serial Dilution

Overnight cell culture is the only method to quantitatively determine the amount of live bacterial cells in a sample (in the unit of colony forming unit, cfu/mL). Serial dilution of the bacterial sample is needed before inoculate onto plate medium. The

procedure is following

1. Starting with 1 mL bacterial sample, dilute the sample 10-fold each time with 9 mL freshly prepared, sterilized, double-filtered saline aseptically until reaching 10^{-6} original concentration, i.e. perform dilution six times.
2. Transfer 0.5 mL 10^{-6} on agar plate with sterile pipette.
3. Spread the bacteria evenly on the plate with sterilized glass beads. Discard the beads in 10% bleach afterward and incubate the agar plate at 37 °C overnight.
4. Count the number of colonies on the agar plate after incubation.

of colonies on the plate x 10^6 (dilution factor) / 0.5 mL = cfu/mL

8.3 - Special Laboratory Cultivation Guideline for *Neisseria gonorrhoeae*

Neisseria gonorrhoeae are fastidious Gram-negative bacteria that require supplementary nutrient in addition to conventional bacteriological medium. In addition, *Neisseria gonorrhoeae* also needs to be grown in 5% CO₂ with constant shaking.

Material:

Agar medium: BD® BBL™ Prepared Chocolate II Agar (GC II agar with hemoglobin with IsoVitaleX®) purchased from Fisher Scientific®.

Broth Medium: Prepare Solution A and Solution B separately in clean, sterile flask. Autoclave Solutions A and B separately at 121 °C for 20 minutes. Allow both solutions to cool to 50 °C in water bath. Aseptically add Solution B to Solution A and mix very well.

Rehydrate 2.0 mL IsoVitaleX® according to package instructions and add aseptically to the mixture. After preparation the broth medium can be stored at 4°C for up to one week.

Solution A contents	Amount (grams)
Proteose Peptone #3	3.0
Corn Starch	0.2
Dipotassium Phosphate (K ₂ HPO ₄)	0.8
Monopotassium Phosphate (KH ₂ PO ₄)	0.2
Sodium Chloride (NaCl)	1.0
DI water	100 mL
<hr/>	
Solution B contents	Amount (grams)
Dried Bovine Hemoglobin	2.0
DI water	100 mL

The bovine hemoglobin is soluble in water, however they aggregate after autoclave. Therefore the growing bacteria will bind to the protein aggregates and makes separation difficult. As such it's recommended to follow the cultivation steps below.

Preparation of stock sample of *N. gonorrhoeae* from lyophilized sample:

1. In a sterile flask, aseptically transfer 20 mL broth medium. Add the lyophilized bacteria pellet to the broth medium. Allow rehydration for 48 hours.
2. After 48 hours, inoculate three GCII plates with 10 uL broth medium each. Incubate for 20 hours with 5% CO₂ at 37 °C.
3. Prepare skim milk storage medium according to the manufacturer instruction. Autoclave for 20 minutes at 121 °C. Prepare three Corning® cryopreservation tubes with 1 mL sterilized skim milk.
4. Aseptically strip off all bacteria colonies from the plate and transfer to the cryopreservation tube (One plate per tube) with skim milk. Vortex the cryopreservation tubes vigorously for about 10 seconds. Store the tubes at liquid nitrogen vapor phase.

Laboratory cultivation of N. gonorrhoeae from stock sample

N. gonorrhoeae (FA1090) is obtained from ATCC®. The broth medium to grow this bacteria strain is 814 broth medium supplement with bovine hemoglobin and IsoVitaleX® (BD®). However, we found that the hemoglobin in the broth medium aggregates and precipitate out of the broth medium after sterilization. When using this broth medium to grow the bacteria, it's almost impossible to completely separate the bacterial cells from the hemoglobin aggregation by centrifugation. To solve this problem we decided to grow the bacteria on the GC II agar and harvest them by stripping them off the plate with sterilized loop. After several rounds of trial and error we develop a reliable procedure to yield log-phase *N. gonorrhoeae* that produce robust signal on our SERS substrate using combination of the broth medium and the GC II agar. First the bacteria are grown on a GC II plate from frozen stock sample overnight at 37 °C with 5% CO₂. Then three to four colonies from the plate is removed with sterilized loop and inoculate into a sterile flask containing 20 mL broth medium. The bacteria is allowed to grow in the broth medium with constant shaking for 20 hours at 37 °C and 5% CO₂. After that, one loop (~ 10 µL) is used to inoculate onto a fresh GC II agar plate and incubate for 18 hours at 37 °C and 5% CO₂. The bacteria cell are harvested from the agar plate by stripping the colonies off the plate with sterilized loop.

8.4 - *In vitro* cultivation for non- LGV serovar *Chlamydia trachomatis*

Introduction

Chlamydia species are Gram-negative, obligate intracellular bacteria which require a mammalian epithelial cell for proliferation and survival. Therefore, it cannot be cultivated with conventional bacteriological broth medium. This property of *Chlamydia* species is the reason why laboratory cultivation for this species is expensive, difficult and labor-intensive. Up until 1965, *Chlamydia* species cultivation is done through passage in the yolk sack of the embryonated hen egg. Since then several mammalian epithelial cell lines are found eligible for *Chlamydia trachomatis* proliferation, making possible for cultivation and isolation of large quantity of *Chlamydia* possible. The procedure describes here use McCoy cell (ATCC® CRL-1696) as host cell line.

Chlamydia trachomatis species is consisted of 15 serovars dividing into three different biovars. All *Chlamydia trachomatis* serovars are Biosafety Level 2 pathogen, with the exception of the LGV serovars which requires Biosafety Level 3 facilities.

Serovars	Biovars/diseases causing
Ab, B, Ba, C	Trachomatis – the leading cause of preventable blindness in developing countries ⁶⁴
D, E, F, G, H, I, J, K	Causing sexually transmitted diseases, including pelvic inflammatory disease, infertility, ectopic pregnancy, neonatal pneumonia and neonatal conjunctivitis ^{60,63}
L1, L2, L3	Lymphogranuloma venereum (LGV)

As different serovar requires different incubation time as well as dilution ratio, it's up to the researcher to determine the ideal ratio for each serovar. This protocol describes procedure for *Chlamydia trachomatis* Serovar D (ATCC® VR-885). Description for

cultivation of the LGV serovars will be included at the end of this section. For more general information, please refer to ATCC® guideline and literature [177].

In vitro Cultivation of *Chlamydia trachomatis* is consisted of three main stages: the growth of host cell, infection by *Chlamydia*, and isolation and storage of elementary body (EB). For Serovar D, this process takes approximately eight days, with 72-96 hours of infection time depends on the concentration of EB inoculated. It's worth-noting that the inclusion bodies cause by Serovar D are much smaller than those by the LGV strains, and a much higher (some protocol reported 10:1) inoculum to host cell ratio is required to create a decent yield of EB. Therefore it's up to the researcher to determine the exact harvest time depends on the growth and size of inclusion body.

Material - Stage 1

Minimal Essential Medium (MEM) supplemented with 10% fetal bovine serum (FBS), Dulbecco Phosphate Buffered Saline (DPBS), trypsin-EDTA, T75 cell culture flask. Low-speed bench-top centrifuge. Additional sterilized centrifuge tubes or micro-centrifuge tubes

- MEM can be purchased from various vendors such as ATCC® or Life Technologies®. However the FBS MUST be purchased from ATCC®, as they are certified to not containing any inhibitory factors for *Chlamydia* growth. The researcher also need to vigorous monitor the growth of *Chlamydia* to ensure the absence of inhibitory factors.
- Since *Chlamydia* is a bacteria, Penicillin-streptomycin (Penn-Strep) or any antibiotic SHOULD NOT be added to the growth medium.

Material - Stage 2

Dulbecco's Minimal Essential Medium (DMEM) with 10% FBS supplement with 1 µg/mL cycloheximide, Sucrose/phosphate/glutamate buffer (SPG) or Hask Balanced Salt Buffer (HBSS), low-speed bench-top centrifuge. Intermediate (x30,000g) centrifuge with refrigerated unit (located on EBR701 or LSEB 6th floor), 10x Diethylaminoethyl-dextran (DEAE-Dextran) in HBSS buffer (final concentration needed, 45 µg/mL). Platform rocker. Inverted microscope (10x and 25x objective), Sterilized Nalgene® centrifuge tube and micro-centrifugation tube, pipette tips.

- HBSS is commercially available and can be used in exchange of SPG. The receipt for SPG is attached at the end of this section.

Material - Stage 3

Sterilized Nalgene® centrifuge tube, 50 mL centrifuge tube and 0.5 mL micro-centrifuge tube, ice-cold HBSS buffer, ice, 1 liter 10% bleach and 70% ethanol in spray bottle.

Procedure

* Stage 1 procedure is essentially the growth and maintenance of the McCoy cell. Refer to Appendix 8.5 - Common tissue culture protocols

Stage 1 - Day 1

1. Seed one McCoy cell stock sample (usually contain $\sim 10^6 - 10^7$ cell/mL) in two T75 flasks. Use 7 mL of DMEM with 10% FBS on each flask. Incubate the flasks at humidified 37 °C incubator with 5% CO₂.

Stage 2 - Day 2

1. Replace the medium with 7 mL fresh complete growth medium.

2. Check confluency under microscope, trypsinized the cell layer to prepare a frozen sample if necessary. Label name, date and cell count results on the container.

Stage 3 - Day 3

1. Check confluency. The desire coverage is 90% - 95%. Trypsinize the cell layer and re-seed back to the flask.
 - This ensure the cell are most viable and metabolically active during infection.
2. Prepare for infection tomorrow. Prepare MEM with 10% FBS and 1 $\mu\text{g}/\text{mL}$ cycloheximide. Prepare and sterilized SPG or use HBSS. Prepare 10x DEAE-dextran in HBSS (i.e. 450 $\mu\text{g}/\text{mL}$). Kept all reagents, medium and centrifuge tubes cold.

Stage 2 - Day 4

1. Final check of cell confluency and viability. Make note of anything unusual.
2. Warm up HBSS and 10x DEAE-dextan in 37 °C water bath. Keep the cap away from the water to avoid contamination. Diluted 10x DEAE-dextran to final concentration (45 $\mu\text{g}/\text{mL}$) with HBSS.
3. Remove growth medium from flask. Rinse the cell layer twice with 10 mL HBSS.
4. Add 5 mL diluted DEAE-dextran to the cell layer. Incubate at room temperature for fifteen minutes.
 - Treating the cell layer with the positively-charged DEAE-dextran can neutral the negative charges on the cell surface, allowing EB to enter easier. As such it's normal that after the treatment some cells (especially on the edges of the flask) fall off from the container wall.

5. Remove the DEAE-dextran. Rinse the cell layer with 10 mL HBSS.
6. Remove one *Chlamydia* stock sample (100 μ L) from the -80 °C freezer. Quickly thaw at 37 °C water bath.
 - *Chlamydia* EB lost viability rapidly at warm temperature. Thaw in < 1 minute.
7. Transfer the stock sample to 7 mL DMEM/10% FBS/cycloheximide. Gently lay the medium over the cell layer.
 - All contaminated disposable container and pipettes must be treated with 10% bleach overnight before disposed in biohazard waste box. Make sure to coat all surfaces with bleach.
8. Place the cell flask on the platform rocker. Rock the cell flask for three hours at room temperature at minimal speed.
 - To avoid contamination, cap the flask tight and seal it with parafilm. Make sure to cover the filter opening.
9. Incubate the cell flask at humidified 37 °C incubator with 5% CO₂.

Stage 2 - Day 5-7

1. Monitor formation and size of inclusion body daily under microscope. Pay close attention to anything unusual (medium color, turbidity, etc). In general the harvest window for this serovar lies between 72-96 hours. (Insert cell image from 24 hrs, 48 hr, 72 hrs).
2. Preparation for harvest (done by the night before harvest)
 - Check all necessary reagents. They must be stored in cold until use.
 - Sterilize necessary containers: pipette tips, centrifuge tubes, micro-centrifuge

tubes and glass beads. Kept sterilized containers sealed and cold until use.

Stage 3 – Day 8 (harvest)

Preparation: Pre-cool bench-top centrifuge and intermediate centrifuge (ERB) to 4 °C. Obtain ice in Styrofoam box. Prepare 500 mL 10% bleach and set aside. Spray in two 50 mL centrifuge tubes, two sterilized Nalgene® centrifuge tubes, dozen sterilized micro-centrifuge tubes, glass beads and 50 µL pipette tips.

* Since *Chlamydia* EB lose viability at room temperature without host cell, it's recommended that total harvest time (exclude the centrifuge time) should be less than 10 minutes. All reagents and containers in contact with the EB should be cold or kept in ice until use, and coat with 10% bleach thoroughly and left overnight before disposal.

1. Remove cell flask from incubator. Final check cell condition and inclusion body size under microscope.
2. Transfer 10-15 glass beads to one of the 50 mL centrifuge tube.
3. Add the beads to flask. Shake vigorously.
- Most host cells will rupture and detached from the flask wall under the mechanical forces of the glass beads.
- The presence of FBS in the medium will cause formation of large amount of foam in the container. Pay extreme caution not to cross-contaminate as the foam contains EB.
4. Transfer the content in the flask to the 50 mL centrifuge tube (including the foam). Immediately submerge the centrifuge tube in ice.
5. Using a new pipette each time, wash the glass beads and the container wall with 5 mL HBSS. Add the content to the other 50 mL centrifuge tube.

6. Centrifuge both 50 mL centrifuge tubes at x 500g for 15 minutes at 4 °C. Make sure to balance by adding HBSS.
7. Decant the liquid to a sterile Nalgene® centrifuge tube. Careful not to disturb the cell debris at the bottom of the tube. Submerge the Nalgene® tube in ice in the Styrofoam box. Fill the other Nalgene® tube with HBSS for counterweight.
8. Bring the Styrofoam box to ERB701. Centrifuge at x 30,000 g for 30 minutes with breaks off.
9. Carefully remove the centrifuge tube from the instrument. Note the small white pellet near the bottom of the tube. This is the EB/RB mixture. Submerge the tube in ice and brought back to the lab.
- Since this is a shared facility which is highly prone to cross-contamination, it's not recommended to open the container even under the bio-hood there.
10. In the hood, carefully decant the liquid to 10% bleach without disturbing the pellet.
11. Using a new pipette, add 1 mL ice-cold HBSS to the side opposite to the pellet. Gently tilt the tube several times so pellet can be washed by the HBSS. Decant the HBSS and use a 50 µL pipette to remove any remaining HBSS.
12. Depends on the size of the pellet, add 200 – 500 µL ice-cold HBSS to the tube. Use a 50 µL pipette to disperse the pellet. Can vortex in addition.
13. Aliquot into 0.5 mL micro-centrifuge tubes with 100 µL each. Label date and name.
14. Store the micro-centrifuge tubes in -80 °C freezer.

15. Coat all containers and pipettes with 10% bleach and left overnight. Wipe down the hood surface with 70% ethanol.

Stage 3 – Day 8 (re-infect)

If subsequent growth is required to obtain more EB, Step 7-14 can be omitted. Instead, at Step 5 use 5 mL ice-cold DMEM/10%FBS/cycloheximide instead of HBSS to wash the glass bead and the container wall and add to 50 mL centrifuge tube. Centrifuge at x500g for 15 minutes. Use the liquid to infect a fresh layer of McCoy cell follow the procedure in **Stage 2 – Day 4**. Note that the working volume limit for T75 flask is 15 mL.

Procedure for cultivation of the LGV serovars

The cultivation of the LGV serovars is essentially the same as described above except two notable difference. First, pre-treatment of the host cell with DEAE-dextran is not needed because the infectivity of LGV serovars are much higher than the non-LGV ones. Cycloheximide may not be needed. Second, the incubation time for EB is much shorter – 28-36 hours instead of 72-96 hours. The inclusion body size is also much larger than the non-LGV ones.

8.5 - Common tissue culture protocols

Contrast to cultivation of vegetative bacterial cells which can happen through suspension in liquid broth medium, almost all mammalian cell must anchor on a suitable surface for proliferation. Cell suspension in liquid medium is indication of cell lysed and death. Therefore agitation or shaking should be avoided to prevent cells from detach from the cell culture container surface. It's recommended to use tissue cell culture flask with non-

wettable, vented filter cap instead of well plates to prevent contamination. Containers and workspace for tissue culture and for cultivation of vegetative bacteria must be separated. If not an option, the area must be thoroughly dis-infected with 70% ethanol spray or 10% bleach between two culture experiments.

TISSUE CULTURE REAGENTS

Phosphate Buffer Solution (PBS) – Can be prepared by adding appropriate number of PBS tablets (Sigma-Aldrich®) to appropriate volume of distilled water and sterilize by autoclave (121 °C for 20 minutes) or can be purchased directly. Un-open PBS can be stored at room temperature until expiration specified on the package. Open PBS is recommended to aliquot into several Corning® medium storage bottle and stored at 4 °C.

Trypsin-EDTA – is recommended to purchase from Gibco® or Sigma-Aldrich instead prepared in the lab. Avoid repeat freeze-thaw. Aliquoted Trypsin-EDTA should be stored at -20 °C until expiration date specified on the package.

Serum – Choice of serum should be based on product sheet provided by the manufacturer or as guided by literature. The most common choice of serum is fetal bovine serum (FBS). It's recommended FBS to be purchased from American Type Cell Collection (ATCC®) as the quality is vigorously and routinely checked and guaranteed high quality. The FBS are used directly without heat-inactivation. Other type of serum I had used includes heat inactivated donor equine serum (DES) and heat inactivated donor calf serum (DCS), both are commercially available. ATCC® also provided detailed instruction for heat-inactivation treatment of serum if needed.

Complete growth medium – The receipt for the complete growth medium should always refer to ATCC® product information or guided by literature. Generally complete growth medium for tissue culture are consisted of the following components:

90 mL base media (DMEM, MEM, RPMI, etc, as specified by ATCC® product information or literature guidance). It's best to purchase the base media from ATCC® or Gibco® instead of attempt to prepare on in the lab. I always choose the base media with high glucose and with L-glutamine.

10% (or 10 mL) Fetal Bovine Serum (or other serum specified by ATCC® product sheet or literature guidance)

Any other additional component specified by the product sheet.

Most tissue culture guideline suggests adding 1% Penicillin-Streptomycin to prevent bacterial growth in the growth medium. However, under special circumstance (eg. cultivation of *Chlamydia trachomatis*) antibiotic should not be used. I found that antibiotic is not always necessary with strict application of aseptic techniques. It's up to the individual researcher to evaluate the risk and benefit of using antibiotic for specific cell lines. It's important to note that regardless adding antibiotic or not, the prepared complete growth medium must be stored aseptically in 4 °C and used up or discarded within 14 days. Sterile Corning® medium storage bottle with air-sealed O-ring should always be used when preparing the complete growth medium.

STERILIZING TECHNIQUES

Strict sterilization techniques must be implemented at all times especially when addition to antibiotic to complete growth medium is not an option (e.g. during cultivation

of *Chlamydia trachomatis*). The first rule of thumb is to treat every surface outside of the biosafety hood as un-sterile. The second rule of thumb is to always wear personal protection when performing experiment – the PPT is to protect the cells being contaminated. The third rule of thumb is to discard everything associated (disposable equipment, media, buffer solution, etc) as soon as a contamination event is discovered and thoroughly clean all surface that had contacted during the contamination event. The biosafety hood must be operated as instructed and wiped down with 70% ethanol before experiment starts. The UV lamp must be on at all time unless for an extended period of inactivity with the biosafety hood. All items enter the biosafety hood must be wiped down with 70% ethanol. Whenever possible, use individually wrapped, disposable containers and pipettes instead of glass ones. After experiment the biosafety hood must be wiped down with 70% ethanol.

Another main “hotspot” for contamination is the incubator since it’s a warm, humid environment all the time. Therefore, it’s recommended the incubator should be clean with 10% bleach regularly. The frequency of cleaning depends on the usage of the incubator but minimally once every months. Condensation near glass door and on top racks must be removed as often as possible. The water used to create the humid environment are placed in a stainless tray at the bottom rack. The water must be sterilized for three hours at 150 °C and leave in the biosafety hood with UV lamp on overnight before putting into the incubator. Sodium hydroxide pellets are added to the water in the tray to prevent any micro-organism growth in the water while in the incubator.

A waste container with 10% bleach should be always available to collect any

discarded liquid. Never leave the waste container un-capped – micro-organisms from the air can fall into the waste container and starts to proliferate. By the same token never waive your hand over open media container even with glove on, as air turbulence can bring micro-organisms into the containers. Always insert sterile pipette into container bottom to transfer media and buffer instead of pouring off the container because the container edge may be contaminated especially there are liquid left from previous transfer.

THAWING CELLS

1. Aseptically transfer 5 mL of completed growth medium to a sterile 15 mL centrifuge tube.
2. Quickly thaw the frozen vial of cells in 37 °C water bath for 1 minutes. The principle is to thaw quickly so cells are not recovering in the DMSO-containing storage solution.
3. Dried off water from the vial. Spray and wipe the vial with 70% ethanol.
4. Transfer the cells/media to the 5 mL completed growth media. Gently re-suspend the cells.
5. Spin down the cell at 750-1000 rpm at room temperature for 5 minutes.
6. While centrifuging, transfer appropriate volume of complete growth medium to tissue culture flask. The volume for different size container is summarized below

Container size	Working volume (mL)
6-well plates	2 mL per well
25 cm ² flask	5 – 10 mL
75 cm ² flask	10 -15 mL
225 cm ² flask	50 – 75 mL

7. Aspirate off supernatant.
8. Re-suspend the cell pellet in 4 mL fresh growth media and evenly divide it into all tissue culture flasks containing appropriate amount of complete growth medium. Square-shake (north-south twice follow by west-east twice) the flask to distribute cell evenly the entire surface.
9. Allow cells to grow at 37 °C with 5% CO₂ with humidity.
10. Check confluency in 24-48 hours. Change media or split the cell if near confluent (want at least 80% confluent). It's recommended to change media 24 hours prior to splitting to ensure highest viability.

SPLITTING CELLS

1. Warm up the complete growth medium, PBS buffer and trypsin-EDTA solution in 37 °C water bath. Spray and wipe with 70% ethanol. For cells grow in serum-free media, a trypsin-inhibitor solution is necessary to neutralize the enzymatic action of trypsin.
2. Remove the complete growth medium from the culture flask.
3. Rinse cell layer once with 5 mL PBS. This is important as it's necessary to remove leftover proteins from the complete growth medium prior to introduction of trypsin.
4. Trypsinize cells with 1-3 mL trypsin-EDTA. The volume used depends on the size of flask but generally should be enough to cover the entire cell layer. Do not over trypsinize or the cells will die. It's recommended to monitor the process under inverted microscope if first time working with the cell line. Trypsin works

best when warmed to 37 °C. Therefore hard to detach cells can be incubated with trypsin in 37 °C to facilitate the trypsinization process.

5. Add equal volume of serum-containing growth media or trypsin inhibitor solution to neutralize the trypsin. The neutralization is thought to be instantaneous.
6. Spin down the cell at 750-1000 rpm for 5 minutes.
7. Aspirate off the trypsin-containing media.
8. Prepare for frozen vial or continue cultivation. Transfer desired amount to newly labeled tissue culture flask (NOT the old ones), label cell line name, date, passage number dilution factor and type of media.

FREEZING CELLS

Freezing cells ensure future supply of the cell line as well as particular passage. However, the freezing process is considered one of the most stressful procedure to the cells and therefore should be carried out only during log phase when majority of the cells in the population is vital and metabolically active. Cell freezing procedure can also act as inherent selection process whereas the less-healthy cells will not be able to survive. Contrary to the thawing process, freezing cells should be carried out slowly and with gradual decrease of temperature to minimize the formation of ice crystal in the cell. Some delicate cell line require special freezing procedure and extra care during freezing. DMSO is used in all freezing procedures to reduce ice crystal formation. All frozen cells should be permanently stored in the vapor phase of liquid nitrogen.

1. Prepare the following two sterile stock solutions fresh, sterile filtered and place in ice prior to freezing.

Solution A: 40% serum, 60% growth medium (DMEM, MEM, etc), 10 mM HEPES

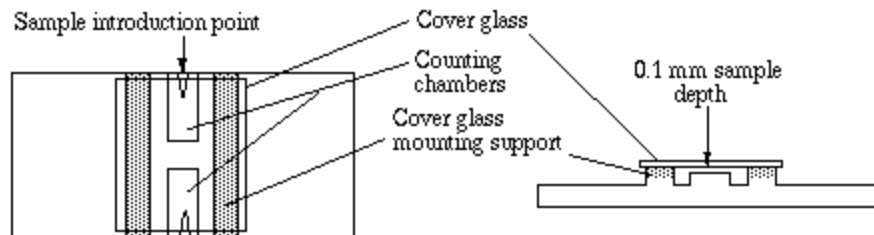
Solution B: 10% DMSO, 90% growth medium (DMEM, MEM, etc), 10 mM HEPES

2. Label sterile cryogenic vials (Corning®, total volume 1.5 mL) with name of the cell line, passage number, cell counts and date freezing with permanent marker and pre-cool in ice. One T75 cells of healthy, confluent adherent cell layer = two vials = one mL Solution A+ Solution B per vial.
3. Trysinize cells. While spinning down the cells, perform cell counts with hemocytometer (see next section).
4. After spinning down, remove supernatant and re-suspend cell pellet in 1 mL Solution A into the vial. Pipet up and down gently.
5. Slowly add 1 mL Solution B to the vial, turning the tube to mix as Solution B is added, pipet up and down gently and ensure thorough mixing.
6. Place vials at upright position in styrofoam tray and place in -80 °C for at least 24 hours, then place in the vapor phase of liquid nitrogen for permanent storage. Some delicate cell lines (usually the normal cell lines and those that are hard to grow) may need to be placed in -20 °C for several hours prior to transfer -80 °C to ensure maximum recovery when thawed.
7. Always leave one test vial to make sure the freezing was successful especially when first working with the cell line.

COUNTING VIABLE CELLS WITH HEMOCYTOMETER

1. In a clean microcentrifuge tube, combine 1:1 dilution of cells in media and Trypan Blue Stain (Sigma®). Quickly mixing with pipet.

2. Load 15-20 μL to the space between a hemocytometer and hemocytometer cover slip. Count numbers of unstained (viable) cells in 1 – 5x5 square field.



Trypan Blue is toxic and will stain viable cells if left for long time at room temperature. Therefore results beyond one minutes after mixing should be discarded.

$$(\# \text{ viable cells}) * 1 \times 10^4 * \text{dilution factor} = \text{viable cell} / \text{mL}$$

When using 1:1 mixture, the dilution factor is 2. Sometimes when cell number is large (> 50 cells per counting grid) further dilution is needed to accurately determined the cell number.

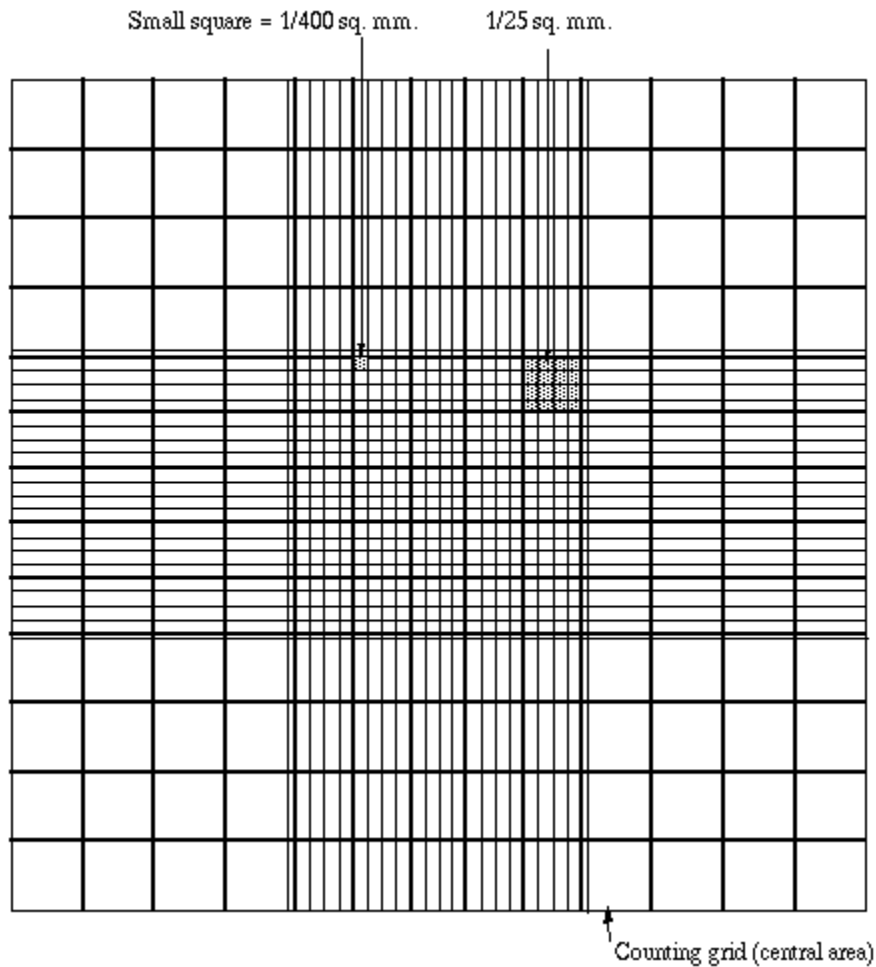


Image source: <http://www.ruf.rice.edu/~bioslabs/methods/microscopy/cellcounting>

8.6 - Receipt for Common Buffer System

1. *DEAE-dextran, 10X*

180 mg DEAE-dextran (Sigma-Aldrich®) adjust volume to 400 mL with HBSS buffer
(450 µg/mL concentration)

Sterilize by filtration with 0.2 micron syringe filter (Do not autoclave as the concentration may change due to evaporation)

Dilute 1:10 for pretreatment of tissue culture monolayer prior to infection (final concentration 45 µg/mL). The volume of DEAE-dextran used and culture condition are summarized below

Size of plate or flask	Cell concentration (cells /mL)	DEAE-dextran (mL)	Final culture volume (mL)
6-well plate	4.0×10^5	2	3
75 cm ² flask	2.0×10^6	5	8-10
150 cm ² flask	1.0×10^7	10	40-50
225 cm ² flask	5.0×10^8	15	75-100

The 10x buffer can be stored at -20 °C for 6 months. The diluted buffer should be discarded after experiment.

2. *K-36 buffer, 10X*

87.1g K ₂ HPO ₄	68.0g KH ₂ PO ₄	74.5g KCl	8.7g NaCl
---------------------------------------	---------------------------------------	-----------	-----------

Bring volume to 1L with deionized water. Adjust pH to 7.0 with 1M KOH.

Autoclave at 121 °C for 20 minutes.

Store up to 1 year at 4°C

3. *Sucrose-phosphate-glutamate buffer*

7.5g sucrose	0.467g Na ₂ HPO ₄ • 7H ₂ O	0.0312g NaH ₂ PO ₄	0.072g L-glutamic acid
--------------	---	--	------------------------

Bring volume to 100 mL with deionized water. Adjust pH to 7.4 with 2M NaOH

Autoclave at 121 °C for 20 minutes

Store up to 1 year at 4°C.

4. *Renografin solutions, 30% 40%, 44% 54%*

Prepare the following in a biological safety cabinet to maintain sterility:

30, 40, 44, 54 mL Renocal-76 or Hypaque-76 (for 30%, 40%, 44% 54% solutions respectively)

10 mL 10X K-36 buffer (see recipe)

Adjust volume to 100 mL with sterile, double-filtered water

Can be stored up to 6 months at 4 °C.

5. *Dulbecco's phosphate buffered saline (DPBS), no calcium, no magnesium*

* DPBS are commercially available through many vendors. The formulations between different vendors are pretty similar. List below is the formulation of DPBS from Gibco®.

KCl, 200 mg/mL	KH ₂ PO ₄ , 200 mg/mL	NaCl, 8000 mg/mL	Na ₂ HPO ₄ • 7H ₂ O, 2160 mg/mL
----------------	---	------------------	--

BIBLIOGRAPHY

-
- ¹ C. L. Haynes, C. R. Yonzon, X. Zhang, R.P. Van Duyne, Surface-enhanced Raman Sensor: early history and the development of sensor for quantitative biowarfare agent and glucose detection, *Journal of Raman Spectroscopy*, 36(2005): 471-484.
 - ² M. Fleischmann, P.J. Hendra, A.J. McQuillan, Raman Spectra of Pyridine Adsorbed at a Silver Electrode, *Chemical Physics letters*, 26(1974):163-166.
 - ³ A. Campion, P. Kambhampati, Surface-enhanced Raman scattering, *Chemical Society Reviews*, 27(1998):241-250.
 - ⁴ D. L. Jeanmaire, R. P. Van Duyne, Surface Raman Spectroelectrochemistry: Part I. Heterocyclic, aromatic, and aliphatic amines adsorbed on the anodized silver electrode, *Journal of Electroanalytical Chemistry and Interfacial Electrochemistry* 84(1977):1-20.
 - ⁵ M. Grant Albrecht, J. A. Creighton, Anomalously Intense Raman Spectra of Pyridine at a Silver Electrode, *Journal of the American Chemical Society* 99(1977):5215-5217.
 - ⁶ P. N. Prasad, Plasmonics, in *Nanophotonics*, 2004, John Wiley & Sons, Inc., Hoboken, NJ, USA.
 - ⁷ G. C. Schatz, R.P. Van Duyne, Electromagnetic Mechanism of Surface-enhanced Spectroscopy, *Handbook of Vibrational Spectroscopy*, at John M Chalmers and Peter R. Griffiths, 2002, John Wiley & Sons, Ltd, Chichester, UK.
 - ⁸ Le Ru, E., C. Etchegoin, P.G., Single-Molecule Surface Enhanced Raman Spectroscopy, *Annual Review of Physical Chemistry* 63(2012) 65-87.
 - ⁹ S. Dason, J. T. Dason, A. Kapoor, Guidelines for the diagnosis and management of recurrent urinary tract infection in women, *Canadian Urological Association Journal* 5 (2011) 316-322.
 - ¹⁰ B. Foxman, Urinary Tract Infection Syndromes: Occurrence, Recurrence, Bacteriology, Risk Factors, and Disease Burden, *Infectious Disease Clinics of North America* 28 (2014): 1-13.
 - ¹¹ G. Schmiemann, E. Kniehl, K. Gebhardt, M. M. Matejczyk and E. Hummers-Pradier, The Diagnosis of Urinary Tract Infection: A Systematic Review. *Deutsches Arzteblatt International* 107 (2010): 361-367.
 - ¹² B. Foxman, Epidemiology of urinary tract infections: Incidence, morbidity, and economic costs. *Disease-a-Month* 49 (2003) 53-70.
 - ¹³ S. M. Schappert and E. A. Rechtsteiner: Ambulatory medical care utilization estimates for 2006. National health statistics reports; no 8, Hyattsville, MD: National Center for Health Statistics (2008).

-
- ¹⁴ T. L. Griebeling, in M. S. Litwin and C. S. Saigal (Eds.), *Urologic Diseases in America*. Department of Health and Human Services, Public Health Service, National Institutes of Health, National Institute of Diabetes and Digestive and Kidney Diseases, Washington, D.C, 2007, p. 587–619.
- ¹⁵ S. M. Schappert, Ambulatory care visits of physician offices, hospital outpatient departments, and emergency departments: United States, 1995, *Vital and Health Statistics Series 13* (1997):1-38.
- ¹⁶ M. L. Wilson, L. Gaideo, Laboratory Diagnosis of Urinary Tract Infections in Adult Patients, *Clinical Infectious Diseases* 38 (2004):1150-1158.
- ¹⁷ T. M. Hooton, W. E. Stamm, Diagnosis and treatment of uncomplicated urinary tract infection, *Infectious Disease Clinics of North America* 11 (1997):551-581.
- ¹⁸ K. Gupta, N. Bhadelia, Management of Urinary Tract Infections From Multidrug-Resistant Organisms, *Infectious Disease Clinics of North America* 28 (2014) 49-59.
- ¹⁹ G. Kahlmeter, An international survey of the antimicrobial susceptibility of pathogens from uncomplicated urinary tract infections: the ECO·SENS Project, *Journal of Antimicrobial Chemotherapy* 51 (2003):69-76.
- ²⁰ T. M. Hooton, S. F. Bradley, D. D. Cardenas, R. Colgan, S. E. Geerlings, J. C. Rice, S. Saint, A. J. Schaeffer, P. A. Tambayh, P. Tenke and L. E. Nicolle, Diagnosis, Prevention, and Treatment of Catheter-Associated Urinary Tract Infection in Adults: 2009 International Clinical Practice Guidelines from the Infectious Diseases Society of America, *Clinical Infectious Diseases* 50 (2010):625-663.
- ²¹ M. L. Wilson, L. Gaide, Laboratory Diagnosis of Urinary Tract Infections in Adult Patients, *Medical Microbiology Invited Article* 38(2004):1150-1156.
- ²² K. C. Carroll, D.C. Hale, D. H. Von Boerum, G.C. Reich, L. T. Hamilton, and J. M. Matsen, Laboratory Evaluation of urinary tract infections in an ambulatory clinic, *American Journal of Clinical Pathology* 101(1994):100-103.
- ²³ L. Nazarko, Nurse prescribing, urinary tract infection and older men, *Nursing Times* 101(2005):69.
- ²⁴ P.G. Pappas, Laboratory in the Diagnosis and Management of Urinary Tract Infections, *Medical Clinics of North America* 75(1991):313-325.
- ²⁵ C. E. Fuller, G. A. Threatte, J. B. Henry, “Basic Examination of the urine”, In: Henry JB, Threatte GA, Herman CJ, et al., eds. *Clinical Diagnosis and Management by Laboratory Methods*, 20th ed. Philadelphia: WB Saunders, 367-402, 2001.
- ²⁶ S. Yang, R. E. Rothman, PCR-based diagnostics for infectious diseases: uses, limitations, and future applications in acute-care settings, *The Lancet Infectious Diseases* 4 (2004);337-348.

-
- ²⁷ D. N. Fredricks, D. A. Relman, Application of Polymerase Chain Reaction to the Diagnosis of Infectious Diseases, *Clinical Infectious Diseases* 29 (1999):475-488.
- ²⁸ P. E. Andreotti, G. V. Ludwig, A. H. Peruski, J. J. Tuite, S. S. Morse, L. F. Peruski, Immunoassay of infectious agents, *BioTechniques* 34 (2003):850-859.
- ²⁹ J. Weile, C. Knabbe: Current applications and future trends of molecular diagnostics in clinical bacteriology, *Analytical and Bioanalytical Chemistry* 394 (2009):731-742.
- ³⁰ N.A. Brunzel, Fundamentals of Urine and Body Fluid Analysis, Philadelphia: W.B. Saunders Company, 272-303, 1994
- ³¹ R. Finch, Regulatory opportunities to encourage technology solutions to antibacterial drug resistance, *Journal of Antimicrobial Chemotherapy* 66 (2011):1945-1947.
- ³² S. Efrima, B. V. Bronk, Silver colloids impregnating or coating bacteria, *Journal of Physical Chemistry B* 102 (1998):5947-5950.
- ³³ R. M. Jarvis, A. Brooker, R. Goodacre, Surface-enhanced Raman scattering for the rapid discrimination of bacteria, *Faraday Discussions* 132 (2006):281-92; discussion 309-19.
- ³⁴ W. R. Premasiri, D. T. Moir, M. S. Klempner, N. Krieger, G. Jones II, L. D. Ziegler: Characterization of the Surface Enhanced Raman Scattering (SERS) of Bacteria, *Journal of Physical Chemistry B*, 109 (2005):312-320.
- ³⁵ M. Kahraman, M. M. Yazici, F. Sahin, O. F. Bayrak, M. Culha, Reproducible surface-enhanced Raman scattering spectra of bacteria on aggregated silver nanoparticles, *Applied Spectroscopy* 61 (2007):479-85.
- ³⁶ H. Chu, Y. Huang, Y. Zhao, Silver nanorod arrays as a surface-enhanced Raman scattering substrate for foodborne pathogenic bacteria detection, *Applied Spectroscopy* 62 (2008):922-931.
- ³⁷ R. M. Jarvis, R. Goodacre, Discrimination of bacteria using surface-enhanced Raman spectroscopy, *Analytical Chemistry* 76 (2004):40-7.
- ³⁸ R. M. Jarvis, R. Goodacre, Characterisation and identification of bacteria using SERS, *Chemical Society Reviews*, 37 (2008):931-936.
- ³⁹ E. Kastanos, K. Hadjigeorgiou, A. Kyriakides and C. Pitris, Classification of bacterial samples as negative or positive for a UTI and antibiogram using surface enhanced Raman spectroscopy, *Proceedings of SPIE* 7911 (2011):791107-791113.
- ⁴⁰ E. Kastanos, A. Kyriakides, K. Hadjigeorgiou, C. Pitris, A Novel Method for Bacterial UTI Diagnosis Using Raman Spectroscopy, *International Journal of Spectroscopy* 2012 (2012).

-
- ⁴¹ K. Hadjigeorgioua, E. Kastanosb, A. Kyriakidesa, C. Pitris: Complete urinary tract infection (UTI) diagnosis and antibiogram using surface enhanced Raman spectroscopy (SERS), *Proceedings of SPIE* 8229 (2012):82290D-1-7.
- ⁴² N. E. Mircescu, H. Zhou, N. Leopold, V. Chiş, N. P. Ivleva, R. Niessner, A. Wieser and C. Haisch, Towards a receptor-free immobilization and SERS detection of urinary tract infections causative pathogens, *Analytical and Bioanalytical Chemistry* 406 (2014): 3051-3058.
- ⁴³ I. S. Patel, W. R. Premasiri, D. T. Moir and L. D. Ziegler: Barcoding bacterial cells: A SERS based methodology for pathogen identification, *Journal of Raman Spectroscopy* 39 (2008): 1660-1672.
- ⁴⁴ W. R. Premasiri, J. C. Lee, A. Sauer-Budge, R. Théberge, C. E. Costello and L. D. Ziegler: The biochemical origins of the surface-enhanced Raman spectra of bacteria: a metabolomics profiling by SERS, *Analytical and Bioanalytical Chemistry* 408 (2016): 4631-4647.
- ⁴⁵ https://www.bd.com/ds/technicalCenter/clsi/clsi-Phoenix_GramNegative_V5.15_V4.31.pdf.
- ⁴⁶ A. Raghino, V. Dimuccio, E. Papadimitriou, B. Bussolati, Extracellular vesicles in the urine: markers and mediators of tissue damage and regeneration, *Clinical Kidney Journal* 8 (2015):23-30.
- ⁴⁷ W. R. Premasiri, Y. Gebregziabher, L. D. Ziegler: On the difference between surface-enhanced Raman scattering (SERS) spectra of cell growth media and whole bacterial cells, *Applied Spectroscopy* 65 (2011):493-9.
- ⁴⁸ W. R. Premasiri, D. T. Moir, L. D. Ziegler: Vibrational Fingerprinting of Bacterial Pathogens by Surface Enhanced Raman Scattering, *Proceedings of SPIE* 5795 (2005).
- ⁴⁹ A. K. Boardman, W. S. Wong, W. R. Premasiri, L. D. Ziegler, J. C. Lee, M. Miljkovic, C. M. Klapperich, A. Sharon, A. F. Sauer-Budge, Rapid Detection of Bacteria from Blood with Surface-Enhanced Raman Spectroscopy, *Analytical Chemistry* 88(2016): 8026-8035.
- ⁵⁰ W. R. Premasiri, P. Lemler, Y. Chen, Y. Gebregziabher and L. D. Ziegler, in Y. Ozaki, K. Kneipp and R. Aroca (Eds.), *Frontiers of Surface-Enhanced Raman Scattering: Single-Nanoparticles and Single Cells*. Wiley & Sons, Chichester, UK, 2014, p. 255-282.
- ⁵¹ H. Link, T. Fuhrer, L. Gerosa, N. Zamboni, U. Sauer, Real-time metabolome profiling of the metabolic switch between starvation and growth, *Nature* 12(2015):1091-1097.
- ⁵² R.D. Tobias, *An Introduction to Partial Least Squares Regression*, SAS Institute Inc., Cary, NC

-
- ⁵³ H. Abdi, Partial Least Squares (PLS) Regression, In: M Lewis-Beck, A. Bryman, T. Futing, Encyclopedia of Social Sciences Research Methods, Thousand Oaks (CA), 2003.
- ⁵⁴ P. A. Chan, A. Robinette, M. Montgomery, A. Almonte, S. Cu-Uvin, J. R. Lonks, K. C. Chapin, E. M. Kojic, E. J. Hardy, Extragenital Infections Caused by Chlamydia trachomatis and Neisseria gonorrhoeae: A Review of the Literature, *Infectious Diseases in Obstetrics and Gynecology* 575 (2016):83-87.
- ⁵⁵ Centers for Disease Control and Prevention. Sexually Transmitted Disease Surveillance 2015. U.S. Department of Health and Human Services, Atlanta, 2016.
- ⁵⁶ European Centre for Disease Prevention and Control. Sexually Transmitted Infections in Europe 2013. European Centre for Disease Prevention and Control, Stockholm, Sweden (2015).
- ⁵⁷ E. Torrone, J. Papp, H. Weinstock, C. Centers for Disease and Prevention: Prevalence of Chlamydia trachomatis genital infection among persons aged 14-39 years--United States, 2007-2012, *MMWR: Morbidity and Mortality Weekly Report* 63 (2014):834-8.
- ⁵⁸ T. Meyer, Diagnostic Procedures to Detect Chlamydia trachomatis Infections, *Microorganisms* 4 (2016):25.
- ⁵⁹ R. L. Cook, S. L. Hutchison, L. Østergaard, R. Braithwaite, R. B. Ness, Systematic review: Noninvasive testing for *Chlamydia trachomatis* and *Neisseria gonorrhoeae*, *Annals of Internal Medicine* 142 (2005):914-925.
- ⁶⁰ B. P. Mulhall, S. Wright, D. Allen, K. Brown, B. Dickson, M. Grotowski, E. Jackson, K. Petoumenos, P. Read, T. Read, D. Russell, D. J. Smith, D. J. Templeton, C. K. Fairley, M. G. Law, High rates of sexually transmissible infections in HIV-positive patients in the Australian HIV Observational Database: A prospective cohort study, *Sexual Health* 11 (2014):291-7.
- ⁶¹ P. Pathela, S. L. Braunstein, S. Blank and J. A. Schillinger: HIV incidence among men with and those without sexually transmitted rectal infections: estimates from matching against an HIV case registry, *Clinical Infectious Diseases* 57 (2013):1203-9.
- ⁶² T. Darville: Chlamydia trachomatis infections in neonates and young children, *Seminars in Pediatric Infectious Diseases* 16 (2005):235-244.
- ⁶³ H. J. Zar: Neonatal chlamydial infections: prevention and treatment, *Pediatric Drugs* 7 (2005):103-10.
- ⁶⁴ S. Resnikoff, D. Pascolini, D. Etya'ale, I. Kocur, R. Pararajasegaram, G. P. Pokharel and S. P. Mariotti: Global data on visual impairment in the year 2002, *Bulletin of the World Health Organization* 82 (2004):844-51.

-
- ⁶⁵ R. Belland, D. M. Ojcius and G. I. Byrne: Chlamydia, *Nature Reviews. Microbiology* 2 (2004):530-1.
- ⁶⁶ R. J. Belland, G. Zhong, D. D. Crane, D. Hogan, D. Sturdevant, J. Sharma, W. L. Beatty and H. D. Caldwell: Genomic transcriptional profiling of the developmental cycle of Chlamydia trachomatis, *Proceedings of the National Academy of Sciences of the United States of America* 100 (2003):8478-8483.
- ⁶⁷ P. Bavoil, A. Ohlin and J. Schachter: Role of Disulfide Bonding in Outer Membrane Structure and Permeability in Chlamydia trachomatis, *Infection and Immunity* 44 (1984): 479-485.
- ⁶⁸ H. D. Caldwell, J. Kromhout and J. Schachter: Purification and partial characterization of the major outer membrane protein of Chlamydia trachomatis, *Infection and Immunity* 31 (1981):1161-76.
- ⁶⁹ R. S. Stephens and C. J. Lammel: Chlamydia outer membrane protein discovery using genomics, *Current Opinion in Microbiology* 4 (2001):16-20.
- ⁷⁰ R.S. Stephens, S. Kalman, C. Lammel, J. Fan, R. Marathe, L. Aravind, W. Mitchell, L. Olinger, R. L. Tatusov, Q. Zhao, E.V. Koonin, R.W. Davis, *Science* 282 (1988):754.
- ⁷¹ A. Nans, H.R. Saibil, R.D. Hayward: Pathogen-host reorganization during Chlamydia invasion revealed by cryo-electron tomography, *Cellular Microbiology* 16(2014):1457-1472.
- ⁷² A. Nans, C. Ford, R.D. Hayward: Host-pathogen reorganisation during host cell entry by Chlamydia trachomatis, *Microbes and Infection* 17(2015): 727-731.
- ⁷³ K. Hybiske, R. S. Stephens: Mechanisms of Chlamydia trachomatis entry into nonphagocytic cells, *Infection and Immunity* 75(2007): 3925-3934.
- ⁷⁴ M. H. Lee, J. Byun, M. Jung, J. J. Yang, K.-H. Park, S.-y. Moon, H. J. Lee and M. S. Lee: Disseminated Gonococcal Infection Presenting as Bacteremia and Liver Abscesses in a Healthy Adult, *Infection & Chemotherapy* 47 (2015):60-63.
- ⁷⁵ K. K. Kerle, J. R. Mascola and T. A. Miller: Disseminated gonococcal infection, *American Family Physician* 45 (1992): 209-14.
- ⁷⁶ D. T. Fleming and J. N. Wasserheit: From epidemiological synergy to public health policy and practice: the contribution of other sexually transmitted diseases to sexual transmission of HIV infection, *Sexually Transmitted Infections* 75 (1999):3-17.
- ⁷⁷ R. D. Kirkcaldy, S. Kidd, H. S. Weinstock, J. R. Papp and G. A. Bolan: Trends in antimicrobial resistance in Neisseria gonorrhoeae in the USA: the Gonococcal Isolate Surveillance Project (GISP), January 2006-June 2012, *Sexually Transmitted Infections* 89 Suppl 4 (2013) iv5-10.

-
- ⁷⁸ S. Creighton, M. Tenant-Flowers, C. B. Taylor, R. Miller and N. Low: Co-infection with gonorrhoea and chlamydia: how much is there and what does it mean? *International Journal of STD and AIDS* 14 (2003):109-13.
- ⁷⁹ S. B. Lyss, M. L. Kamb, T. A. Peterman and et al.: Chlamydia trachomatis among patients infected with and treated for neisseria gonorrhoeae in sexually transmitted disease clinics in the United States, *Annals of Internal Medicine* 139 (2003):178-185.
- ⁸⁰ E. J. Watson, A. Templeton, I. Russell, J. Paavonen, P. A. Mardh, A. Stary and B. S. Pederson: The accuracy and efficacy of screening tests for Chlamydia trachomatis: a systematic review, *Journal of Medical Microbiology* 51 (2002):1021-31.
- ⁸¹ J. R. Papp, J. Schachter, C. A. Gaydos and B. Van der Pol: Recommendations for the Laboratory-Based Detection of Chlamydia trachomatis and Neisseria gonorrhoeae-2014, *MMWR: Morbidity and Mortality Weekly Report* 63 (2014):1-19.
- ⁸² M. A. Chernesky, J. B. Mahony, S. Castriciano, M. Mores, I. O. Stewart, S. J. Landis, W. Seidelman, E. J. Sargeant and C. Leman: Detection of Chlamydia trachomatis antigens by enzyme immunoassay and immunofluorescence in genital specimens from symptomatic and asymptomatic men and women, *Journal of Infectious Diseases* 154 (1986):141-8.
- ⁸³ M. Alary, C. Gbenafa-Agossa, G. Aina, M. Ndour, A. C. Labbe, D. Fortin, M. Steele and R. W. Peeling: Evaluation of a rapid point-of-care test for the detection of gonococcal infection among female sex workers in Benin, *Sexually Transmitted Infections Journal* 82 Suppl. 5 (2006) v29-32.
- ⁸⁴ C. A. Gaydos, T. C. Quinn, D. Willis, A. Weissfeld, E. W. Hook, D. H. Martin, D. V. Ferrero and J. Schachter: Performance of the APTIMA Combo 2 assay for detection of Chlamydia trachomatis and Neisseria gonorrhoeae in female urine and endocervical swab specimens, *Journal of Clinical Microbiology* 41 (2003):304-9.
- ⁸⁵ D. M. Whiley, J. W. Tapsall and T. P. Sloots, Nucleic Acid Amplification Testing for Neisseria gonorrhoeae: An Ongoing Challenge, *The Journal of Molecular Diagnostics* 8 (2006) 3-15.
- ⁸⁶ <http://chlamydiae.com/twiki/bin/view/Diagnostics/NucleicacidAmplificationTests>.
- ⁸⁷ W. R. Premasiri, D. T. Moir, M. S. Klempner and L. D. Ziegler, in K. Kneipp, R. Aroca, H. Kneipp and E. Wentrup-Byrne (Eds.), *New Approaches in Biomedical Spectroscopy*. Oxford University Press, New York, 2007, p. 164.
- ⁸⁸ W. R. Premasiri, A. F. Sauer-Budge, J. C. Lee, C. M. Klapperich and L. D. Ziegler, Rapid bacterial diagnostics via surface enhanced Raman microscopy, *Spectroscopy* 27(2012) 40-49.

-
- ⁸⁹ W. R. Premasiri, Y. Chen, P. M. Williamson, D. C. Bandarage, C. Pyles and L.D. Ziegler, Rapid Urinary Tract Infection Diagnostics by Surface-Enhanced Raman Spectroscopy (SERS): Identification and Antibiotic Treatment Determination, *Analytical and Bioanalytical Chemistry* 409 (2017):3043-3054.
- ⁹⁰ R. Wiggins, S. Graf, N. Low, P.J. Horner, Real-time quantitative PCR to determine chlamydial load in men and women in a community setting, *Journal of Clinical Microbiology* 47 (2009):1824-1829.
- ⁹¹ M.E. Blocker, R.G. Krysiak, F. Behets, M.S. Cohen, M.M. Hobbs, Quantification of Chlamydia trachomatis Elementary Bodies in Urine by Ligase Chain Reaction, *Journal of Clinical Microbiology* 40 (2002):3631-3634.
- ⁹² M. Bissessor, S. N. Tabrizi, C. K. Fairley, J. Danielewski, B. Whitton, S. Bird, S. Garland, M. Y. Chen, Differing Neisseria gonorrhoeae bacterial loads in the pharynx and rectum in men who have sex with men: implications for gonococcal detection, transmission, and control, *Journal of Clinical Microbiology* 49 (2011):4304-6.
- ⁹³ D. Priest, J. J. Ong, E. P. Chow, S. Tabrizi, S. Phillips, M. Bissessor, C. K. Fairley, C. S. Bradshaw, T. R. Read, S. Garland, S.; M. Chen, Neisseria gonorrhoeae DNA bacterial load in men with symptomatic and asymptomatic gonococcal urethritis, *Sexually Transmitted Infection* Published Online First: 01 February 2017. doi: 10.1136/sextrans-2016-052950
- ⁹⁴ K.H. Johnston, E.C. Gotschlich, Isolation and Characterization of the Outer Membrane of Neisseria gonorrhoeae, *Journal of Bacteriology* 119 (1974): 250-257.
- ⁹⁵ K. L. Seib, H. J. Wu, S. P. Kidd, M. A. Apicella, M. P. Jennings, A. G. McEwan, Defenses against oxidative stress in Neisseria gonorrhoeae: a system tailored for a challenging environment. *Microbiology and Molecular Biology Reviews* 70 (2006):344-61.
- ⁹⁶ I. Schröder, E. Johnso, S. de Vries, Microbial Ferric Iron Reductases. *FEMS Microbiology Reviews* 27 (2003): 427 – 447.
- ⁹⁷ C. Ratledge, L. G. Dover, Iron Metabolism in Pathogenic Bacteria, *Annual Review of Microbiology* 54(2000):881-941
- ⁹⁸ H.C. Mahler, W. Friess, U. Grauschopf, S. Kiese, Protein aggregation: pathways, induction factors and analysis. *Journal of Pharmaceutical Sciences* 98 (2009):2909-2934.
- ⁹⁹ M. Vazquez-Rey, D.A. Lang: Aggregates in monoclonal antibody manufacturing processes. *Biotechnology and Bioengineering* 108 (2011):1494-1508.

-
- ¹⁰⁰ J.F. Carpenter, B.S. Kendrick, B.S. Chang, M.C. Manning, T.W. Randolph, Inhibition of Stress-Induced Aggregation of Protein Therapeutics, *Methods in Enzymology* 309 (1999): 236 -255.
- ¹⁰¹ B.S. Chang, B. Yeung, Physical Stability of Protein Pharmaceuticals. Formulation and Process Development Strategies for Manufacturing Biopharmaceuticals (2010) 69-104. John Wiley & Sons, Inc.
- ¹⁰² E. Podstawka, Y. Ozaki, L.M. Proniewicz, Part II: Surface-Enhanced Raman Spectroscopy Investigation of methionine containing heterodipeptides adsorbed on colloidal silver, *Applied Spectroscopy* 58(2004):1147-1156.
- ¹⁰³ A.L. Jenkins, R.A. Larsen, T.B. Williams, Characterization of Amino Acids Using Raman Spectroscopy, *Spectrochimica Acta Part A* 61(2005):1585-1594.
- ¹⁰⁴ G.D. Chumanov, R.G. Efremov, I.R. Nabiev, Surface-enhanced Raman Spectroscopy of Biomolecules. Part I. – Water-Soluble Proteins, Dipeptides and Amino Acids, *Journal of Raman Spectroscopy* 21(1990): 43-48.
- ¹⁰⁵ T.M. Cotton, J.H. Kim, G.D. Chumanov, Surface-enhanced Raman Spectroscopy Investigation of Fluoroquinolone/DNA/DNA Gyrase/Mg²⁺ Interactions: Part I. Adsorption of Pefloxacin on Colloidal Silver – Effect of Drug Concentration, Electrolytes, and pH, *Journal of Raman Spectroscopy* 22(1991):729-742.
- ¹⁰⁶ S. Cinta-Pinzaru, S. Cavalu, N. Leopold, R. Petry, W. Kiefer, *Journal of Molecular Structure*, 2001, 565:225.
- ¹⁰⁷ J. Hu, R.S. Sheng, Z.S. Xu, Y. Zeng, *Spectrochimica Acta Part A* 51(1995):1087-1096.
- ¹⁰⁸ A.M. Ahern, R.L. Garrel, *Langmuir* 7(1991): 254-261.
- ¹⁰⁹ S. Stewart, P.M. Fredericks, *Spectrochimica Acta Part A* 55 (1999):1615-1640.
- ¹¹⁰ E.S. Grabbe, R.P. Buck, *Journal of the American Chemical Society* 111(1989): 8362-8366.
- ¹¹¹ S. Stewart, P.M. Fredericks, *Spectrochimica Acta Part A* 55(1999):1641-1660.
- ¹¹² R. J. Bastidas, C. A. Elwell, J. N. Engel and R. H. Valdivia: Chlamydial intracellular survival strategies, *Cold Spring Harbor Perspectives in Medicine* 3(2013): a010256.
- ¹¹³ H.A Saka, R. H. Valdivia (2010). Acquisition of nutrients by Chlamydiae: unique challenges of living in an intracellular compartment, *Current Opinion in Microbiology* 13 (2010): 4-10.
- ¹¹⁴ S. Frokjaer, D. E. Otzen (2005). Protein Drug stability: a formulation challenge, *Nature Reviews. Drug Discovery* 4(4): 298 - 306.

-
- ¹¹⁵ M. Vazquez-Rey, D. A. Lang, Aggregates in Monoclonal Antibody Manufacturing Processes, *Biotechnology and Bioengineering*, 108(2011):1494-1508.
- ¹¹⁶ C. David. (2012). Raman Spectroscopy for proteins. In *Horiba Scientific Webinar*. Retrieved from http://www.horiba.com/fileadmin/uploads/Scientific/Documents/Raman/HORIBA_webinar_proteins.pdf
- ¹¹⁷ J. T. Pelton, L.R. McLean, Spectroscopic methods for analysis of protein secondary structure, *Analytical Biochemistry* 277(2000):167-176.
- ¹¹⁸ V. Militello, C. Casarino, A. Emanuele, A. Giostra, F. Pullara, M. Leone, Aggregation kinetics of bovine serum albumin studied by FTIR spectroscopy and light scattering, *Biophysical Chemistry* 107(2004):175-187.
- ¹¹⁹ A.L. Fink, Protein aggregation: folding aggregates, inclusion bodies and amyloid, *Folding & Design* 3(1998):R9-R23.
- ¹²⁰ A Dong, S. J. Prestrelski, S. D. Allison, J.F. Carpenter, Infrared spectroscopic studies of lyophilization- and temperature-induced protein aggregation, *Journal of Pharmaceutical Sciences* 84(1995): 415-424.
- ¹²¹ S. Krimm, J. Bandekar, Vibrational spectroscopy and conformation of peptides, polypeptides and proteins, *Advances in Protein Chemistry* 38(1986):181-364.
- ¹²² A. Barth, Infrared spectroscopy of proteins, *Biochimica et Biophysica Acta* 1767(2007):1073-1101.
- ¹²³ Y. Wang, K. Murayama, Y. Myojo, R. Tsenkova, N. Hayashi, Y. Ozaki, Two-dimensional Fourier transform near-infrared spectroscopy study of heat denaturation of ovalbumin in aqueous solutions, *Journal of Physical Chemistry B* 102(1998):6655-6662.
- ¹²⁴ MATLAB and Bioinformatics Toolbox Release 2016b, The MathWorks, Inc. Natick, Massachusetts, United States.
- ¹²⁵ D.S. MacLean, Q.S. Qian, C.R. Middaugh, Stabilization of proteins by low molecular weight multi-ions, *Journal of Pharmaceutical Sciences* 91 (2002):2220-2229.
- ¹²⁶ R.A. Curtis, J. Ulrich, A. Montaser, J.M. Prausnitz, H.W. Blanch, Protein-protein interactions in concentrated electrolyte solutions - hofmeister-series effects, *Biotechnology and Bioengineering* 79 (2002):367-380.
- ¹²⁷ T. Arakawa, Hydration as a major factor in preferential solvent protein interactions, *Crystal Growth & Design* 2 (2002):549-551.
- ¹²⁸ R. L. Baldwin, How Hofmeister Ion Interactions Affect Protein Stability, *Biophysical Journal* 71(1996):2056-2063.

-
- ¹²⁹ E. Y. Chi, S. Krishnan, T. W. Randolph, J. F. Carpenter, Physical Stability of Proteins in Aqueous Solution: Mechanism and Driving Forces in Nonnative Protein Aggregation, *Pharmaceutical Research* 20(2003): 1325-1336.
- ¹³⁰ S. Amin, G. V. Barnett, J. A. Pathak, C. J. Roberts, P. S. Sarangapani, Protein aggregation, particle formation, characterization, & rheology, *Current Opinion in Colloid & Interface Science* 19(2014):438-449.
- ¹³¹ N. S. Wigginton, A. de Titta, F. Piccapietra, J. Dobias, V. J. Nesatyy, M. J. F. Suter, R. Bernier-Latmani, Binding of Silver Nanoparticles to Bacterial Proteins Depends on Surface Modifications and Inhibits Enzymatic Activity, *Environmental Sciences & Technology* 44(2010): 2163-2168.
- ¹³² J. L. Clement, P. S. Jarrett, Antibacterial Silver, *Metal Based Drugs* 1(1994):467-482.
- ¹³³ T. Miclaus, C. Beer, J. Chevallier, C. Scavenius, V. E. Bochenkow, J. J. Enghild, D. S. Sutherland, Dynamic Protein Coronas Revealed as a Modulator of Silver Nanoparticle Sulphidation *in vitro*, *Nature Communications* 7(2016): 11770.
- ¹³⁴ N. Duran, C. P. Silveira, M. Duran, D. S. T. Martinez, Silver Nanoparticle Protein Corona and Toxicity: a mini-review, *Journal of Nanobiotechnology* 12(2015): 55-72.
- ¹³⁵ L. Treuel, M. Malissek, S. Grass, J. Diendorf, D. Mahl, W. Meyer-Zaika, M. Epple, Quantifying the influence of polymer coatings on the serum albumin corona formation around silver and gold nanoparticles, *Journal of Nanoparticle Research* 14(2012):1-12.
- ¹³⁶ M. Sleutel, E.S. Van Driessche, W. Pan, E. K. Reichel, D. Maes, P. G. Vekilov, Does Solution Viscosity Scale to the Rate of Aggregation of Folded Proteins?, *Journal of Physical Chemistry Letters* 3(2012): 1258-1263.
- ¹³⁷ C. R. Thomas, A. W. Nienow, P. Dunnill, Action of shear on enzymes: Studies with alcohol dehydrogenase, *Biotechnology and Bioengineering* 21(1979): 2263-2278.
- ¹³⁸ C. R. Thomas, A. W. Nienow, P. Dunnill, Action of shear on enzymes: Action of shear on enzymes: Studies with catalase and urease, *Biotechnology and Bioengineering* 21(1979): 2279-2302.
- ¹³⁹ World Health Organization (2017) Cancer Fact sheet. <http://www.who.int/mediacentre/factsheets/fs297/en/>. Access April 26, 2017.
- ¹⁴⁰ R.W. Ruddon. Cancer biology. 4th ed. New York: Oxford University Press, 2007.
- ¹⁴¹ J.L. Griffin, and J.P. Shockcor (2004).Metabolic Profiles of Cancer Cells, *Nature Reviews. Cancer* 4(7): 551-561.
- ¹⁴² D. Hanahan and R. A. Weinberg, Hallmarks of Cancer: The Next Generation, *Cell* 144(2011):646-674.

-
- ¹⁴³ O. Warburg, On the Origin of the Cancer Cell, *Science* 123(1956):309-314.
- ¹⁴⁴ G. Kroemer and J. Pouyssegur, Tumor Cell metabolism: Cancer's Achilles' Heel, *Cancer Cell* 13(2008) 472-482.
- ¹⁴⁵ S. Cardaci and M.R. Ciriolo, TCA Cycle Defects and Cancer: When Metabolism Tunes Redox State, *International Journal of Cell Biology* 2012(2012):1-9.
- ¹⁴⁶ D. B. Kell and H. V. Westerhoff, Towards a rational approach to the optimization of flux in microbial biotransformations, *Trends in Biotechnology* 4(1986):137-142.
- ¹⁴⁷ J. L. Spratin, N. J. Serkova, and S. G. Eckhardt, Clinical Applications of Metabolomics in oncology: a review, *Clinical Cancer Research*, 15(2009): 430-440.
- ¹⁴⁸ O. Ben-Yoseph, *et al.*, Glycerol 3-phosphate and lactate as indicators of the cerebral cytoplasmic redox state in severe and mild hypoxia respectively, a ¹³C- and ³¹P-NMR study, *Biochemical Journal* 291(1993):915-919.
- ¹⁴⁹ J. M. Hakumaki *et al.*, Quantitative ¹H NMR Diffusion Spectroscopy of BT4C Rat Glioma during thymidine kinase-mediated gene therapy *in vivo*: Identification of apoptotic response, *Cancer Research*, 58(1998):3791-3799.
- ¹⁵⁰ J. R. Griffin and M. Stubbs, Opportunities for studying cancer by metabolomics: preliminary observations on tumor deficient in hypoxia-inducible factor 1, *Advances in Enzyme Regulation* 43(2003): 67-76.
- ¹⁵¹ M. C. Preul, *et al.*, Accurate, noninvasive diagnosis of human brain tumors by using proton magnetic resonance spectroscopy, *Nature Methods* 2(1996) 323-325.
- ¹⁵² K. K. Lehtimaki, *et al.*, Metabolite changes in BT4C rat gliomas undergoing ganciclovir-thymidine kinase gene therapy-induced programmed cell death as studied by ¹H NMR spectroscopy *in vivo*, *ex vivo*, and *in vitro*, *Journal of Biological Chemistry* 278(2003) 45915-45923.
- ¹⁵³ C. L. Florian, N.E. Preece, K.K. Bhakoo, S.R. Williams and M.D. Noble, Characteristic metabolic profiles revealed by ¹H NMR spectroscopy for three types of human brain and nervous system tumors, *NMR in Biomedicine*. 8(1995) 253-264.
- ¹⁵⁴ S. Lee, S. Kim, J. Choo, S.Y. Shin, Y.H. Lee, H. Y. Choi, S. Ha, K. Kang, C. H. Oh: Biological imaging of HEK293 cells expressing PLC γ 1 using surface-enhanced Raman microscopy, *Analytical Chemistry* 79(2007): 916-922.
- ¹⁵⁵ H. Chon, S. Lee, S. W. Son, C. H. Oh, J. Choo: Highly sensitive Immunoassay of lung cancer marker carcinoembryonic antigen using surface-enhanced Raman scattering of hollow gold nanospheres. *Analytical Chemistry* 81(2009):3029-3034.
- ¹⁵⁶ X. Huang, I. H. El-Sayed, W. Qian, M. A. El-Sayed: Cancer cells assemble and align gold nanorods conjugated to antibodies to produce highly enhanced, sharp and

-
- polarized surface Raman spectra: a potential cancer diagnostic marker. *Nano Letters* 7(2007):1591-1597.
- ¹⁵⁷ X. Qian, X. H. Peng, D. O. Ansari, Q. Yin-Goen, G. Z. Chen, D. M. Shin, L. Yang, A. N. Young, M.D. Young, S. Nie: In vivo tumor targeting and spectroscopic detection with surface-enhanced Raman nanoparticle tags. *Nature Biotechnology* 26(2008): 83-90.
- ¹⁵⁸ M. Y. Sha, H. Xu, M. J. Natan, R. Cromer: Surface-enhanced Raman scattering tags for rapid and homogeneous detection of circulating tumor cells in the presence of human whole blood, *Journal of the American Chemical Society* 130(2008): 17214-17215.
- ¹⁵⁹ H.W. Tang, X. B. Yang, J. Kirkham, D.A. Smith, Probing intrinsic and extrinsic components in single osteosarcoma cells by near-infrared surface-enhanced Raman scattering, *Analytical Chemistry* 79(2007): 3646-3653.
- ¹⁶⁰ X. Wang, X. Qian, J. J. Beitler, Z. G. Chen, F. R. Khuri, M. M. Lewis, H. J. Shin, S. Nie, D.M. Shin: Detection of circulating tumor cells in human peripheral blood using surface-enhanced Raman scattering nanoparticles, *Cancer Research*, 71(2011):1526-1532.
- ¹⁶¹ B. Yan, B. M. Reinhard: Identification of tumor cells through spectroscopic profiling of the cellular surface chemistry, *The Journal of Physical Chemistry Letters* 1(2010):1595-1598.
- ¹⁶² S. Feng, R. Chen, J. Lin, J. Pan, G. Chen, Y. Li, M. Cheng, Z. Huang, J. Chen, H. Zeng, Nasopharyngeal cancer detection based on blood plasma surface-enhanced Raman spectroscopy and multivariate analysis, *Biosensors and Bioelectronics* 25(2010): 2414-2419.
- ¹⁶³ S. Feng, J. Pan, Y. Wu, D. Lin, Y. Chen, G. Xi, J. Lin, R. Chen, Study on gastric cancer blood plasma based on surface-enhanced Raman spectroscopy combined with multivariate analysis, *Science in China Life Sciences* 54(2011):828-834.
- ¹⁶⁴ D. Lin, S. Feng, J. Pan, Y. Chen, J. Lin, G. Chen, S. Xie, H. Zeng, R. Chen, Colorectal cancer detection by gold nanoparticle based surface-enhanced Raman spectroscopy of blood serum and statistical analysis, *Optics Express* 19(2011): 13565-13577.
- ¹⁶⁵ P. Papageorgis, A. W. Lambert, S. Ozturk, F. Gao, H. Pan, U. Manne, Y. O. Alekseyev, A. Thiagalingam, H. M. Abdolmaleky, M. Lenburg, S. Thiagalingam: Smad signaling is required to maintain epigenetic silencing during breast cancer progression, *Cancer Research* 70(2010): 968-978.
- ¹⁶⁶ G. Burnstock, Purinergic nerves, *Pharmacological Reviews* 24(1972):509-581.

-
- ¹⁶⁷ G. Burnstock, Physiology and pathophysiology of purinergic neurotransmission, *Physiological Reviews* 87(2007):659-797.
- ¹⁶⁸ J. Stagg, M. J. Smyth, Extracellular adenosine triphosphate and adenosine in cancer, *Oncogene* 29(2010):5346-5358.
- ¹⁶⁹ V. Kumar, Adenosine as an endogenous immunoregulator in cancer pathogenesis: Where to go? *Purinergic Signaling* 9(2013):145-165.
- ¹⁷⁰ F. Di Virgilio, Purines, Purinergic Receptors, and Cancer, *Cancer Research* 72 (2012): 5441-5447.
- ¹⁷¹ M.P. Abbracchio, G. Burnstock, A. Verkhratsky, H. Zimmermann, Purinergic signaling in the nervous system: an overview, *Trends in Neurosciences* 32(2009):19-29.
- ¹⁷² M.P. Rathbone, L. Christjanson, S. Deforge, B. Deluca, J. W. Gysbers, S. Hindley, M. Jovetich, P. Middlemiss, S. Takhal S, Extracellular purine nucleosides stimulate cell division and morphogenesis: pathological and physiological implications, *Medical Hypotheses* 37(1992):232-240.
- ¹⁷³ J. Chen, Y. Zhao, Y. Liu, The role of nucleotides and purinergic signaling in apoptotic cell clearance – implications for chronic inflammatory diseases, *Frontiers in Immunology* 5(2014):656-665.
- ¹⁷⁴ G. Hasko, J. Linden, B. Cronstein, P. Pacher, Adenosine receptors: therapeutic aspects for inflammatory and immune diseases, *Nature Reviews. Drug Discovery* 7(2008):759-770.
- ¹⁷⁵ G.G. Yegutkin, Nucleotide- and nucleoside-converting ectoenzymes: Important modulators of purinergic signaling cascade, *Biochimica et Biophysica Acta*, 1783(2008):673-694.
- ¹⁷⁶ R. L. Elstrom, D. E. Bauer, M. Buzzai, R. Karnauskas, M. H. Harris, D. R. Plas, H. Zhuang, R. M. Cinalli, A. Alavi, C. M. Rudin, C. B. Thompson, Akt Stimulates Aerobic Glycolysis in Cancer Cells, *Cancer Research* 64(2004):3892-3899.
- ¹⁷⁷ M.A. Scidmore (2005) *Current. Protocol. Microbiology*. Chapter 11:Unit 11A 11.

CURRICULUM VITAE

